

EFFECTIVE MASSES OF FREE CARRIERS IN LEAD TELLURIDE: THEIR  
TEMPERATURE DEPENDENCE AND CONTRIBUTION TO TRANSPORT PROPERTIES

by  
HENRY ALBERT LYDEN

A.B. in Physics, Williams College  
(1957)

S.B.E.E., M.I.T.  
(1957)

S.M.E.E., M.I.T.  
(1959)

SUBMITTED IN PARTIAL FULFILLMENT OF THE  
REQUIREMENTS FOR THE DEGREE OF  
DOCTOR OF SCIENCE

at the  
MASSACHUSETTS INSTITUTE OF TECHNOLOGY

Signature of Author -----  
Department of Electrical Engineering

Certified by -----  
Thesis Supervisor

Accepted by -----  
Chairman, Department Committee on Graduate Students

✓



Room 14-0551  
77 Massachusetts Avenue  
Cambridge, MA 02139  
Ph: 617.253.5668 Fax: 617.253.1690  
Email: docs@mit.edu  
<http://libraries.mit.edu/docs>

## **DISCLAIMER OF QUALITY**

Due to the condition of the original material, there are unavoidable flaws in this reproduction. We have made every effort possible to provide you with the best copy available. If you are dissatisfied with this product and find it unusable, please contact Document Services as soon as possible.

Thank you.

**Due to the poor quality of the original document, there is some spotting or background shading in this document.**

EFFECTIVE MASSES OF FREE CARRIERS IN LEAD TELLURIDE: THEIR  
TEMPERATURE DEPENDENCE AND CONTRIBUTION TO TRANSPORT PROPERTIES

by

Henry Albert Lyden

Submitted to the Department of Electrical Engineering on February 16, 1962,  
in Partial Fulfillment of the Requirements For the Degree of Doctor of Science

ABSTRACT

Single crystals of both n-type and p-type PbTe were grown by the Bridgman-Stockbarger technique. Very smooth and highly-reflective crystals were obtained when the PbTe material lowered through the furnace had been previously distilled in a vacuum ( $\sim 10^{-5}$  mm).

From measurements of the Hall Effect and of the electrical conductivity on 3 n- and 2 p-type samples of PbTe, all with free-carrier concentrations of  $N=3-4 \times 10^{18}$  carriers/cm<sup>3</sup>, the mobility ( $\mu$ ) of holes and electrons has been obtained over the temperature range 77° to 300°K. This mobility has a temperature dependence represented by  $\mu \propto T^{-r}$  where ( $2 < r < 3$ ) for  $T > 150^\circ\text{K}$ . The origin of this behavior has been investigated by determining the temperature dependence of the reduced Fermi potential energy ( $\eta$ ), of the density-of-states effective mass ( $m_d^*$ ), and of the conductivity effective mass ( $m_c^*$ ).

For obtaining  $m_c^*$  as a function of temperature, a new procedure has been developed. It has been possible to derive an equation which enables one to determine  $m_c^*$  knowing  $N$ ,  $\mu$ ,  $\epsilon_\infty$  (which is the lattice dielectric constant of the material at very high frequencies), and the wavelength of the reflectivity minimum associated with the free-carrier dispersion. Using this new technique, values for  $m_c^*$  have been obtained between 4° and 300°K. Over this range  $m_c^*$  increases monotonically from 0.052 to 0.105 for n-type PbTe, and from 0.044 to 0.11 for p-type.

It has also been determined that  $m_d^*$  behaves in a very similar fashion. The values that have been obtained for  $m_d^*$  at 77° and 300°K are  $m_{dn}^* = 0.20$  and 0.30 and for  $m_{dp}^* = 0.14$  and 0.25.

It has been shown that an acoustical mode mobility can be synthesized, using the data for  $\eta$ ,  $m_d^*$ , and  $m_c^*$ , which agrees quite well with the experimental mobility for  $T > 200^\circ\text{K}$  for both n- and p-type material. Moreover, a combination of acoustical and optical mode mobilities is capable of fitting the observed mobility over the entire temperature range,  $80^\circ$  to  $300^\circ\text{K}$ .

From the amount of optical mode scattering required to fit the mobility data it is deduced that the static dielectric constant is not much different from  $\epsilon_\infty$ . It has been determined that  $\epsilon_s - \epsilon_\infty \approx 2.5$  for PbTe at  $300^\circ\text{K}$ . In addition it is inferred that PbTe is predominantly covalent in nature instead of ionic, as is usually assumed.

Finally, the thermal conductivity has been measured between  $100^\circ$  and  $300^\circ\text{K}$ . The data obtained substantiate the results of Kanaii and Nii in that no extra conduction mechanism, comparable to that attributed to exciton conduction by Ioffe and by Deviatkova, was observed.

Thesis Supervisor: Arthur C. Smith  
Title: Assistant Professor of Electrical Engineering

## ACKNOWLEDGMENTS

The author is especially indebted to Professor Arthur C. Smith for his ready availability and pertinent counsel throughout the course of this work. In addition, a special acknowledgement must be made to the group at Lincoln Laboratory under the direction of Dr. Benjamin Lax and Dr. John Mavroides for making their facilities and personnel available for this work. In particular, among the personnel of this group, thanks are extended to Dr. Dana Dickey, to whom credit goes for the development of the infra-red spectrometer used in this investigation, for his interest and his many contributions with regard to the infra-red measurements of this study. Also within this group, special thanks are extended to Mr. Michael Fulton for his very capable assistance in making the infra-red measurements.

To Professor Richard B. Adler and David C. White special thanks are rendered in acknowledgement of their service as thesis readers. For his willing cooperation and for his capable attendance to the details of the laboratory special thanks go to Mr. David Puotinen. They also go to Dr. Robert E. Nelson for his ready assistance with regard to the Hall Effect measurements and to Dr. Jose M. Borrego for his helpful cooperation with the material preparation. The assistance of Mr. Curtis Hoffman in helping with the thermal conductivity measurements is gratefully acknowledged.

For her many contributions, not the least of which include helping to reduce the data and typing most of the rough draft, sincere thanks are extended to Mrs. Marjorie Lyden. For the final preparation of the manuscript, appreciation is extended to the Publications Department of the Electronic Systems Laboratory and especially to Miss Mary Berry. The contribution of Mr. Harold Tonsing of that laboratory to the preparation of the drawings is sincerely appreciated.

Finally, with respect to the important aspect of financial assistance, the support of the United States Air Force under Contract No. AF-19(604)-4153 is gratefully acknowledged.

## TABLE OF CONTENTS

	page
ABSTRACT	ii
ACKNOWLEDGMENTS	iv
INTRODUCTION	1
CHAPTER I. BACKGROUND AND LITERATURE SURVEY	3
CHAPTER II. DETERMINATION OF THE CONDUCTIVITY EFFECTIVE MASS	13
CHAPTER III. PREPARATION OF MATERIAL	27
CHAPTER IV. EXPERIMENTAL PROCEDURE AND ESTIMATION OF ERRORS	37
CHAPTER V. EXPERIMENTAL RESULTS AND ANALYSIS	47
Thermoelectric Power	47
Hall Effect	53
Density-of-states Effective Mass	54
Infra-red Reflectivity of n-Type PbTe	57
Comparison With Theoretical Reflectivity	68
Lattice Contribution to Reflectivity	72
Synthesis of Acoustical Mode Mobility	75
Determination of Optical Mode Mobility	78
Combination of Acoustical and Optical Mobilties	85
Infra-red Reflectivity of p-Type PbTe	92
Fitting of the Mobility of p-Type PbTe	98
Magnetoplasma Effect	101
Thermal Conductivity of PbTe	108
CHAPTER VI. CONCLUDING DISCUSSION	117
APPENDIX A. DIFFERENTIATION OF THE EQUATION FOR THE REFLECTIVITY OF FREE CARRIERS	125
APPENDIX B. APPLICATION OF EQUATION 2-10 TO THE CASE OF N-TYPE GERMANIUM	131

## INTRODUCTION

The temperature dependence of the mobility of the semiconducting compound PbTe has posed something of a mystery in that it apparently does not conform to the theoretical behavior. We have probed the origins of this behavior in this investigation. For doing this, a procedure has been developed whereby it is possible to determine the conductivity effective mass from the wavelength of the infra-red reflectivity minimum resulting from the free-carrier dispersion. Using this procedure, the conductivity effective mass ( $m_c$ ) has been determined as a function of temperature between 4° and 300°K for 3 n-type and 2 p-type samples of lead telluride. A very pronounced temperature dependence has been observed. At 4°K we obtained the values  $m_{cn} = 0.052 m_o$  and  $m_{cp} = 0.044 m_o$ . The values of  $m_c$  increase monotonically to the values at 300°K which have been determined to be  $m_{cn} = 0.105 m_o$  and  $m_{cp} = 0.11 m_o$ .

In addition, the thermoelectric power has been measured between 77° and 300°K for these same five samples, whose free carrier concentrations were all about  $3 - 4 \times 10^{18}$  carriers/cm<sup>3</sup>. From these data, the reduced Fermi potential energy and the density-of-states effective mass ( $m_d$ ) were determined over this same temperature range. At 77°K we have observed  $m_{dn} = 0.20 m_o$  and  $m_{dp} = 0.14 m_o$ , whereas at 300°K they have increased to  $m_{dn} = 0.30 m_o$  and  $m_{dp} = 0.25 m_o$ .

These values of the effective masses have been used to deduce the number of equivalent ellipsoids of constant energy ( $N_v$ ). For the conduction band, we find  $N_v = 4$  indicating that the (111) minima are at the edge of the zone. For the valence band, we find that  $N_v \approx 2.5$  from which it has been inferred that a valence band maximum at the center of the zone has a prominent role in the energy band picture.

An acoustical mode mobility has been synthesized from these data and it has been found that the actual temperature dependence for PbTe is considerably greater than even the non-degenerate limit of  $T^{-3/2}$ . Moreover, for both n-type and p-type material the temperature dependence of the synthesized acoustical mode mobility agrees quite well with the observed mobility behavior for temperatures  $> 200^\circ\text{K}$ . Below this temperature, it has been found that optical mode scattering is important. A combination of these two scattering mechanisms, acoustical and optical, have given a very close agreement with the observed

mobility temperature dependence over the complete temperature range, 77° to 300°K.

From the amount of optical mode scattering required to fit the observed mobility behavior, it has been deduced that PbTe should not be classified as a predominately polar compound since it has a very low degree of ionicity. As a result, its static dielectric constant is just slightly greater than its high frequency dielectric constant. Values for both the effective ionic charge,  $S = 0.07$ , and the static dielectric constant,  $\epsilon_s = \epsilon_\infty + 2.5$  have been deduced.

Finally, the thermal conductivity ( $\kappa$ ) of these same samples of PbTe has been measured between 100° and 300°K. This investigation was undertaken to ascertain if  $\kappa$  obeys the simple theory or if in fact an extra conduction mechanism is present as has been reported. We have found no evidence of any extra component in  $\kappa$ . It is apparently composed of an electronic component described by the Wiedemann-Franz relation and by a lattice component which obeys the usual  $T^{-1}$  dependence.



## CHAPTER I

### BACKGROUND AND LITERATURE SURVEY

Investigative research into the thermal, electrical, and optical properties of the compounds of the lead sulfide family (lead sulfide, selenide, and telluride) has been extensively reported in the literature. It is not our purpose to present here a comprehensive review of all of this research. Such reviews do, in fact, already exist.<sup>1-3\*</sup> There have come to light, as a result of this previous research, some properties which do not completely conform with the predicted semiconductor behavior and the question has arisen as to why and how such a behavior can exist. We are concerned here with just such a question, and so we will limit the background material to a discussion of the properties which have a direct bearing on this investigation.

The property which is most pertinent to our present investigation is the temperature dependence of the free carrier mobility. This property has received considerable attention and has been widely reported in the literature.<sup>4-8</sup> All of these reports agree that the dependence of the mobility on temperature,  $\mu_{ac} T^{-r}$ , is such that the exponent  $r$  lies in the range  $2 < r < 3$  for both n- and p-type material and for all temperatures above  $\sim 200^\circ\text{K}$ . Such temperature dependences have been observed in other semiconductors (e.g. p-type germanium and n- and p-type silicon). Nevertheless, it differs from that theoretically predicted for semiconductors above their Debye temperature where scattering is by acoustical modes. Such a scattering mechanism leads to a theoretical temperature dependence in which the exponent  $r$  lies in the range  $1 \leq r \leq 3/2$  where the limits hold for material which is degenerate or non-degenerate, respectively.

---

\*Superscripts refer to numbered items at the end of each chapter.

The Hall coefficient and its temperature dependence is also pertinent to our present investigation. It has been shown, for crystals having cubic symmetry and ellipsoidal surfaces of constant energy along the symmetry axes, that the Hall coefficient is given by<sup>8</sup>

$$R = \frac{b}{Ne} \left[ \frac{3K(K+2)}{(2K+1)^2} \right] \quad (1-1)$$

where  $N$  is the free-carrier concentration,  $e$  is the electronic charge,  $K$  is the effective mass ratio  $m_1/m_t$  (assuming that the mean free time is isotropic), and  $b$  is a numerical factor varying between the limits  $3\pi/8$  and  $1$  corresponding to classical and degenerate statistics, respectively. The results reported in the literature show that, for material in its extrinsic region, the Hall coefficient is a constant, independent of temperature, down to  $77^\circ\text{K}$  and only slightly temperature dependent ( $0-20\%$  change) down to  $4^\circ\text{K}$ . From magneto-resistance data (as will be discussed in a subsequent paragraph) we know that the anisotropy factor  $K$  is not a strong function of temperature. That is, the range of values is apparently such that  $3 < K < 5$ . The corresponding range for the factor in brackets in Eq. 1-1 is  $0.95$  to  $0.87$ . Consequently, it is reasonable to conclude that the concentration of free carriers in both n- and p-type lead telluride is nearly constant from  $4^\circ\text{K}$  upward throughout the extrinsic region which usually extends to temperatures of  $\sim 500^\circ\text{K}$  for concentrations of  $\sim 5 \times 10^{18}$  carriers/cm<sup>3</sup>.

Studies of the thermoelectric power are not as numerous as the above, and the most comprehensive of those reported to date appear in the Russian literature.<sup>6,7,9-11</sup> It has been shown that the thermoelectric power exhibits most of the characteristics predicted by the theoretical expressions for semiconductors. However, the more detailed analysis presented in references 9 and 10 shows, in the case of PbSe, that there are slight deviations from the usual behavior which have been interpreted on the basis of a temperature-dependent density-of-states effective mass.

In addition to the above investigations, extensive studies of the magnetoresistance in PbTe have been reported by Allgaier,<sup>12,13</sup> in particular, and also by Shogenji<sup>14,15</sup> and Uchiyama.<sup>14</sup> Detailed comparisons of the magnetoresistivity data with the theory for single-band, cubically-symmetric, multivalley models, in which the surfaces of constant energy in k-space are taken to be ellipsoids-of-revolution, indicate that these surfaces are oriented along the  $\langle 111 \rangle$  axes for both n- and p-type PbTe.\* There are therefore either eight or four equivalent ellipsoids of constant energy in each band. The number depends on whether the extrema lie wholly within the Brillouin zone or at the zone boundary. Moreover, Allgaier reports<sup>13</sup> that the mass-anisotropy ratio  $K$  has the values 4.7 at room temperature and 4.2 at 77°K in p-type PbTe. His room temperature data also indicates that  $K$  is 3.6 in n-type PbTe. However, another report states that  $K$  is 4.5 at room temperature and decreases to 3.3 at 77°K in n-type PbTe,<sup>17</sup> but this latter report supports the conclusion that the surfaces of constant energy in the conduction band are oriented along the  $\langle 111 \rangle$  axes. These same authors in another report, in which the oscillatory magnetoresistance was measured at 1.7° and 4.2°K, again show that their data may be interpreted in terms of this energy band model.<sup>18</sup> Furthermore, they conclude that the conduction-band minima occur at the Brillouin zone edge from their findings that there are four equivalent ellipsoids of constant energy in the conduction band.

The energy gap of the lead sulfide group has also been the object of extensive investigation. The early literature on the subject indicated that the forbidden gap in PbTe was roughly 0.6 eV. However, more

---

\* A recent abstract describing the results of piezoresistance and elastoresistance measurements on p-type PbTe concludes that the presence of a second valence band is indicated.<sup>16</sup>

recently it has been established that this early value is too high by a factor of about two. The most extensive investigations have been those reported by Gibson,<sup>19</sup> Avery,<sup>20</sup> and Scanlon.<sup>21</sup> Gibson made optical transmission measurements in the infra-red over a temperature range from 20° to 600°K using samples of thickness ranging between 0.05 and 3 mm. Because of the relatively large thicknesses involved he was restricted in his measurements to regions of low absorption ( $\alpha \sim 10^2 \text{ cm}^{-1}$ ). The principal conclusions of this investigation are well-known and can be summarized as follows:

1. The absorption edge is independent of the free-carrier concentration and is the same for n- and p-type material.
2. The edge shifts to shorter wavelengths as the temperature of the material is increased - a shift which is contrary to that observed in almost all other semiconductors.
3. Below 400°K this shift is linear with temperature and has a value of approximately  $4 \times 10^{-4} \text{ eV}/^\circ\text{C}$ .
4. The absorption at wavelengths greater than that of the absorption edge has been interpreted as free-carrier absorption.
5. Above 400°K the absorption edge wavelength becomes temperature independent.

In the studies made by Avery, many of these conclusions were substantiated, but there were some significant differences. In this latter work, reflections from cleaved surfaces were utilized. As a result of the nature of the experiment, only regions of high absorption ( $\alpha \sim 10^4 \text{ cm}^{-1}$ ) could be investigated so that the data obtained by Gibson and Avery do not overlap. The first three conclusions of Gibson were verified by Avery. (Conclusion #4 was outside of the scope of Avery's work since he was restricted to the short wavelength side of the scope of Avery's work since he was restricted to the short wavelength side of the absorption edge). However, the latter obtained a result which was considerably different from that obtained by Gibson with regard to the temperature behavior of the absorption edge above 400°K (conclusion #5). Instead of observing a decrease in the temperature dependence, Avery observed that the edge moved more rapidly with temperature. An attempt was made to reconcile these two results by assuming that there were two different

energy band excitations involved, but Avery concluded that such an explanation was not wholly satisfactory.<sup>20b</sup> Another possible explanation lies in the instability of the material itself. At elevated temperatures these compounds both decompose and oxidize resulting in irreversible changes in the crystal properties. It could be that such a change has occurred during one of these investigations. Avery has paid considerable attention to the effects of oxidation and conducted his experiments under very closely controlled vacuum conditions so that if this should be the cause of the discrepancy then one might consider that the error is more likely to lie in Gibson's results.

Scanlon was able to perform high resolution optical transmission studies on very small-sized samples with thicknesses ranging from 1 mm down to a few microns. His measurements provide continuous data over the long wavelength absorption edge from absorption coefficients of 50 to  $50,000 \text{ cm}^{-1}$ . Unfortunately, Scanlon's measurements were made at only one temperature ( $\sim 300^\circ\text{K}$ ), and so they cannot settle the variance in the results above  $400^\circ\text{K}$ . However, they do provide a standard for comparison with the data of Avery and Gibson at room temperature. It can be seen that the absorption edge presented by all three are in essential agreement,<sup>22</sup> but the results of Avery and Scanlon are somewhat more similar in that the absorption edge determined by them is sharper than that determined by Gibson.

Along with his data on the absorption edge of the lead sulfide group, Avery presents values for the refractive index at 6 microns. For PbTe he gives the value  $n_o = 5.48 \pm 0.10$ . This compares very well with the value  $n_o = 5.5$  obtained by Moss<sup>23</sup> ( $n_o^2$  gives the relative dielectric constant of the lattice in the absence of any contribution from free carriers). Moreover, Avery observed<sup>20b</sup> that the refractive index of PbS decreased steadily at a rate of  $6 \times 10^{-4}$  per  $^\circ\text{C}$  as the material was heated from 20 to  $300^\circ\text{C}$ . Moss also showed that for PbTe the relation between the refractive index and the wavelength of the absorption edge obeys the equation<sup>23</sup>

$$\frac{n_o}{\lambda_g} = \text{constant}, \quad (1-2)$$

an equation which has been found to have general validity for photoconductive materials of high refractive index. Consequently, it follows directly that

$$\frac{dn_o}{dT} = \frac{n_o}{4E_g} \frac{dE_g}{dT} \quad (1-3)$$

where  $E_g$  is the energy gap in electron volts. From this equation, with information regarding the temperature dependence of the energy gap (at least below 400°K), and with a knowledge of the refractive index  $n_o$  at room temperature, it is possible to calculate its value at other temperatures.

Finally, we turn to the thermal conductivity of the lead sulfide family, and of lead telluride in particular. Here, as in the studies of the thermoelectric power, the most extensive ones are found in the Russian literature. They have reported that this property in PbTe exhibits a very unusual behavior. Their data indicates the presence of a component, other than that due to the lattice and to free carriers, which becomes important even below room temperature (as low as 250°K) and which has the effect of increasing the total thermal conductivity.<sup>24,25</sup> They show that this increase is not attributable to the so-called bipolar thermal conduction, because from Hall coefficient measurements, the samples appear to remain extrinsic to temperatures above 500°K. Moreover, their data indicate that the additional component is independent of the impurity concentration which varied over an order-of-magnitude from  $5 \times 10^{17}$  to  $10^{19}$  carriers/cm<sup>3</sup> and that it is apparently a function of an excitation energy. The conclusion reached by the Russians is that the unusual behavior is caused by transitions to higher energy states of bound hole-electron pairs (excitons) and the subsequent movement of these excitons through the lattice.

However, another report based on the investigations of Kanai and Nii contradicts the above conclusion.<sup>26</sup> In this latter investigation, the thermal diffusivity of several PbTe samples was measured, and after converting the data with the aid of specific heat values, they obtained a thermal conductivity which varies inversely with temperature up to around 500°K where bipolar effects become important and cause the thermal conductivity to increase. They concluded from this behavior that no unusual component, similar to that reported by the Russians, is present. Moreover, a subsequent Russian study of the thermal conductivity of lead selenide indicates that no extra contribution due to excitons is present in that member of the lead sulfide family.<sup>9</sup> All of which leaves the temperature behavior of the thermal conductivity of PbTe, as yet, not completely resolved.

This discussion of the properties of the lead sulfide family, and of PbTe in particular, has been an attempt to present the state of the knowledge which exists with respect to those properties which are measured in this investigation or which are utilized in the subsequent analysis.

## CHAPTER I

### BIBLIOGRAPHY

1. Scanlon, W.W., Polar Semiconductors, a review article in Solid State Physics vol. 9, 83-137, Academic Press (1959).
2. Hutson, A.R., Properties of Some Oxides and Sulfides, Semiconductors A. C.S. Monograph edited by Hannay, N.B., 590-9, Rheinhold Publishing Corp., N.Y. (1958).
3. Putley, E.H., The Hall Effect and Related Phenomena, 223-31, Butterworths Semiconductor Monographs, London (1960).
4. Putley, E.H., The Hall Coefficient, Electrical Conductivity, and Magnetoresistance of PbS, PbSe, and PbTe. Proc. Phys. Soc. of London, B 68, 22-34 (1955).
5. Petritz, R. L. and Scanlon, W.W., Mobility of Electrons and Holes in the Polar Crystal, PbS, Phys. Rev. 97, 6, 1620-6 (1955).
6. Gerstein, E. Z. Savitskaia, T., and Stilbans, L., A Study of the Thermoelectric Properties of PbTe. Sov. Phys. Tech. Phys. 2, 2302-13 (1957).
7. Kolomets, N. V., Stavitskaia, F., and Stilbans, L., A Study of the Thermoelectric Properties of PbSe and PbTe, Sov. Phys. Tech. Phys. 2, 59-66 (1957).
8. Allgaier, R. S. and Scanlon, W. W. Mobility of Electrons and Holes in PbS, PbSe, and PbTe between Room Temperature and 4.2° K, Phys. Rev. 111, 4, 1029-37 (1958).
9. Devyatkova, E. D. and Smirnov, I. A., Thermal Conductivity and the Dependence of the Lorentz Number of PbSe on Temperature and on the Degree of the Electron-Gas Degeneracy, Sov. Phys. Tech. Phys. 2, 1786-92 (Feb. 1961).
10. Smirnov, I. A. Moizhes, B., and Neusberg, E. D., The Effective Carrier Mass in Lead Selenide, Sov. Phys. Tech. Phys. 2, 1793-1804 (Feb. 1961).
11. Putley, E. H., Thermoelectric and Galvanomagnetic Effects in PbSe and PbTe, Proc. Phys. Soc. of London B 68, 35-42 (1955).
12. Allgaier, R. S. Magnetoresistance in PbS, PbSe, and PbTe at 295°<sup>o</sup>, 77.4°<sup>o</sup>, and 4.2°K, Phys. Rev. 112, 3, 828-36 (Nov. 1, 1958).
13. Allgaier, R. S., Weak-Field Magnetoresistance in P-Type PbTe at Room Temperature and at 77°K., Phys. Rev. 119, 2, 554-61 (July 15, 1960).



11. Shogenji, K. and Uchiyama, S., The Galvanomagnetic Effects in Single Crystal of PbTe, J. Phys. Soc. (Japan) 12, 1164 (1957).
15. Shogenji, K., On Galvanomagnetic Effects in P-Type Crystals of PbTe, J. Phys. Soc. (Japan) 14, 1360-71 (1959).
16. Burke, J., Houston, B., and Allgaier, R., Room-Temperature Piezoresistance and Elastoresistance in P-Type PbTe, Bull. Am. Phys. Soc. 6, 136 (March 20, 1961).
17. Ellett, M., Cuff, K., and Kuglin, C., Band Structure and Transport Properties in N-Type PbTe, Bull. Am. Phys. Soc. 6, 18 (Feb. 1, 1961).
18. Kuglin, C., Ellett, M., and Cuff, K., Oscillatory Magnetoresistance in N-Type PbTe, Phys. Rev. Letters 6, 4, 177-9 (Feb. 15, 1961).
19. Gibson, A. F., The Absorption Spectra of Single Crystals of PbS, PbSe and PbTe, Proc. Phys. Soc. (London) B 65, 378-88 (1952).
20. Avery, D. G.
  - (a) The optical Constants of PbS, PbSe, and PbTe in the Region  $0.5-3\mu$  Region of the Spectrum, Proc. Phys. Soc. (London) B 66, 133-40 (1953).
  - (b) Further Measurements on the Optical Studies of PbS, PbSe, and PbTe, Ibid, 67, 2-8 (1954).
21. Scanlon, W. W., Recent Advances in the Optical and Electronic Properties of PbS, PbSe, PbTe and their Alloys, J. Phys. Chem. Solids 8, 423-8 (Jan. 1959).
22. Ref. 2 p. 593.
23. Moss, T. S., Inter-Relation between Optical Constants for Lead Telluride and Silicon, Proc. Phys. Soc. (London) B, 66, 141-4 (1953).
24. Ioffe, A. F., Heat Transfer, Can. J. Phys. 34, 1342 (1956).
25. Deviatkova, E. D., Investigation of the Thermal Conductivity of PbTe, Sov. Phys. Tech. Phys. 2, 414-8 (1957).
26. Kanai, Y. and Nii, R., Experimental Studies on the Thermal Conductivity in Semiconductors, Phys. Chem. Solids 8, 338-9 (Jan. 1958).



## CHAPTER II

### DETERMINATION OF THE CONDUCTIVITY EFFECTIVE MASS

In recent years there have been several hypotheses advanced, and some experimental work presented as support, in an effort to explain the source of the observed temperature dependence ( $\mu_{oc} T^{-5/2}$ ) of the free-carrier mobility in the lead sulfide family. (The dependence predicted theoretically in  $\mu_{oc} T^{-3/2}$  for non-degenerate and  $\mu_{oc} T^{-1}$  for degenerate semiconductors in the presence of acoustical mode lattice scattering.) However, none of these attempts have been wholly satisfactory. Either because of a divergence between theory and experiment or because of a lack of experimental evidence, these efforts have been inadequate. It is with regard to the determination of the reasons behind this behavior of the mobility that we are primarily concerned in this investigation.

Previous analyses of this problem, which has arisen in connections with many semiconductors other than those of the lead sulfide family, can be summarized as follows:

1. A combination of one- and two-phonon scattering processes proposed for lead telluride instead of the usually assumed one-phonon scattering process.<sup>1</sup>
2. A combination of acoustical and optical mode scattering as suggested for lead sulfide,<sup>2</sup> for p-type germanium,<sup>3,4</sup> and n-type indium antimonide.<sup>5</sup>
3. The development of a theory for optical mode scattering which predicts a  $T^{-5/2}$  dependence as derived for diamond structures (e.g. germanium and silicon.)<sup>6</sup>
4. The development of a theory for intervalley scattering in semiconductors with multivalley bands.<sup>7</sup>
5. Consideration of the effect on the mobility of a temperature-dependent effective mass in lead selenide<sup>8</sup> and in germanium.<sup>9</sup>

Of these several choices, very few can be positively disqualified as the explanation for the temperature dependence of the mobility in the lead sulfide group. The intervalley scattering theory can probably be so disqualified because this theory predicts an effect only near and below the

Debye temperature, which for PbTe has been determined to be  $< 140^{\circ}\text{K}$ ,<sup>10</sup> while the  $T^{-5/2}$  dependence has been observed at  $500-600^{\circ}\text{K}$ .<sup>1,2</sup> In addition, the combination of acoustical and optical mode scattering has been applied to lead sulfide with the result that reasonable agreement was achieved at temperatures below the Debye temperature, but theory and experiment diverged at higher temperatures.<sup>2</sup> This may indicate that the theory needs development or that it just does not apply in this case. It is even more difficult to assess a priori the merits of the other choices. Nevertheless, it is still possible to perform a definitive experiment--namely, the determination of the free-carrier effective mass and its temperature dependence. The results of such an experiment may be used directly to verify number five above and indirectly to verify the other possibilities because the effective mass is an unknown parameter in the mobility in every case.

When it is possible to describe a scattering process in terms of a relaxation time ( $\tau$ ), the free-carrier mobility takes the form:

$$\mu = \frac{e\langle\tau\rangle}{m_c} \quad (2-1)$$

where  $e$  is the electronic charge,

$m_c$  is the conductivity effective mass,  
and  $\langle\tau\rangle$  is the relaxation time averaged over all of the free electrons. For the case of acoustical mode lattice scattering, the deformation potential theory yields a mobility of the form:<sup>11</sup>

$$\mu \propto \frac{1}{m_c} m_d^{-3/2} T^{-1} E^{-1/2} \quad (2-2)$$

where  $m_d$  is the density-of-states effective mass,

$T$  is the temperature, and

$E$  is the average thermal energy of the free carriers.

In the non-degenerate case, the average thermal energy is proportional to the temperature, and the mobility has an explicit temperature dependence of

$T^{-3/2}$ . However, an additional temperature dependence can enter through the effective masses.

Finally, we note that while  $m_c = m_d$  for spherical surfaces of constant energy, they take on a more complex form when the surfaces are not spheres at the center of the Brillouin zone but are ellipsoids-of-revolution along a set of symmetry axes of the zone. When such is the case, it is found that:

$$m_d = (m_l m_t^2)^{1/3} \quad (2-3)$$

and

$$\frac{1}{m_c} = \frac{1}{3} \left( \frac{1}{m_l} + \frac{2}{m_t} \right)$$

where  $m_l$  is the value of the effective mass tensor associated with the longitudinal axis of the ellipsoidal energy surface and  $m_t$  is that associated with each of the two transverse axes of the surface.

From Eq. 2-2, one sees that the effective mass plays an important role in the standard mobility theory. Also, it is seen that both the conductivity and the density-of-states effective masses are involved. Consequently, any consideration of the effect of a temperature-dependent effective mass on the mobility should necessarily involve a determination of both of these effective masses. It is because of this very point that a previous analysis of lead selenide is incomplete.<sup>8</sup> That is, in that investigation, only the temperature dependence of the density-of-states effective mass was determined, and so it remains to evaluate the temperature dependence of the conductivity effective mass.

The question that naturally arises is how this temperature dependence may be determined. In the past this determination has posed considerable difficulty. For example, the conductivity effective mass in germanium and silicon has been measured at liquid helium temperature, where the mean free time of free carriers between collisions is sufficiently long, using cyclotron resonance techniques.<sup>12,13</sup> More recently, infra-red techniques

have been employed for this determination. In one instance, the conductivity effective masses in germanium, silicon and indium antimonide were obtained from a combination of reflection and transmission measurements conducted at room temperature.<sup>14</sup> In another instance, only reflection measurements were required, in conjunction with varying intensities of magnetic field, to determine the conductivity effective masses of mercury selenide and indium antimonide (presumably at room temperature).<sup>15</sup>

Cyclotron resonance techniques have so far been inapplicable in the case of PbTe, because the material has not been produced as pure as these techniques require. However, the latter investigations utilizing infra-red techniques offer the key to the answer of how to determine the temperature dependence of the conductivity effective mass, and so we shall consider them more fully.

In the far infra-red, at wavelengths longer than that of the intrinsic absorption edge (see Chapter I, discussion on energy gap), the electromagnetic radiation interacts with the free carriers of the material. The theory of this free carrier dispersion is developed in detail in a recent book by Moss.<sup>16</sup> Through a combined classical and quantum mechanical approach, it is shown that the following relations hold for the real refractive index  $n$  and the absorption index (extinction coefficient)  $k$ :

$$n^2 - k^2 - \epsilon_{\infty} = - \frac{N e^2}{m_c \epsilon_0} \frac{\tau^2}{1 + \omega^2 \tau^2} \quad (2-4)$$

$$2nk\omega = \frac{N e^2}{m_c \epsilon_0} \frac{\tau}{1 + \omega^2 \tau^2} \quad (2-5)$$

where  $\epsilon_{\infty}$  is the relative dielectric constant of the medium in the absence of any contribution from free carriers at very high frequencies,

$N$  is the free carrier concentration,

$\epsilon_0$  is the dielectric constant of free space,

and  $\omega$  is the radial frequency of the radiation.

Several points should be noted with regard to Eqs. 2-4 and 2-5. It is seen that the effective mass that is involved is the conductivity effective mass. This has been shown to be the case for the energy band model in which ellipsoidal surfaces of constant energy lie along rotation axes of the cubic point group (as has been postulated for both the conduction and valence bands in PbTe). Furthermore, the presence of the mean free time ( $\tau$ ), without having averaged with respect to the distribution function, implies that an energy-independent mean free time has been assumed. However, it can be shown, if  $\tau$  depends on the energy raised to a power  $\tau = \tau_0 E^s$  and if the exponent  $s = -1/2$  as in the case of lattice scattering, that the error arising from this assumption is probably no worse than  $\sim 10\%$ .<sup>16</sup> Finally, it should be noted that although an energy-independent  $\tau$  has been assumed, no conditions have been imposed upon the magnitude of the quantity ( $\omega\tau$ ) with respect to unity.

The total dispersion of incident radiation arises from contributions by the lattice as well as by the free carriers. However, at wavelengths beyond the absorption edge (which for PbTe is  $\sim 6$  microns and shorter than the fundamental lattice mode (which for PbTe, whose Debye temperature is approximately 140°K, would be expected to occur near 100 $\mu$ ), only the contribution of the free carriers need be considered. This assumption regarding the dominance of free-carrier dispersion will be discussed in greater detail in Chapter V in conjunction with the analysis of the experimental data. However, it is clear that the validity of such an assumption can be checked by comparing the theoretical expressions 2-4 and 2-5 with the experimental results.

In addition to the above dispersion relations, we have for the reflectivity of the material in the case of normally incident radiation and infinitely thick samples:

$$R = \frac{(n - 1)^2 + k^2}{(n + 1)^2 + k^2} \quad (2-6)$$

and for the transmission in the absence of interference fringes and for  $k^2 \ll n^2$ :

$$T = \frac{(1 - R)^2 e^{-ax}}{1 - R^2 e^{-2ax}} \quad (2-7)$$

Furthermore,  $\alpha$  is related to  $k$  by:

$$\alpha = \frac{4 \pi k}{\lambda} \quad (2-8)$$

Using these relationships, it is possible to understand the procedure followed by Spitzer and Fan in their determination of the conductivity effective mass.<sup>14</sup> Measurement of  $R$  and  $T$  enables one to determine  $\alpha$  from Eq. 2-7 and, consequently,  $k$  from Eq. 2-8. Knowing  $k$  and  $R$ , it is then possible to determine  $n$  from Eq. 2-6. Finally, a knowledge of  $\epsilon_{\infty}$  (obtained from  $R$  in the range of 5-10 $\mu$  where  $k \sim 0$ ),  $n$ ,  $k$ , and  $N$  allows one to calculate  $m_c$  from either Eq. 2-4 or 2-5. In their calculations, Spitzer and Fan utilized Eq. 2-4. Moreover, it was possible to make the approximation  $\omega^2 \tau^2 \gg 1$  so that their results are independent of the energy dependence of the mean free time.

The other method noted above for determining the conductivity effective mass from infra-red reflection in conjunction with a magnetic field utilizes the fact that, in the presence of properly polarized radiation, the magnetic field shifts the minimum in the reflectivity to both sides of the zero-field minimum.<sup>15</sup> That is, one observes a splitting of this zero-field minimum and the appearance of two minima. The displacement of these minima to either side of the zero-field minimum is directly proportional to the cyclotron resonance frequency  $\omega_c = eB/m_c$ . Consequently, in their investigation Lax and Wright determined the shift as a function of magnetic field strength and then determined  $m_c$  from the slope of this dependence.

Both of these procedures have certain experimental drawbacks with respect to the problem at hand, namely, the problem of measuring the temperature dependence of the conductivity effective mass in PbTe. The first procedure requires the measurement of both reflection and transmission data in conjunction with a dewar system. The requirement of a dewar system complicates appreciably the optics of both of these measurements. In addition, for the transmission measurements, samples of a f



microns thickness are required. It is possible to achieve such thicknesses in PbTe only with very careful grinding and polishing techniques, and then it is possible to obtain only very small ( $\sim 600 \times 50 \mu$ ) surface areas so that special optical techniques must be utilized.<sup>17</sup>

On the other hand, the magnetoplasma effect of Lax and Wright requires the combination of optics for reflection measurements, a dewar system, and reasonably high magnetic fields ( $>20$  kilogauss).<sup>15</sup> This is a difficult combination to realize. Moreover, the magnetoplasma effect is most easily obtained in those materials which have a very pronounced minimum in their reflectivity. This is the case, for example, in materials with a free carrier mobility of  $10,000 \text{ cm}^2/\text{volt-sec}$ . The mobility of PbTe certainly satisfies this criterion near liquid nitrogen temperature and below, but around room temperature it has decreased to the order of  $1000 \text{ cm}^2/\text{volt-sec}$ . In addition, at temperatures above liquid nitrogen temperature, the reflectivity minimum in PbTe becomes broader and tends to obscure the shift produced by a magnetic field. This can be seen from the fact that the shift from the zero-field minimum is given by:<sup>15</sup>

$$\Delta\omega = \frac{eB}{2m_t} \frac{K+2}{2K+1} \quad (2-9)$$

If we assume that  $m_t \sim 0.68 m_0$  (where  $m_0$  is the free-electron mass) and that  $K \sim 4.0$ , then we conclude:

$$\Delta\omega = 1.1 \times 10^{11} B \text{ (Kilogauss) rad/sec.}$$

For a maximum field of 25 kilogauss and a minimum reflectivity at  $\sim 27 \mu$ , this shift corresponds roughly to one micron. Such a shift is readily resolved when the minimum is deep, but it is quite difficult to do so for a shallow minimum.\*

---

\* This will become apparent in a later section in which the experimental results are presented, because the magnetoplasma shift was obtained experimentally.

Because of the difficulties outlined above, an alternative procedure has been utilized. It can be seen from the equation for the reflectivity and from the two dispersion Eqs. 2-4 and 2-5 that a family of theoretical reflection curves can be generated which has  $m_c$  as a variable. From this family, that curve and effective mass value can be chosen which best fits the experimental data. This procedure would be tedious to be sure, and it turns out that still another alternative is available for obtaining the conductivity effective mass from infra-red reflection measurements without requiring at the same time either transmission measurements or a magnetic field. This alternative procedure follows from the fact that the general expression for the reflectivity can be differentiated with respect to frequency. The condition of zero slope at the minimum then yields an equation for the effective mass in terms of the frequency of the reflectivity minimum and other measurable parameters. The equation that results is the following:

$$m_c^{*3} - \frac{3\epsilon_\infty - 1}{4\epsilon_\infty [\epsilon_\infty - 1]} \frac{\frac{1}{2} + 5 + 8\rho^2}{(1 + 3\rho^2)} Z m_c^{*2} + \frac{3\epsilon_\infty - 2}{2\epsilon_\infty [\epsilon_\infty - 1]^2} \frac{(1 + 2\rho^2)}{(1 + 3\rho^2)} Z^2 m_c^* + \frac{Z^3}{4\epsilon_\infty [\epsilon_\infty - 1]^2 (1 + 3\rho^2)} = 0$$

(2-10)

where  $m_c^* = m_c/m_0$ ,  $\rho = \omega_0\tau$ ,  $Z = Ne^2/m_c\epsilon_0\omega_0^2$ , and  $\omega_0$  is the frequency of the reflection minimum. (The complete derivation of this equation is contained in Appendix A.

This equation is quite general in that no approximations are made with respect to the magnitude of  $(\omega\tau)$  nor with respect to the magnitude of  $\epsilon_\infty$ .

However, it does contain the implicit assumption that the mean free time is energy independent. This latter is not very serious for three reasons.

- i) It often turns out that  $\rho$  is large with respect to unity so that  $\rho^2$  tends to dominate each factor. Consequently, each of the coefficients tends to be independent of  $\rho$ , except for the last term which is usually a small correction term.
- ii) The energy dependence of lattice scattering is rather small ( $\tau_{oc} E^{-1/2}$ ) and thus differs very slightly from the energy independent case.
- iii) To observe the free carrier reflectivity minimum at convenient wavelengths ( $\sim 30\mu$ ), it is often necessary to utilize free carrier concentrations which result in at least partial, if not total, degeneracy. In the case of total degeneracy,  $\tau$  is independent of energy which corresponds exactly with the assumption in this analysis.

As a check on this theory, the reflection curve for n-type germanium reported by Spitzer and Fan<sup>14</sup> can be considered. The sample investigated by them had a carrier concentration of  $3.9 \times 10^{18}$  electrons/cm<sup>3</sup>,  $\mu_n = 520$  cm<sup>2</sup>/volt-sec.,  $\epsilon_\infty = 16$  and a reflectivity minimum at  $\lambda_0 \approx 23\mu$ . By making an initial estimate for the conductivity effective mass, say  $m_c^* = 0.12$  as determined by cyclotron resonance, one can obtain an initial estimate for  $\rho$ . Using this value of  $\rho$  and the values for  $N$ ,  $\epsilon_\infty$ , and  $\omega_0$  listed above, Eq. 2-10 can be solved for  $m_c^*$ . This enables one to calculate a revised estimate for  $\rho$  and the procedure is repeated until the solution of Eq. 2-10 yields the same value for  $m_c^*$  as before. (This example is carried out in detail in Appendix B.) In actual fact, because  $\rho$  is large with respect to unity and therefore Eq. 2-10 is almost independent of  $\rho$ , this procedure converges very quickly. The value obtained for the conductivity effective mass using this procedure for the above example is  $m_c^* = 0.145$ . This compares very well with the value  $m_c^* = 0.15$  calculated by Spitzer and Fan.

As an additional check on the theory, for example to show that the free carrier dispersion can completely account for the observed reflectivity, a theoretical reflection curve can be generated using the effective mass calculated from Eq. 2-10. When this is done, one finds that the reflectivity curve, reported by Spitzer and Fan for the n-type sample of germanium

considered above, is reproduced as exactly as it is possible to determine the values from their report. (The values calculated to achieve this fit are shown in Figure 2-1.) Moreover, such a precise fit lends additional support to the claim that the assumption of an energy independent mean free time does not seriously affect the results.

Before turning to the investigation of PbTe, it is possible to gain more insight into the general solution presented as Eq. 2-10. For example, the plasma frequency is oftentimes expressed in the simple form :

$$\omega_o^2 = \frac{Ne^2}{m_c \epsilon_c \epsilon_\infty} \quad (2-11)$$

Now, if both  $\rho$  and  $\epsilon_\infty$  are considered to be large with respect to unity and  $Z \sim 1$ , then Eq. 2-10 reduces to the quadratic:

$$m_c^{*2} - \frac{2Z}{\epsilon_\infty} m_c^* + \frac{Z^2}{\epsilon_\infty^2} = 0 \quad (2-12)$$

which has the solution:

$$m_c^* = \frac{Z}{\epsilon_\infty} = \frac{Ne^2}{m_o \epsilon_o \epsilon_\infty \omega_o^2} \quad (2-13)$$

Equations 2-11 and 2-13 are obviously identical. This indicates that the assumptions inherent in the use of Eq. 2-11 are the above, namely  $\rho$  and  $\epsilon_\infty \gg 1$ .

Moreover, if the conductivity effective mass were calculated, for the n-type sample of germanium considered here, by means of Eq. 2-11 instead of Eq. 2-10, the value computed is  $m_c^* = 0.115$ . This value is considerably different from the value  $m_c^* = 0.145$  determined using Eq. 2-10 and from the value  $m_c^* = 0.15$  obtained by Spitzer and Fan. This difference serves as justification for the derivation of the more exact Eq. 2-10.

Finally, it should be noted that oftentimes Eq. 2-10 can be very well approximated by a quadratic equation.

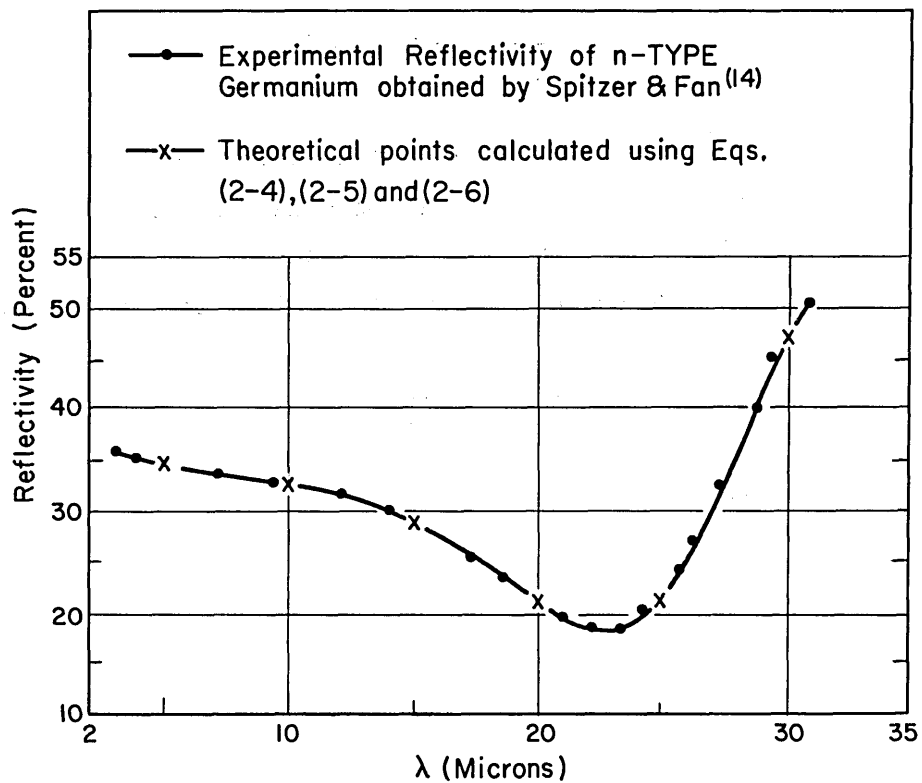


Fig. 2-1 The reflectivity as a function of wavelength for n - type germanium with  $N = 3.9 \times 10^{18}$  electrons/cm<sup>3</sup>. Both the experimental data reported by Spitzer and Fan and theoretical values calculated using an effective mass  $m_c = 0.145m_0$  are shown.

$$\begin{aligned}
 m_c^{*2} - \frac{3\epsilon_\infty - 1}{4\epsilon_\infty [\epsilon_\infty - 1]} \frac{\frac{1}{\rho^2} + 5 + 8\rho^2}{(1 + 3\rho^2)} Z m_c^* \\
 + \frac{3\epsilon_\infty - 2}{2\epsilon_\infty [\epsilon_\infty - 1]^2} \frac{(1 + 2\rho^2)}{(1 + 3\rho^2)} Z^2 = 0
 \end{aligned} \tag{2-14}$$

This equation can be solved directly, with the result that there are apparently two solutions. In actual fact there is only one allowable solution. The root with the plus sign must be chosen, because the root with the minus sign results in a total relative dielectric constant  $\epsilon$

$$\epsilon = n^2 - k^2 = \epsilon_\infty - \frac{Ne^2}{\epsilon_0 m_c} \frac{\tau^2}{1 + \rho^2} \tag{2-15}$$

which is less than unity.

## CHAPTER II

### BIBLIOGRAPHY

1. Gershtein, E., Savitskaia, T., and Stilbans, L., A Study of the Thermoelectric Properties of Lead Telluride, Sov. Phys. Tech. Phys. 2, 2302-13 (1957).
2. Petritz, R. and Scanlon, W., Mobility of Electrons and Holes in the Polar Crystal, PbS, Phys. Rev. 97, 6, 1620-6 (1955).
3. Ehrenreich, H. and Overhauser, A., Scattering of Holes by Phonons in Germanium, Phys. Rev. 104, 2, 331-42 (1956). Lattice Scattering Mobility of Holes in Germanium, *ibid*, 3, 649-59 (1956).
4. Harrison, W., Scattering of Electrons by Lattice Vibrations in Non-Polar Crystals, Phys. Rev. 104, 5, 1281-90 (1956).
5. Ehrenreich, H., Electron Scattering in InSb. J. Phys. Chem. Solids 2, 131-49 (1957).
6. Tolpygo, K. and Fedorchenko, A., The Interaction of an Electron Hole with the Lattice Vibrations in a Homopolar Crystal, Sov. Phys. JETP 4, 5, 713-20 (1957).
7. Herring, C., Transport Properties of a Many-Valley Semiconductor, Bell Sys. Tech. J. 34, 237-90 (1955).
8. Smimov, I., Moizhes, B. and Nensberg, E., The Effective Carrier Mass in Lead Selenide, Sov. Phys. Tech. Phys. 2, 1793-1804 (Feb. 1961).
9. MacFarlane, G., McLean, F., Quarrington, J. and Roberts, V., Fine Structure in the Absorption Edge Spectrum of Ge., Phys. Rev. 108, 1377-83 (1957).
10. Parkinson, D. and Quarrington, J., Molar Heats of Lead Sulfide, Selenide and Telluride, Proc. Phys. Soc. (London) A 67, 569-79 (1954).
11. Shockley, W., Electrons and Holes in Semiconductors - Chap. 11, Van Nostrand (Princeton, N.J., 1950).
12. Dresselhaus, G., Kip, A. and Kittel, C., Cyclotron Resonance of Electrons and Holes in Silicon and Germanium Crystals, Phys. Rev. 98, 368-84 (1955).
13. Dexter, R., Zeiger, H. and Lax, B. Cyclotron Resonance Experiments in Silicon and Germanium, Phys. Rev. 104, 637-44 (1956).

14. Spitzer, W. and Fan, H., Determination of Optical Constants and Carrier Effective Mass of Semiconductors, Phys. Rev. 106, 5, 882-90 (1957).
15. Lax, B. and Wright, G., Magnetoplasma Reflection in Solids, Phys Rev. Letters 4, 1, 16-18 (1960).
16. Moss, T., Optical Properties of Semiconductors, Butterworths Semiconductor Monographs (London 1959).
17. Scanlon, W. W., Recent Advances in the Optical and Electrical Properties of PbS, PbSe, PbTe and their Alloys, J. Phys, Chem. Solids 8, 423-8 (Jan. 1959).



## CHAPTER III

### PREPARATION OF MATERIAL

Several articles have appeared in recent years which discuss, in particular, the growth of lead telluride single crystals,<sup>1,2,3</sup> its phase diagram,<sup>4,5</sup> and dislocations in the grown crystals.<sup>6</sup> The pertinent conclusions of these studies can be summarized as follows:

It is not very difficult to obtain large single crystals of lead telluride by the Bridgman or Stockbarger techniques. However, the presence of oxygen atoms in the melt can have the undesirable effect of bonding to the quartz crucible being lowered through the furnace, thus resulting in either a crack in the crucible or strains and dislocations in the grown crystal. The presence of oxygen can have the additional effect of masking the solubility of excess lead in the grown crystal so as to make it virtually impossible to obtain n-type PbTe in this way.<sup>2</sup> Consequently, reproducible results in the growth of single crystals of lead telluride, which are doped by off-stoichiometric proportions of lead and tellurium, can be obtained only if care is taken to eliminate oxygen from the starting materials. Moreover, the task of growing uniformly doped single crystals using off-stoichiometric proportions of lead and tellurium is further complicated by the fact that the congruent melting temperature ( $\sim 924^{\circ}\text{C}$ )<sup>4</sup> does not coincide with stoichiometric proportions of lead and tellurium. Instead, the congruent melting temperature lies on the tellurium-rich side and corresponds to a concentration which ranges between 50.002<sup>4</sup> and 50.007<sup>5</sup> atomic percent of tellurium. In addition, the maximum solubility limits for this compound occur at about  $775^{\circ}\text{C}$ . where these limits have been determined to be 49.994 to 50.013 atomic percent of tellurium.<sup>5</sup> The implication of this phase diagram is that n-type crystals grown by the Bridgman and Stockbarger techniques will be non-uniformly doped unless care is taken to control the composition of the melt or unless the crystals are later annealed in a lead-rich atmosphere.

The technique of obtaining oxygen-free lead telluride outlined by Lawson<sup>2</sup> has been tried and has been found to be very tedious and not completely satisfactory. Considerable difficulty was encountered in trying to control stoichiometry due to losses of material by vaporization.

An alternative procedure has been followed, and very pure and mirror-like single crystals have been obtained. The basic materials used in this procedure have been commercially available, 99.999 % pure lead and tellurium. The tellurium, just prior to being used, is distilled twice at a temperature of 550-600°C. under a running vacuum of 1-10 microns of mercury. Even though the handbooks state that the sublimation temperature of TeO<sub>2</sub> is approximately equal to the melting temperature of tellurium, it has been observed that this procedure leaves behind a residue which adheres to the Vycor tube holding the material. Moreover, from studies of the electrical properties of the distilled tellurium, it has been concluded that this procedure effects a considerable purification of the starting material.<sup>7</sup> The oxide is removed from the surface of the lead rods by immersing them in concentrated hydrochloric acid for about twenty minutes and then washing them in hot demineralized water to remove the lead chloride. The amounts required for reaction are then weighed out in roughly stoichiometric proportions. This weighing need not be too precise since subsequent steps in this procedure automatically compensate for some degree of imprecision at this point. However, the atomic percent of lead should be between 50 and 51 %. These materials are placed inside a graphite crucible and covered with a snugly fitting graphite cap which has an opening for evacuation that can be plugged with a movable plunger. (See Fig. 3-1 and Reference 8 for additional details of this reaction phase of the procedure).

This crucible is then placed inside a quartz tube and attached to a vacuum system which is pumped down to a pressure of about one micron of mercury and flushed with helium. Then, in an atmosphere of helium of 2-3 lbs./in.<sup>2</sup> above atmospheric pressure, the materials are reacted by means of an induction furnace. The helium gas inhibits the vapor losses of the constituent materials. As exhibited by the very slight condensation of vapors on the wall of the quartz tube, the losses are minimal. This

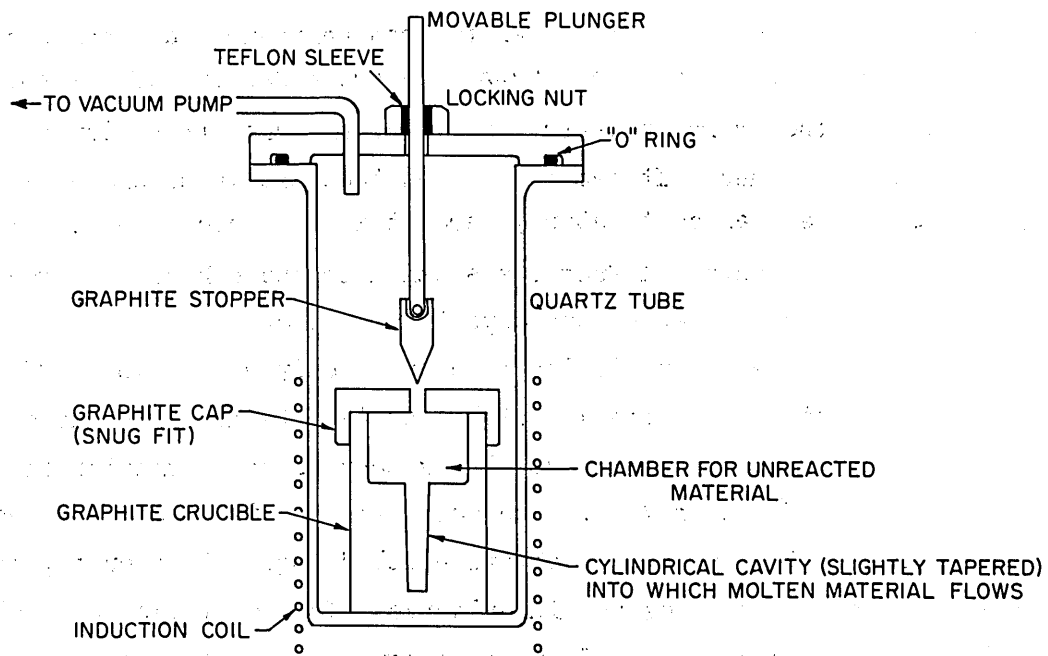


Fig. 3-1 Detail of apparatus used for the reaction of PbTe as developed by Borrego.

reaction phase of the procedure can be accomplished in about one hour, and the composition is not critical as long as there is, if any, a slight excess of lead.

The cast rod of PbTe is removed from the graphite crucible and sealed in a quartz tube under a vacuum of  $10^{-5}$  -  $10^{-6}$  mm of mercury. A crimp is put in this quartz tube which divides it roughly into two equal sections with the rod of PbTe in one of them. The end containing the PbTe rod is placed in a horizontal furnace maintained at approximately  $950^{\circ}\text{C}$ .; the other end of the quartz tube protrudes out of the end of the furnace, and the crimp prevents the molten material from flowing from one section to the other. It has been noted that the vapor pressure of PbTe at  $950^{\circ}\text{C}$ . is several centimeters,<sup>9</sup> and it is sufficient to effect a distillation of the material from one section to the other. However, this distillation requires about two days to complete.

If this latter distillation is carried only about two-thirds of the way to completion, then the material that is obtained from the distillation is invariably p-type, and the resulting carrier concentration is approximately  $3.5 \times 10^{18}$  holes / $\text{cm}^3$ . The material that is obtained is very shiny, and before melting it down to obtain a solid ingot of material, many small crystals with cubic faces are in evidence. This distillation of lead telluride has the effect of further removing oxides and any carbon that may have been introduced in the reaction phase of the process.

This distillate is then removed from the tube and sealed under a vacuum of  $10^{-5}$  -  $10^{-6}$  mm in a quartz crucible together with a small amount of lead shot or distilled tellurium which is required to produce the desired carrier concentration. This crucible is then lowered through a Bridgman or Stockbarger furnace. For the crystals grown for this investigation the lowering rate has been 3-4 mm/hr and the temperature along the length of the furnace changes from approximately  $970^{\circ}$  to  $800^{\circ}\text{C}$  with a gradient of  $15\text{-}20^{\circ}\text{C}/\text{cm}$ . The crystals that are obtained have a very smooth and highly reflective surface and have been determined to be single-crystalline from back reflection x-ray profiles of the surface and cross-section of the ingot. When crystals are prepared in this way, the

crystal never seems to bond to the quartz crucible, and from the smooth, reflective state of the ingot surface, there is apparently a minimum of strain introduced in the crystal itself. If the additional step involving the distillation of PbTe is omitted, then it is necessary to carbonize the inside of the quartz crucible or else to place the material in a graphite crucible inside of a quartz envelope. Both of these methods have been used with the result that large single crystals were also obtained, but the physical appearance of the ingots was considerably inferior to that obtained with distilled material and quartz crucible. The surface of crystals so grown, instead of being smooth and reflective, was dull and oftentimes considerably pock-marked. These characteristics lead one to believe that some carbon has been introduced into the ingot and that the lattice has been strained considerably. (Figure 3-2 shows a photograph of sections of ingots prepared in the ways described above.)

Of course, n-type crystals grown using distilled PbTe still have concentration gradients, often changing from p-type to n-type along the length of the ingot. This is a direct result of the phase diagram and can be rectified only by a long annealing process in the presence of a lead-rich reservoir of lead telluride as outlined in Reference 5. Such an annealing process has been undertaken for samples 2 and 3 of this investigation. These samples were sealed in separate quartz crucibles along with a charge of Pb and PbTe, where the total atomic percent of Pb was roughly 55 %, and each was annealed for 50-60 hours at a temperature of 750°C.

A breakdown of the procedure which was followed in the crystal growth of each of the samples utilized in this investigation is presented in Table 3-1. For the infra-red reflection experiment, the sample size required was 0.80" x 0.20" x 0.10" (length x width x thickness). In obtaining these samples from the single-crystalline ingots, a cubic (100) face was located by x-ray. The ingot was cut along this face with an abrasive wheel at the slow rate of 1 cm/hr. The other faces of the sample were obtained with a combination of 320 grit emery paper, masking tape, and a laboratory sandblaster. This procedure was very slow, but the

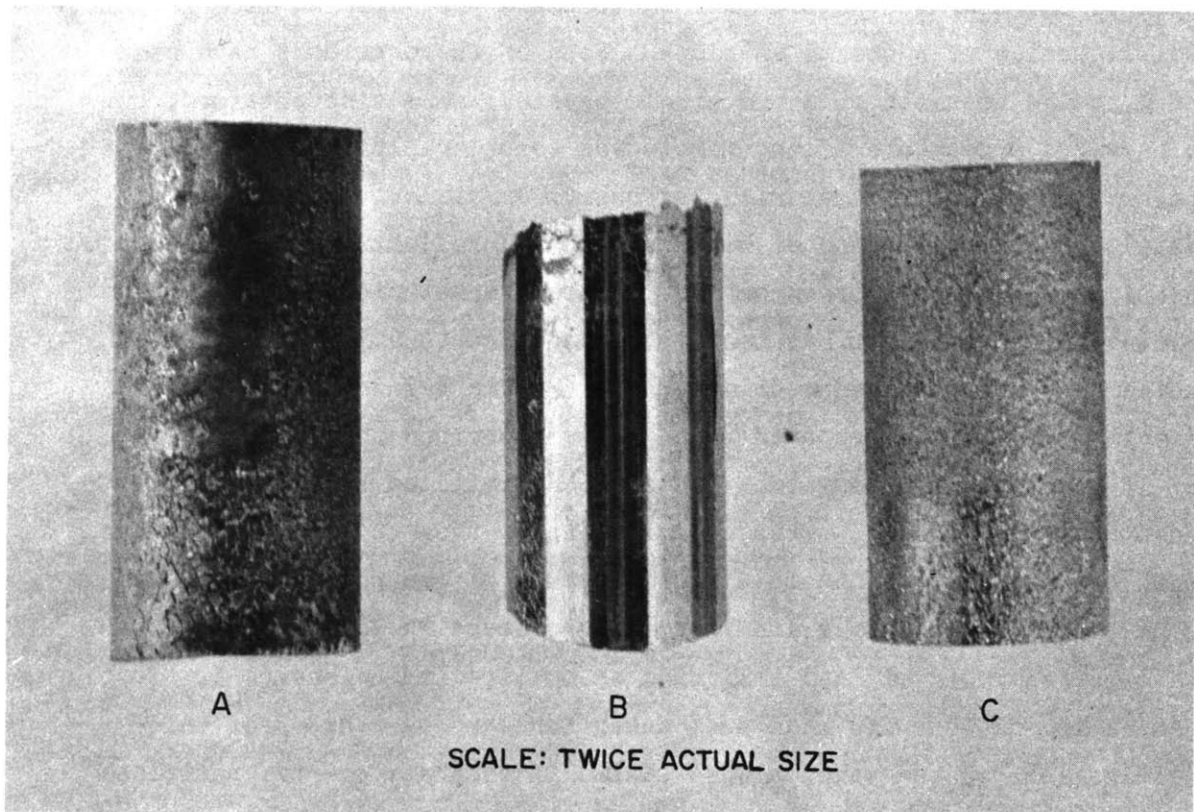


Fig. 3-2 Photograph of sections of single-crystalline Ingots of PbTe grown in a Bridgman - Stockbarger Furnace using the following crucible configurations:

- A. undistilled PbTe in a carbonized quartz crucible
- B. distilled PbTe in a plain quartz crucible
- C. undistilled PbTe in a graphite crucible sealed in a quartz envelope.

results of the cutting wheel were too inconsistent to attempt to use it for cutting thin slices. After the sample was completely shaped, one surface was polished using the following scale of grits: 240, 320, 600, Linde A, and Linde B. The resulting surface was quite reflective with a very slight amount of imperfections and fogging. The final step in the preparation was a polishing etch composed of:<sup>10</sup>

10 parts saturated KOH solution  
10 parts ethylene glycol  
1 part 30 % hydrogen peroxide

This polishing etch is a very mild etch, and it is only useful on a highly polished surface. The samples used in the subsequent measurements were either the same samples used in the infra-red reflection measurements or, as in the case of the Hall and electrical conductivity, were smaller samples cut from the infra-red samples.

The specific details with regard the effects of the sample preparation from crystal growth through the final polishing -- on the electrical and optical properties of the samples used in this investigation will be deferred to Chapter V where they will be included in the analysis of the experimental data.

Sample Number	Type	Material Preparation			Annealing Process		Crystal Orientation for Reflection Data Face Perpendicular to:	
		Distilled PbTe	Undistilled PbTe Carbonized Quartz Crucible	Graphite Crucible	Excess Pb At. %	Time in hrs. at 750° C.	Incident Light	Mag. Field
1	n	no	yes	no	none		100	*
2 <sup>+</sup>	n	no	yes	no	55	50	*	*
3	n	no	no	yes	55	60	100	*
4	p	yes	no	no	none		100	100
5	p	yes	no	no	none		100	100

\* not determined

+ doped with bismuth

Table 3-1: A Breakdown of the Procedures Followed in the Material and Sample Preparation for the Infra-red Study of the Effective Mass



## CHAPTER III

### BIBLIOGRAPHY

1. Lawson, W. D., A Method of Growing Single Crystals of Lead Telluride and Lead Selenide, *J. Appl. Phys.* 22, 12, 1444-7 (Dec. 1951).
2. Lawson, W. D., Oxygen Free Single Crystals of Lead Telluride, Selenide, and Sulfide, *J. Appl. Phys.* 23, 4, 495-6 (April 1952).
3. Lawson, W. D., and Nielson S., Preparation of Single Crystals, a semiconductor monograph, Academic Press (1958).
4. Miller, E., Komarek, K., and Cadoff, I., Stoichiometry of Lead Telluride, *Trans. of Metal. Soc. of A. I. M. A.* 215, 6, 882-9 (Dec. 1959).
5. Brebrick, R. F. and Allgaier, R. S., Composition Limits of Stability of PbTe, *J. Chem. Phys.* 32, 6, 1826-31 (June 1960).
6. Houston, B. B. and Norr, M. K., Dislocation Etch Pits on P-Type Lead Telluride, *J. Appl. Phys.* 31, 3, 615-6 (March 1960).
7. Wedlock, B. and Norton, F., Purification of Tellurium by Distillation, 1961 Conference on Ultra-purification of Semiconductor Materials sponsored by the Electronics Research Directorate of Air Force Cambridge Research Center.
8. Borrego-Larralde, J. M., Doctor of Science Thesis at the Massachusetts Institute of Technology, Cambridge, Mass., pp. 48-50 (Sept. 1961).
9. Brady, E. L., Preparation and Properties of PbTe, *J. Electrochem. Soc.* 101, 9, 466-73 (1954).
10. Lavine, Mrs. M., Lincoln Laboratory, Lincoln, Massachusetts. Private communication.



## CHAPTER IV

### EXPERIMENTAL PROCEDURE AND ESTIMATION OF ERRORS

Before considering the experimental data obtained for these 3n- and 2p-type samples of PbTe, we shall discuss the experimental techniques used to obtain the data and give an estimation of the errors involved.

The thermoelectric power measurement is probably one of the easiest to make. It only requires that a temperature difference be established across the sample. The only additional restriction is that the end contacts are required to be isothermal surfaces for large area electrical contacts. This can be readily achieved by "wetting" the surface of the sample by means of ultra-sonic soldering with Cerroseal solder, and then by soldering the sample into place between the heater and heat-sink. In our experimental set-up the measurements were made with respect to copper. The thermocouples for making temperature measurements were in contact with the soldered junctions so that it is expected that the temperature drops at the interfaces were quite small ( $< 2\%$  of the overall temperature difference). Moreover, it has been possible to remove and re-solder samples into place and to obtain data which is reproducible to  $\sim 2\%$ . Thus, we estimate that the errors involved in this measurement are between 2 - 4%.

For the Hall Effect and electrical conductivity measurements, the sample holder and apparatus used is the same as that discussed in extensive detail in reference 1. Briefly, the method utilized an AC current source and a DC magnetic field. This combination is sufficient to eliminate Peltier effects at the voltage probe contacts and thermo-galvanomagnetic effects at the Hall probes.

The magnet utilized in this investigation was a 6" Varian electromagnet (model V-4007) with a regulated power supply (Varian model V-2200). The gap spacing was 2", and the magnetic field within this gap was observed to be uniform to within 1% up to a radius of 2" from the center of the pole pieces. The magnetic field was calibrated for field strengths between 3 and 7.2 kilogauss by means of a Rawson fluxmeter. This calibration was reproducible within  $\pm 1 - 2\%$ .

It is estimated that the values obtained for  $N$  from the product  $R_{\sigma}$  are determined within the limits of  $\pm 5\%$ .

The infra-red reflectivity measurements were conducted at the National Magnet Laboratory of the Massachusetts Institute of Technology. The experimental set-up used for these measurements was developed by Dr. Dana Dickey of that laboratory. The optics were standard for the most part. An NaCl plate was used to chop the light from a globar source. For dispersing the light beam, a grating ruled with a line density of 1000 lines per inch and "blazed" at  $44.1\mu$  was used. To measure the reflected light intensity a thermocouple detector with a diamond window was employed.

In order to be able to span the wavelength range of interest from 18 to  $40\mu$  without changing the chopper and internal filters, it was necessary to select various combinations of filters to be placed externally in the beam in front of the thermocouple detector. The basis for this selection revolved around the idea that, at a particular orientation of the main dispersion grating, the light transmitted and focused on the sample is actually composed of a fundamental plus higher order harmonics. However, the gratings and filters were such that no signal of wavelength shorter than  $\sim 17\mu$  was present so that for wavelengths of the fundamental up to  $50\mu$  only first and second order harmonics have to be considered. To use the main grating in second order the only modification required was to place a KBr filter in the beam before the detector. Since the transmission characteristic of this filter is to pass 90% of the intensity for wavelengths shorter than  $30\mu$  and to be opaque for wavelengths greater than  $35\mu$ , the main grating can be utilized in the range of fundamental frequencies in the wavelengths between 36 and  $50\mu$  to obtain reflectivities in the wavelength range of 18 to  $25\mu$ . As noted above, for wavelengths of the fundamental greater than  $50\mu$ , third order frequencies can also be passed by the KBr filter in the beam. Consequently, this sets the upper limit of the useful wavelength range for utilizing the main grating in second order.

To use the main grating in first order, it is necessary to consider the amount of second order present in the beam. This becomes a problem as one goes to wavelengths  $> 34\mu$ . In order to utilize the equipment in first order at wavelengths greater than  $34\mu$ , the procedure used has been the following:

Two strips of sooted polyethylene were placed in the beam. These strips have the effect of attenuating significantly wavelengths  $< 20\mu$ . To determine the amount of second order remaining in the beam, after recording the intensities of the incident light and of the light reflected from the sample surface, an NaCl filter was placed in the beam in series with the polyethylene strips. This filter has the characteristic that it is opaque for wavelengths above  $\sim 25\mu$  and passes 90 % of all light intensity for wavelengths  $< 20\mu$ . Thus, in the range  $\lambda > 34\mu$  where second order effects are a problem, this filter removes the first order signal and passes just the contribution made by the second order present in the beam. This second set of recordings then provided the zero reference for the amount of first order signal present in beam. This technique enabled us to extend our useful range, for the existing chopper and filter configuration, out to  $40\mu$ . This long wavelength limit was established by the fact that at that wavelength the second order contribution was beginning to represent a significant contribution ( $\sim 10\%$ ) to the total signal. The short wavelength limit for first-order use of the main grating was established at  $\sim 25\mu$  based solely on the low level of the fundamental signal present at shorter wavelengths. However, since the grating was blazed at  $44.1\mu$ , there is a considerable amount of second order signal at  $22\mu$ .

It should be noted that using the grating in second order has the same effect as slowing down the grating drive motor by a factor of two. That is, for each degree of rotation of the grating, the frequency range scanned in first order is twice that for second order. Consequently, the frequency resolution is better in second order than in first.

The calibration of the grating position as a function of wavelength was conducted in second order because of the increased wavelength sensitivity in that mode. The calibration was obtained by comparing the recorded water-vapor absorption spectrum with that contained in a Perkin-Elmer instruction manual. It was possible to achieve sufficient resolution to calibrate the grating position to an accuracy of better than  $0.1\mu$  which represents a fraction of one percent at these wavelengths.

The overall accuracy ascribed to the determination of the conductivity effective mass from the position of the reflectivity minimum is estimated as

follows: The position of the minimum is determined by  $N$ ,  $\epsilon_{\infty}$ ,  $\mu$ , the resolution and calibration of the instrument, and by the broadness of the minimum itself. We neglect any error arising from the free carrier mobility,  $\mu$ . It is shown in the next chapter that a large change in  $\mu$  is required to produce a noticeable shift in the minimum, and we shall assume that our determination of  $\mu$  is accurate to  $\pm 5\%$ . Therefore, to a first approximation we may consider that the effective mass is given by Eq. 2-11 which is rewritten below:

$$m_c = \frac{Ne^2 \lambda_0^2}{4\pi^2 c^2 \epsilon_0 \epsilon_{\infty}} \quad (4-1)$$

where  $c$  is the velocity of light,  $\lambda_0$  is the wavelength of the reflectivity minimum as before and the other symbols are also unchanged.

We have already estimated that  $N$  is probably determined to an accuracy of  $\pm 5\%$ . The parameter  $\epsilon_{\infty}$  is determined as a function of temperature by means of Eq. 1-2 which states

$$\epsilon_{\infty}^2 E_g = \text{constant} \quad (4-2)$$

This relation has been shown to be valid specifically for the case of PbTe by Moss<sup>2</sup>. At room temperature the value of  $\epsilon_{\infty}$  has been established to be  $\epsilon_{\infty} = 30 \pm 3\%$ . This establishes the limit of error imposed upon the absolute values of  $m_c$  at room temperature. However, for other temperatures, it is assumed that changes in  $\epsilon_{\infty}$  are correct to within  $\pm 10\%$  of the change predicted by Eq. 4-2. This amounts to a rather small percentage error in relative magnitudes of effective masses at different temperatures. As it will be shown later, the total change in  $\epsilon_{\infty}$  between 300°K and 4°K is 8 units (from 30 to 38.2). Thus the error introduced by  $\epsilon_{\infty}$  in the temperature dependence of  $m_c$  is assumed to be less than  $3\%$ .

Finally, we note that  $m_c$  is a function of  $\lambda_0^2$ . We have estimated that a negligible error is introduced in  $\lambda_0$  through the calibration of the main grating. However, there still remains an uncertainty in  $\lambda_0$  due to the broadness of the reflectivity minima. These minima are sharpest at the lowest

temperatures where the error ascribed to  $\epsilon_{\infty}$  is expected to be a maximum. Thus, the errors due to these two parameters tend somewhat to offset one another. The actual uncertainty in  $\lambda_0$  is estimated to be less than  $\pm 0.5\mu$  at room temperature and less than  $\pm 0.2\mu$  at  $4^{\circ}\text{K}$ . At room temperature, this represents an error in  $\lambda_0^2$  of 3 % (for  $\lambda_0 = 3\text{-}\mu$ .)

All told, therefore, we estimate that the errors involved in the determination of  $m_c$  are on the order of  $\pm 10\%$ .

Finally, we consider the measurement of the thermal conductivity. A steady-state, longitudinal heat flow method has been used. The basic concepts are elementary, involving no more than a resistance heater in physical contact with one end of the sample, a heat sink in contact with the other end and thermocouples for measuring the temperature difference between the two ends. However, in actual practice there are many details which must be attended to if one hopes to obtain reproducible and reliable data. We will enumerate a few of these:

1. The end contacts are very important and especially so since the temperatures are monitored outside of the sample. Good thermal contacts have been achieved in this investigation by "wetting" the sample ends with Cerroseal solder by means of ultrasonic soldering. The sample is then soldered into place between the heat source and heat sink.
2. The sample heater can be a source of difficulty if the region of joule heating is in close proximity to the sample-to-heater interface. Such a configuration can lead to a non-uniform heat flow across this boundary. Thus, it has been found helpful to have the joule heating take place in a region about one-half inch above this interface, with a piece of solid copper filling the intervening region to allow the heat flow to distribute itself uniformly.
3. It is imperative that all leads (i.e., thermocouple, voltage, and current leads) leaving the system be completely thermally grounded to the heat sink so as to provide a reproducible temperature gradient along the leads. This has been provided for in these measurements by silver-soldering a  $\frac{1}{4}$ "- diameter copper rod to the baseplate around which each lead has been

wrapped a minimum of ten turns. (The wires themselves had a fine enamel coating to provide electrical insulation from the rod.)

4. In order to reproduce the same environmental conditions each time and also to eliminate conductive heat losses through the surrounding medium, it has been necessary to evacuate the sample holder. We have maintained a vacuum of 1-5 $\mu$  in the system during all measurements. A schematic of the apparatus and a detail of the sample holder used in this investigation are shown in Figs. 4-1 and 4-2.

In addition to putting the system together reproducibly, it is necessary to calibrate the heat losses for the system when no sample is in place. This has been done both before the series of measurements and following these measurements, with the result that the calibration did not differ by more than 1 % between these two calibration runs.

In addition to the calibration, another potential source of error is the heat lost by radiation from the sample surface. This can be evaluated in the following manner: Heat radiated from a surface obeys the standard Stefan-Boltzmann Law of Radiation, namely

$$P = \sigma_s A(T^4 - T_o^4) \quad (4-1)$$

where P is the rate at which thermal energy radiates from the surface, A is the radiating surface area which is at a temperature T and which radiates into an environmental temperature  $T_o$ , and  $\sigma_s$  is the Stefan-Boltzmann radiative constant =  $5.67 \times 10^{-12}$  watts/cm<sup>2</sup>C<sup>4</sup>. Moreover, it has been assumed that the surface is a black-body (i.e., that the surface emissivity is unity). This represents the absolute maximum that such a surface can radiate. In order to calculate this maximum amount of heat lost through the surface, we note the following: for small  $\Delta T = T - T_o$ , the factor in parenthesis can be approximated by  $(T^4 - T_o^4) \approx T^3 (\Delta T)$ ; the sample size used in this investigation was typically a cube whose dimension is 0.50 cm; finally, a reasonable approximation is to assume that the temperature gradient is linear along the sample so that the average temperature difference between the sample surface and the environment is  $\Delta T/2$ . From



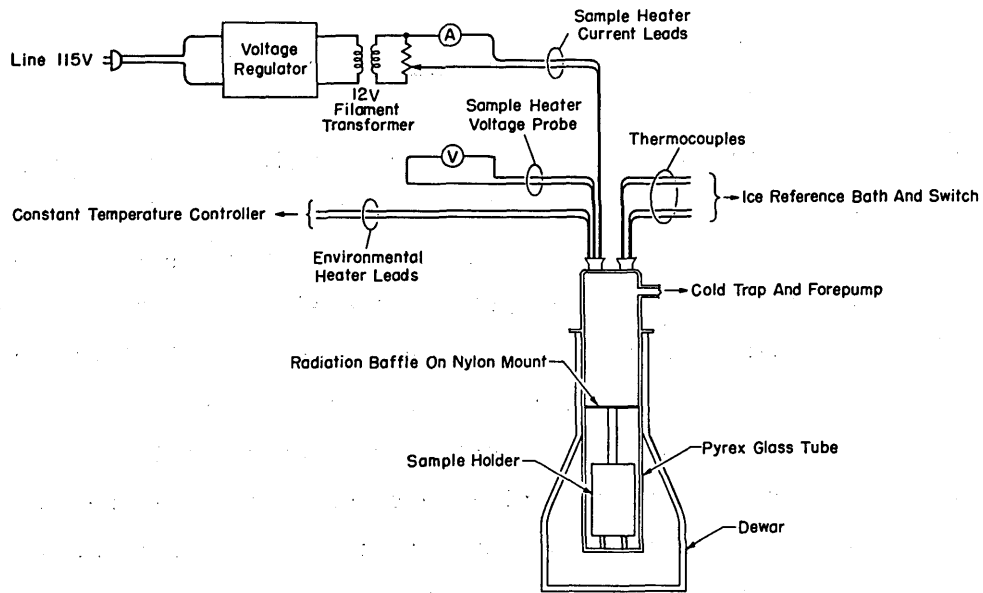


Fig. 4-1 Schematic of the thermal conductivity measuring apparatus.

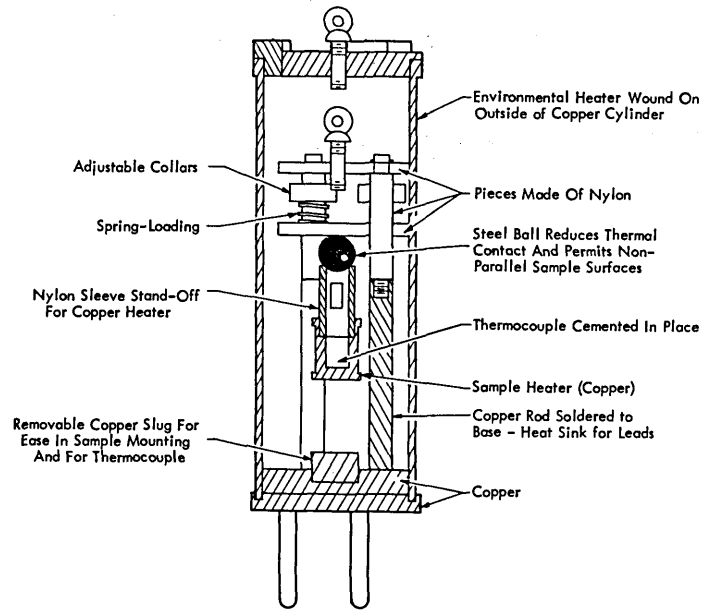


Fig. 4-2 Detail of sample holder for thermal conductivity measurements.

Eq. 4-1 we calculate

$$\frac{P}{\Delta T} = 0.15 \text{ milliwatts}/^{\circ}\text{C}$$

for  $T = 300^{\circ}\text{K}$ . The thermal power which flows longitudinally through the sample can be calculated to be  $10 \text{ mw}/^{\circ}\text{C}$  (for  $\kappa = 20 \text{ mw}/\text{cm}^{\circ}\text{C}$ ). This indicates that the radiation heat losses through the sample surface, which are a maximum at  $300^{\circ}\text{K}$  for this investigation, are still  $< 1.5 \%$  of the total thermal power passing through the sample. Moreover, it should be noted that a neglect of the heat losses from the sample surface gives rise to an increase in the apparent thermal conductivity of the material. Thus, if anything, the neglect of this radiative heat loss has the effect of producing a  $\kappa$  which apparently has an additional component. However, we shall see that the temperature dependence which is obtained does not indicate this at all.

In order to check the thermal contact between the sample and the heat source and heat sink the thermoelectric power of the samples has been measured as a function of temperature in this same experimental set-up. The values obtained for the thermoelectric power check within  $\pm 3 \%$  with those obtained from the independent measurement of this parameter.

Based on these considerations, we estimate that the limits of error for this measurement are approximately  $\pm 5 \%$ .

## CHAPTER IV

### BIBLIOGRAPHY

1. Nelson, R., Preparation and Electronic Transport Properties of Mercury Telluride, p. 28-37, Doctor of Science thesis at the Massachusetts Institute of Technology, Cambridge, Mass. (June, 1961).
2. Moss, T. S., Inter-Relation between Optical Constants for Lead Telluride and Silicon, Proc. Phys. Soc. (London) B, 66, 141-4 (1953).



## Chapter V

### EXPERIMENTAL RESULTS AND ANALYSIS

The thermoelectric power for each of the five samples (3n-type and 2p-type) has been determined between 77°K and 300°K, and the results are shown in Fig. 5-1. This data has been interpreted by means of the theoretical expression for the thermoelectric power, which is applicable for Fermi-Dirac statistics, ellipsoidal energy surfaces and extrinsic conduction, namely<sup>1</sup>

$$Q = \pm \frac{k}{e} \left[ \frac{(5/2 + s) F_{3/2 + s}}{(3/2 + s) F_{1/2 + s}} \right] \dots \eta \quad (5-1)$$

where  $s$  is characteristic of the scattering mechanism and is the exponent of the kinetic energy in the mean free time  $\tau = \tau_0 E^s$ ,  $\eta$  is the reduced Fermi potential ( $E_f/kT$ ) and  $F_r$  is a Fermi-Dirac integral of the form

$$F_r(\eta) = \int_0^\infty \xi^r f_0(\xi, \eta) d\xi$$

in which  $\xi$  is the reduced kinetic energy of the free carriers ( $E/kT$ ), and  $f_0$  is the Fermi distribution function

$$f_0(\xi, \eta) = \frac{1}{1 + e^{(\xi - \eta)}}$$

The value to be assigned to  $s$  in Eq. 5-1 is a little uncertain. However, there is some basis for assuming that acoustical mode lattice scattering predominates above 100°K, and therefore  $s = -1/2$ . (The discussion of this topic has been deferred to this point in order to place in sharper focus the effect of this parameter on the subsequent analysis.) Probably the most direct method for evaluating this energy dependence is through the determination of the Nernst-Ettingshausen effect. A very detailed investigation of this effect in all three members of the PbS family has been reported in the literature.<sup>2</sup> Briefly, this analysis utilized measurements of the longitudinal and transverse Nernst-Ettingshausen electric fields which for the case of weak magnetic fields, isothermal conditions ( $dT/dy = dT/dz = 0$ ) and extrinsic conduction have been expressed in the form:

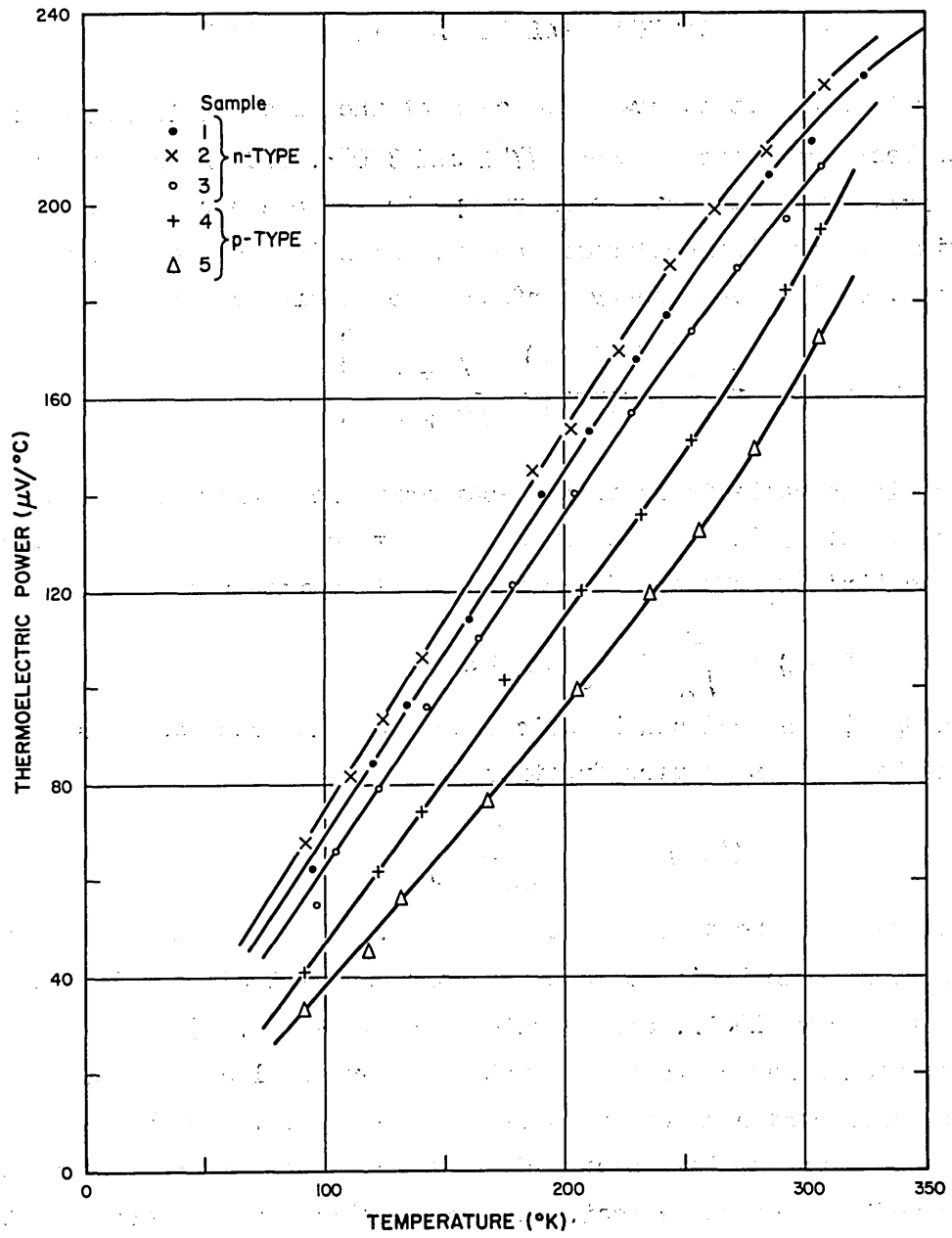


Fig. 5-1 Thermoelectric power of 3 n- and 2 p- type samples from 77° to 300°K.

$$E_y = s a_s \frac{k}{e} \mu B \frac{dT}{dx} \quad (5-2)$$

and

$$E_x = 2s \left( b_s - \frac{a_s^2}{2} \right) \frac{k}{e} (\mu B)^2 \frac{dT}{dx} \quad (5-3)$$

where  $E_y$  and  $E_x$  are the electric fields developed along the x and y axes, the temperature gradient is along the x-axis, the magnetic field  $B$  is along the z-axis, and  $a_s$  and  $b_s$  are constants depending only on  $s$  and are of the order of unity. By defining a non-dimensional field  $F_i = E_i / \frac{k}{e} \frac{dT}{dx}$  it is possible to obtain a ratio from Eqs. 5-2 and 5-3 which is wholly a function of  $s$ , namely

$$\frac{F_y}{F_x} = \frac{s a_s^2}{2b_s - a_s^2} \quad (5-4)$$

Equation 5-4 was evaluated for various values of  $s$  from  $-1/2$  to  $+3/2$  with the result that the function is positive for  $s < 0$ , negative for  $s > 0$ , and zero for  $s=0$ . In all, the Nernst-Ettingshausen effect was measured in seven samples, three of which were PbTe. In every case the ratio  $F_y^2 / F_x$  was negative and indicated a value of  $s$  somewhere in the range  $-1/2 < s < 0$ . Since the choices considered were scattering by: the acoustical modes of a covalent lattice for which  $s = -1/2$ , the vibrational modes of an ionic lattice above the Debye temperature ( $\theta \approx 130^\circ\text{K}$  for PbTe) for which  $s = +1/2$ , or ionized impurities for which  $s = +3/2$ , the conclusion reached in the above analysis was that lattice bonding must be predominately covalent (as opposed to ionic) and that the scattering is dominated by the acoustical modes of the lattice.

Moreover, this same conclusion was reached in an analysis in which the Lorentz number in the Wiedemann-Franz law for free carrier thermal conductivity was determined in PbSe.<sup>3</sup> The same result has also been inferred from studies of the thermoelectric power of PbTe.<sup>4</sup>

Probably the most significant feature of the investigations into the scattering mechanism is that none have supported any other hypothesis except that  $s = -1/2$ . Consequently, this is the value of  $s$  that is used in the subsequent analysis.

Equation 5-1 has been evaluated with the aid of a table of Fermi-Dirac functions<sup>5</sup> for  $\eta$  in the range -0.3 to 4.0. For calculations involving  $\eta > 4$ , a simplified relation which is appropriate for strongly degenerate material has been utilized,<sup>6</sup>

$$Q = \frac{\pi^2}{3} \frac{k}{e} \frac{(3/2 + s)}{\eta} \quad (5-5)$$

Moreover, for these latter calculations, a small correction factor (1.04) was used to make the values of Eqs. 5-1 and 5-5 coincide for  $\eta = 4$ . By comparing the calculated values ( $Q_{calc}$ ) with those determined experimentally ( $Q_{exp}$ ), it is possible to determine the temperature dependence of  $\eta$  in each of the five samples. The results of these calculations are presented in Table 5-1.

Having thus determined the value of  $\eta$  for each of the five samples over the range  $80^\circ < T < 300^\circ K$ , it is possible to obtain the temperature dependence of the kinetic energy factor in the mean free time. For the assumed acoustical mode lattice scattering,  $\tau = \tau_0 E^{-1/2}$ . Hence, it follows that

$$\langle \tau \rangle = \tau_0 \langle E^{-1/2} \rangle = \tau_0 (kT)^{-1/2} \frac{\int_0^\infty f_0 d\xi}{\int_0^\infty \xi^{1/2} f_0 d\xi} = \tau_0 (kT)^{-1/2} \frac{F_0}{F_{1/2}} \quad (5-6)$$

Equation 5-6 has been evaluated for  $0 \leq \eta \leq 4$  and the results are shown in Fig. 5-2. In particular, the following points are noted:

- i) The contribution of the energy dependence of the mean free time to the temperature dependence of the free carrier mobility, for  $T < 300^\circ K$ , is something weaker than the non-degenerate limit of  $T^{-1/2}$  (for the free carrier concentrations considered here). In fact, for these samples, below  $100^\circ K$  for the n-type and below  $150^\circ K$  for the p-type, the energy dependent factor contributes nothing to this over-all temperature dependence.



$\eta$	Q calc ( $\mu$ volt/ $^{\circ}$ C)	Temperature at which Q exp. = Q calc. ( $^{\circ}$ K)				
		T <sub>1</sub>	T <sub>2</sub>	T <sub>3</sub>	T <sub>4</sub>	T <sub>5</sub>
7.5	37					96
6.5	43				92	107
5.5	50				103	119
5.0	55			88	110	128
4.5	61	87	82	96	119	138
4.0	68	98	91	107	131	152
3.5	75	107	100	117	141	164
3.0	86	122	114	132	157	182
2.5	98	138	130	148	174	202
2.0	112	156	147	167	195	225
1.5	130	180	170	192	222	253
1.0	151	208	197	220	253	281
0.5	176	241	229	256	285	310
0.0	205	283	272	302	319	
-0.2	219	308	296	327		
-0.3	225	321	308			

Table 5-1, The temperature dependence of the reduced Fermi potential of samples 1-5 obtained from an analysis of the thermoelectric power data of Fig. 5-1 using Eqs. 5-1 and 5-5.

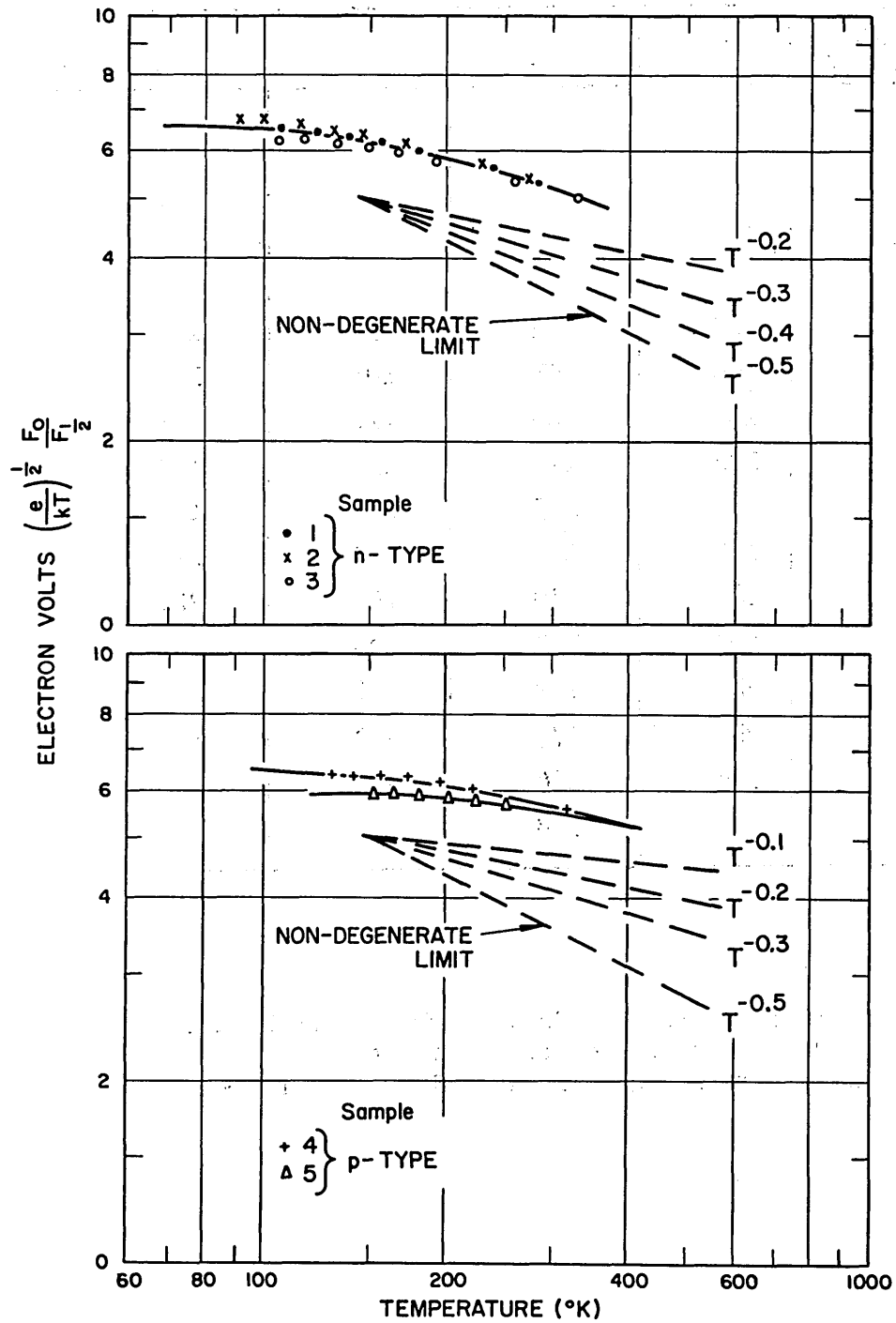


Fig. 5-2 The temperature dependence of  $\langle E^{-1/2} \rangle$ , which is the kinetic energy factor in the mean free time associated with acoustical mode lattice scattering and which is averaged over all of the free carriers.

- ii) At 300°K, the contribution to the temperature dependence of the mobility is approximated by  $T^{-0.3}$  for these n-type samples and  $T^{-0.2}$  for the p-type.
- iii) Finally, the lack of any temperature dependence at the low temperatures indicates that the material can be considered to be completely degenerate in that range. This implies that the actual energy dependence of the mean free time decreases in importance since the free carrier kinetic energy is essentially a constant for total degeneracy. Because of this last result, the assumption of an energy independent mean free time in the differentiation of the reflectivity equation should be a valid approximation.

The free carrier concentration has been obtained from Hall measurements by utilizing Eq. 1-1, namely

$$R = \frac{b}{N_e} \left[ \frac{3K(K+2)}{(2K+1)^2} \right] \quad (5-7)$$

And, in the light of the analysis above, it is reasonable to conclude that at 77°K, the numerical factor  $b$  is unity, corresponding to total degeneracy. The term in brackets can be evaluated using values for  $K$  which are reported in the literature (see discussion in Chapter I). In connection with this it should be noted that the term in brackets is very nearly equal to 0.9 for  $K$  between 3 and 6, a range of  $K$  which includes all values so far reported for both p- and n-type material at 77°K. Consequently, this term in Eq. 5-7 has been approximated by the value 0.9 for both p- and n-type material. The results of the analysis of the Hall data are presented in Table 5-2.

Sample #	Type	Free Carrier Concentration
1	n	$2.9 \times 10^{18}$
2	n	2.2
3	n	3.8
4	p	3.3
5	p	3.6

Table 5-2. Results from the analysis of the Hall data using Eq. 5-7.

Moreover, Hall measurements were made at 300°K and they differed only slightly from the values obtained at 77°K. In no case was this difference as much as 15% which can readily be accounted for by changes in  $b$  and in the bracketed

term of Eq. 5-7. For example, the non-degenerate limit for  $b$  is  $3\pi/8 = 1.18$  as compared with the value of unity for full degeneracy. Because of these results, which agree qualitatively with the reports in the literature, we conclude that the free carrier concentration in all five samples remains constant up to  $300^\circ\text{K}$ . Having established the free carrier concentration and the temperature dependence of  $\eta$ , it is possible to calculate a value for the density-of-states effective mass. This can be obtained from the relation:

$$m_d^* = \frac{m_d}{m_0} = \left( \frac{N}{4\pi} \right)^{2/3} \left( \frac{h^2}{2m_0 kT} \right) \left[ F_{1/2}(\eta) \right]^{-2/3} \quad (5-8)$$

The results of this calculation are presented in Figs. 5-3 and 5-4. The data show that  $m_d^*$  has a very definite temperature dependence. This is in qualitative agreement with findings in PbSe<sup>7</sup> and in PbTe<sup>8</sup> but contrary to those of another report for PbTe.<sup>9</sup> At temperatures near  $100^\circ\text{K}$ , the apparent temperature dependence is very slight. However, at  $300^\circ\text{K}$  for n-type material  $m_{dn}^* \propto T^{1/2}$ , and for p-type this dependence is slightly greater  $m_{dp}^* \propto T^{3/5}$ . Moreover, at  $77^\circ\text{K}$  we note that  $m_{dp}^* < m_{dn}^*$  while at  $300^\circ\text{K}$  they are approximately equal. Again this is contrary to the findings in a recent report<sup>9</sup> which asserts that  $m_{dp}^* > m_{dn}^*$  for all temperatures below  $300^\circ\text{K}$ . However, it does agree with the relationship between  $m_{dp}^*$  and  $m_{dn}^*$  deduced in an earlier report for PbS where the values  $m_{dp}^* = 0.1$  and  $m_{dn}^* = 0.22$  were obtained near  $100^\circ\text{K}$ .<sup>10</sup> Finally, it is noted that the absolute values obtained here are in substantial agreement with those presented in the literature for PbTe (eg.  $m_{dn}^* = 0.25$  at  $300^\circ\text{K}$ ,<sup>8</sup>  $m_{dn}^* = 0.15$  at  $77^\circ\text{K}$ ,<sup>8</sup> and  $m_d^* = 0.16$  at  $77^\circ\text{K}$ ,<sup>11</sup>).

The free carrier mobility has been determined between  $77^\circ\text{K}$  and  $300^\circ\text{K}$ . For this determination, the electrical conductivity was measured over the above temperature range. Noting that, for an extrinsic conductor, this parameter may be represented by the formula

$$\sigma = Ne\mu \quad (5-9)$$

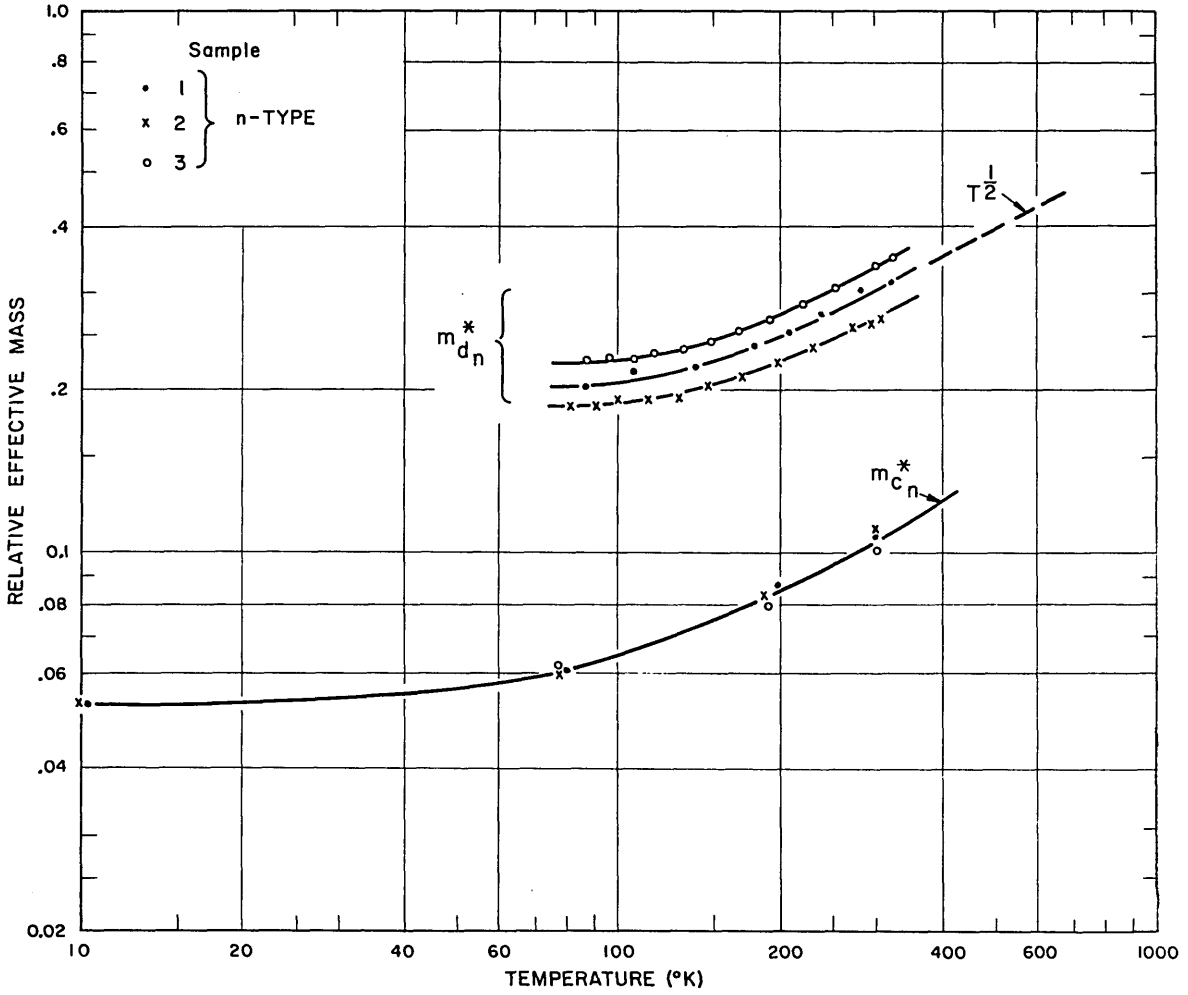


Fig. 5-3 The density-of-states and conductivity effective masses for 3 n-type samples of PbTe.  $m_d^*$  is calculated from Eq. 5-8 and  $m_c^*$  from Eq. 2-10.

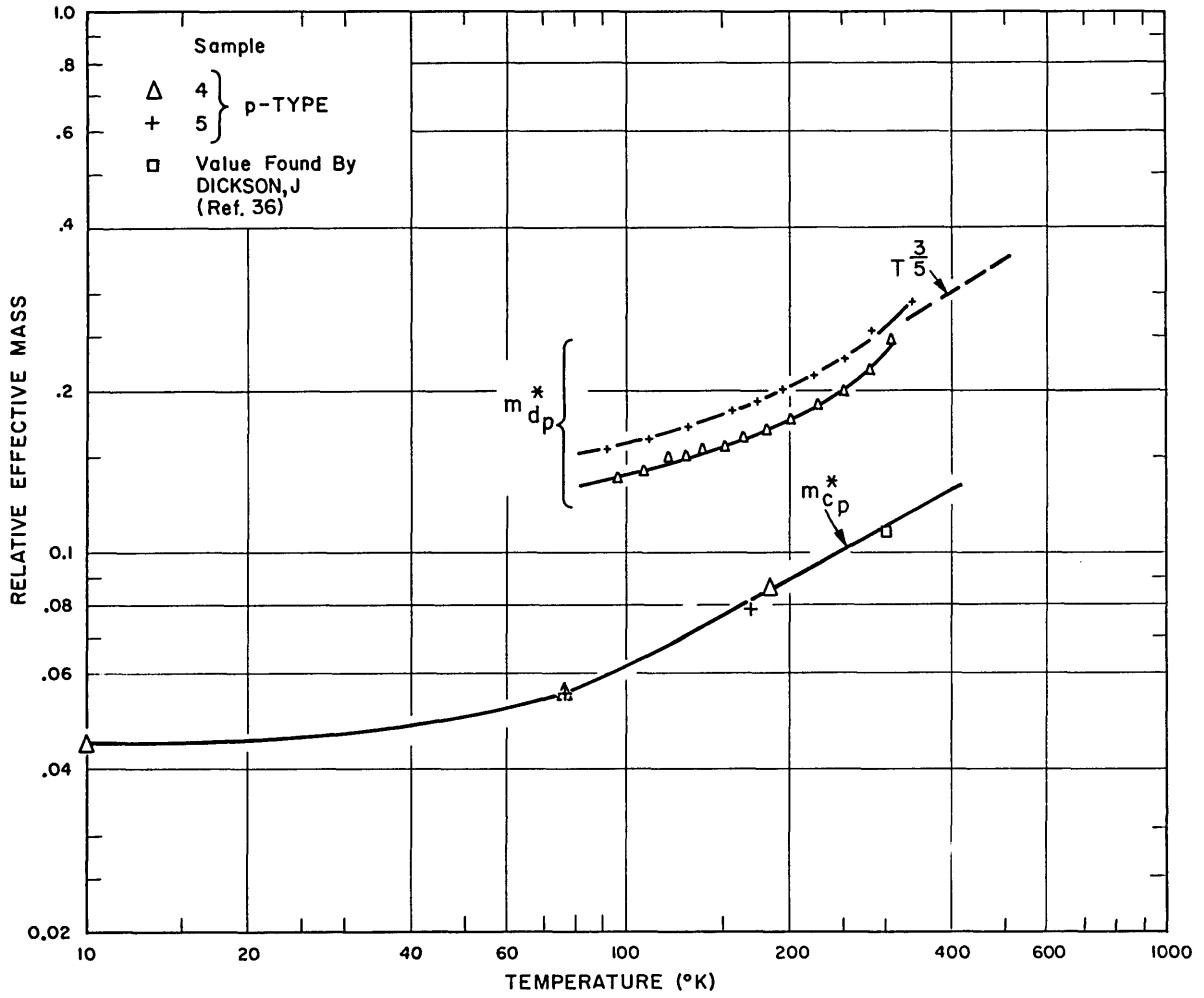


Fig. 5-4 The density-of-states and conductivity effective masses for 2 p-type samples of PbTe.  $m_d^*$  is calculated from Eq. 5-8 and  $m_c^*$  from Eq. 2-10.

it follows directly from Eqs. 5-9 and 5-7 that the mobility may be calculated from the relation:

$$\mu = R_{77^{\circ}\text{K}} \sigma \frac{(2K + 1)^2}{3K(K + 2)} \quad (5-10)$$

The mobility values determined using Eq. 5-10 are shown in Fig. 5-5.

The infra-red reflectivity data are grouped under three separate headings because the analysis of the data naturally divides itself in this way. The three subdivisions are: i) zero-field reflectivity of n-type PbTe, ii) zero-field reflectivity of p-type PbTe and iii) magnetoplasma effects. We will consider each of these in the above order.

The (zero-field) reflectivity of the n-type samples is presented in Figs. 5-6, 5-7 and 5-8. The qualitative features that are readily apparent are the following:

- i) The reflectivity does exhibit a minimum in this range of wavelengths which, however, becomes broader and more shallow as the temperature increases.
- ii) The position of the minimum varies with the free-carrier concentration.
- iii) The position of the minimum has a distinct temperature dependence - moving to longer wavelengths as the temperature is increased.

For obtaining the conductivity effective mass from these curves, the wavelength of the minimum reflectivity has been obtained by visual inspection of the data. In addition, it has been necessary to make certain assumptions with regard to  $\epsilon_{\infty}$ , which is the relative dielectric constant of the lattice in the absence of any free carrier contribution at very high frequencies. It has been reliably established that  $\epsilon_{\infty} = 30$  at  $300^{\circ}\text{K}$ .<sup>12</sup> For obtaining the value of  $\epsilon_{\infty}$  at other temperatures, we have utilized the relationship<sup>12</sup>

$$n_o^4 E_g = \text{constant} \quad (5-11)$$

and the values for the energy gap  $E_g$  reported by Avery<sup>13</sup> and by Gibson.<sup>14</sup> (In this temperature range their results are in agreement.) The values obtained from

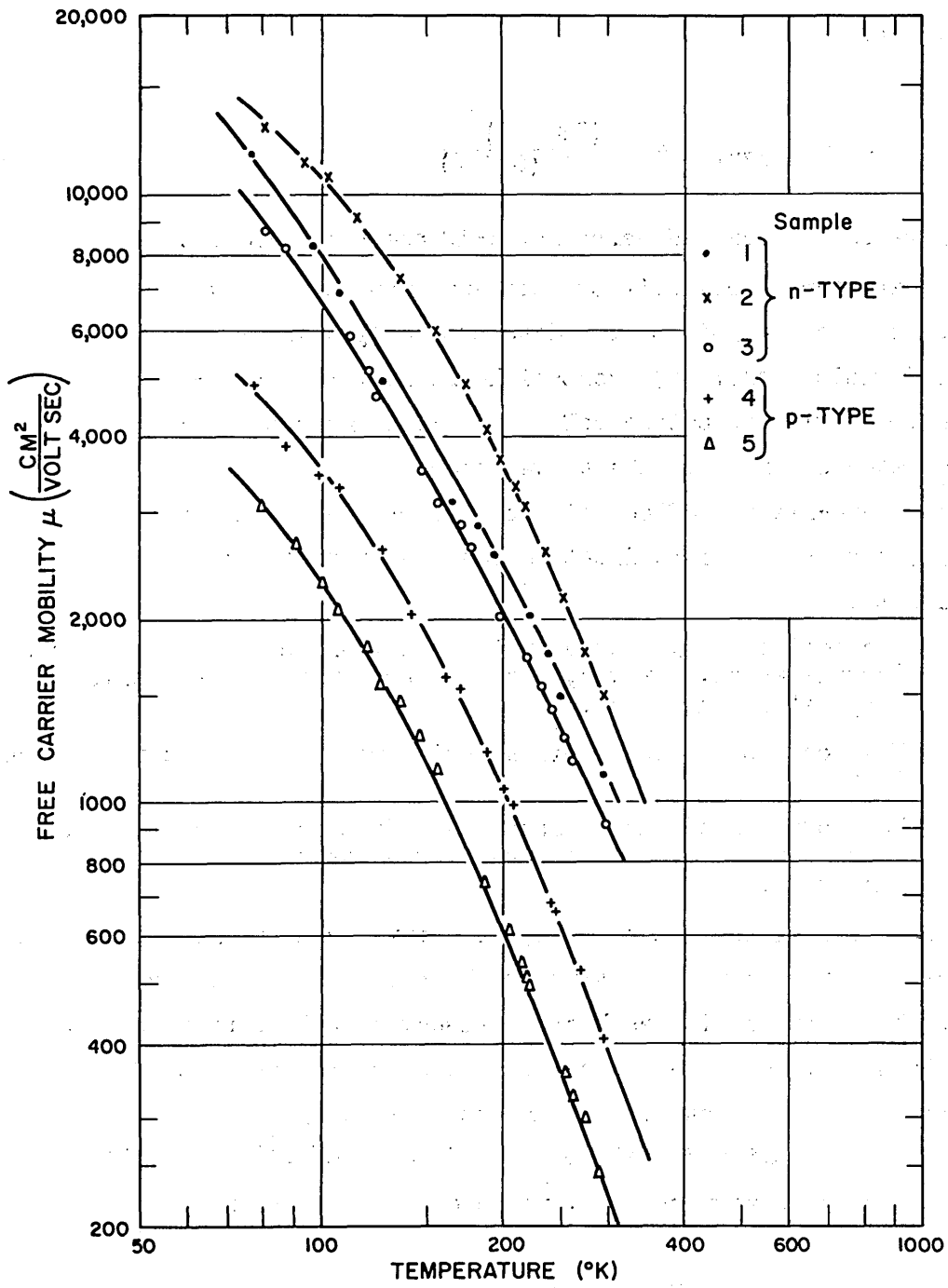


Fig. 5-5 The free carrier mobility for 3 n - and 2 p - type samples of PbTe calculated from Eq. 5-10, are shown as a function of temperature between 77° and 300°K.



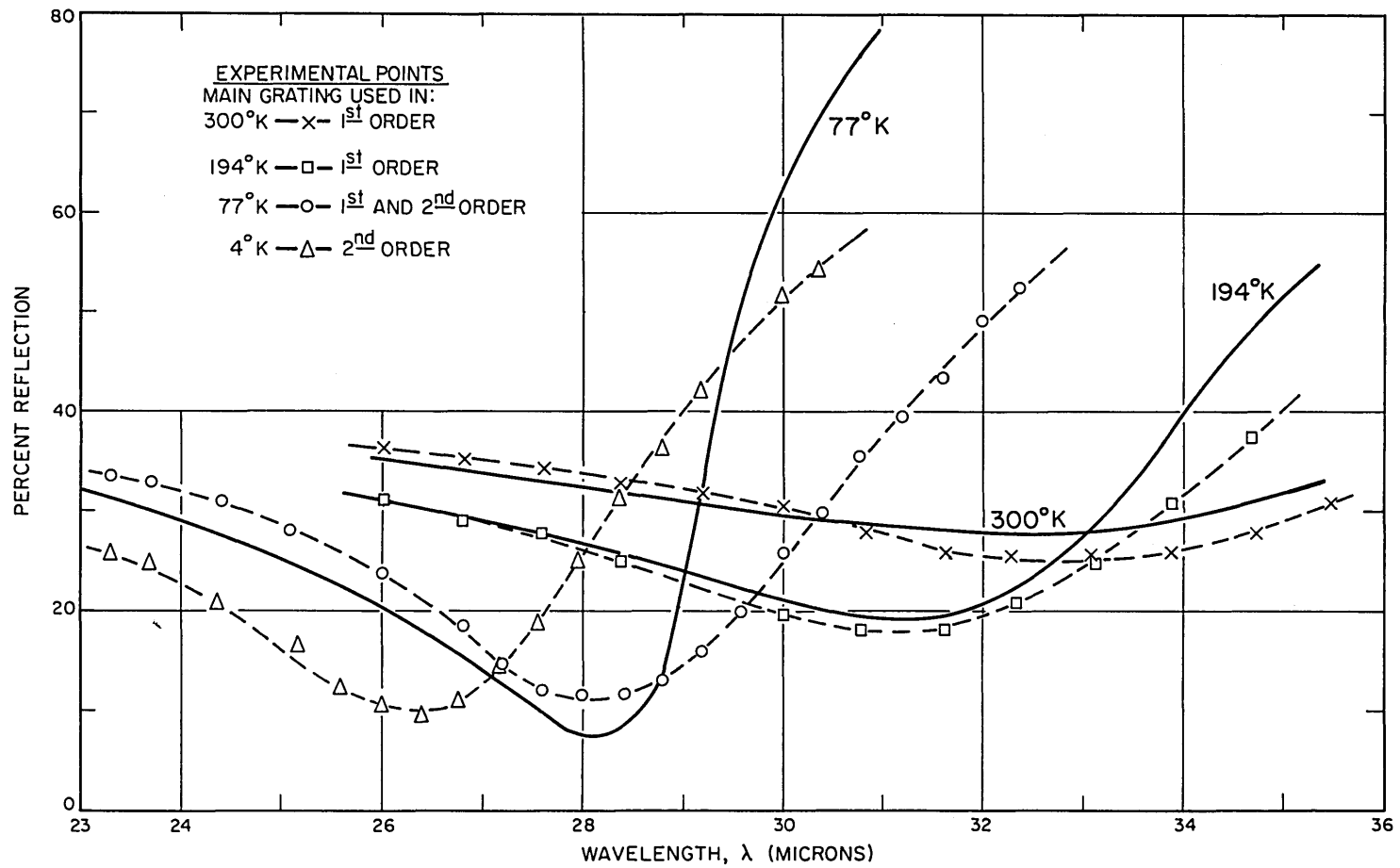


Fig. 5-6 The zero-field infra-red reflectivity of sample 1 as a function of wavelength at 4°, 77°, 194°, and 300°K along with theoretical curves at 77°, 194°, and 300°K shown as solid curves.

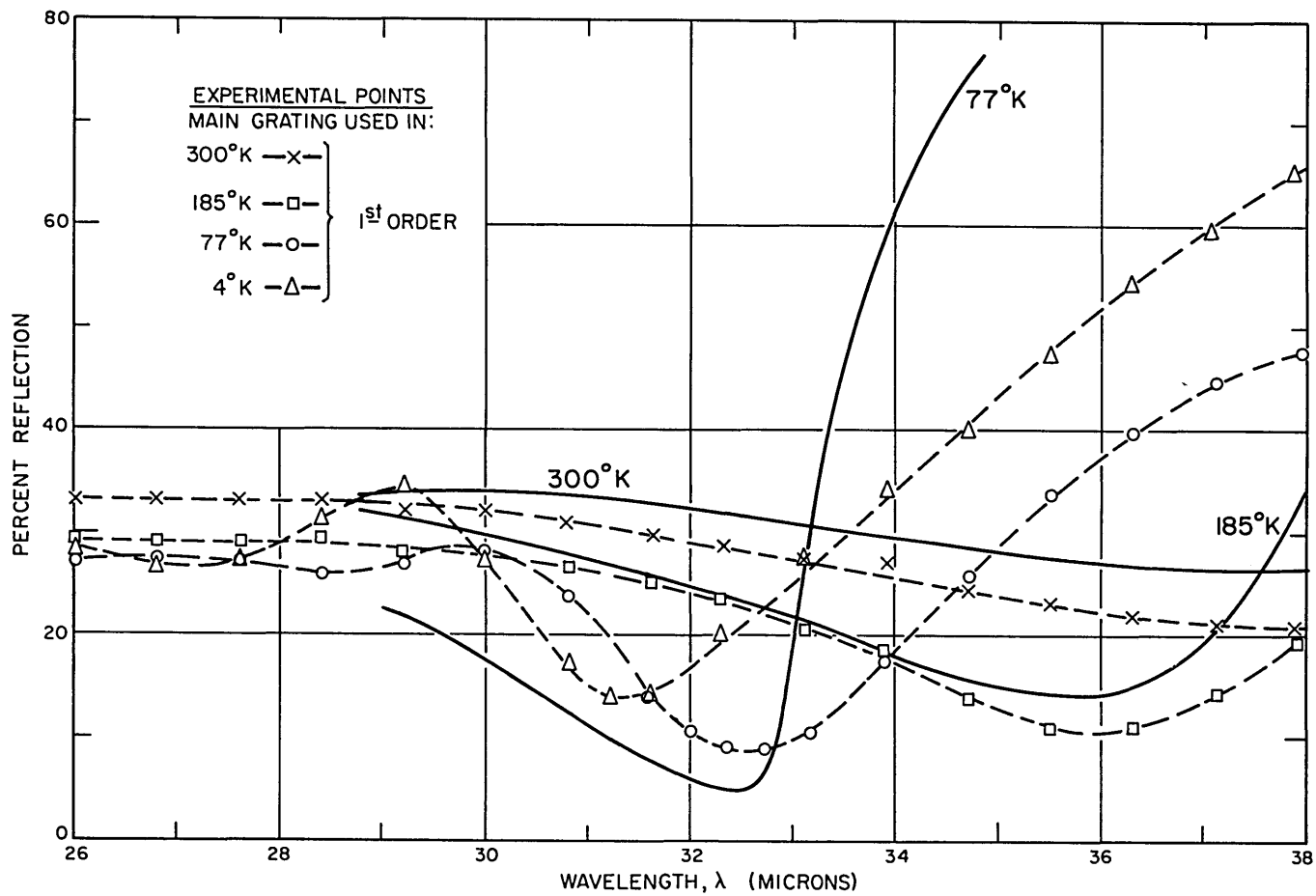


Fig. 5-7 The zero-field infra-red reflectivity of sample 2 as a function of wavelength at 4°, 77°, 185°, and 300° K along with theoretical curves at 77°, 185°, and 300°K shown as solid curves.

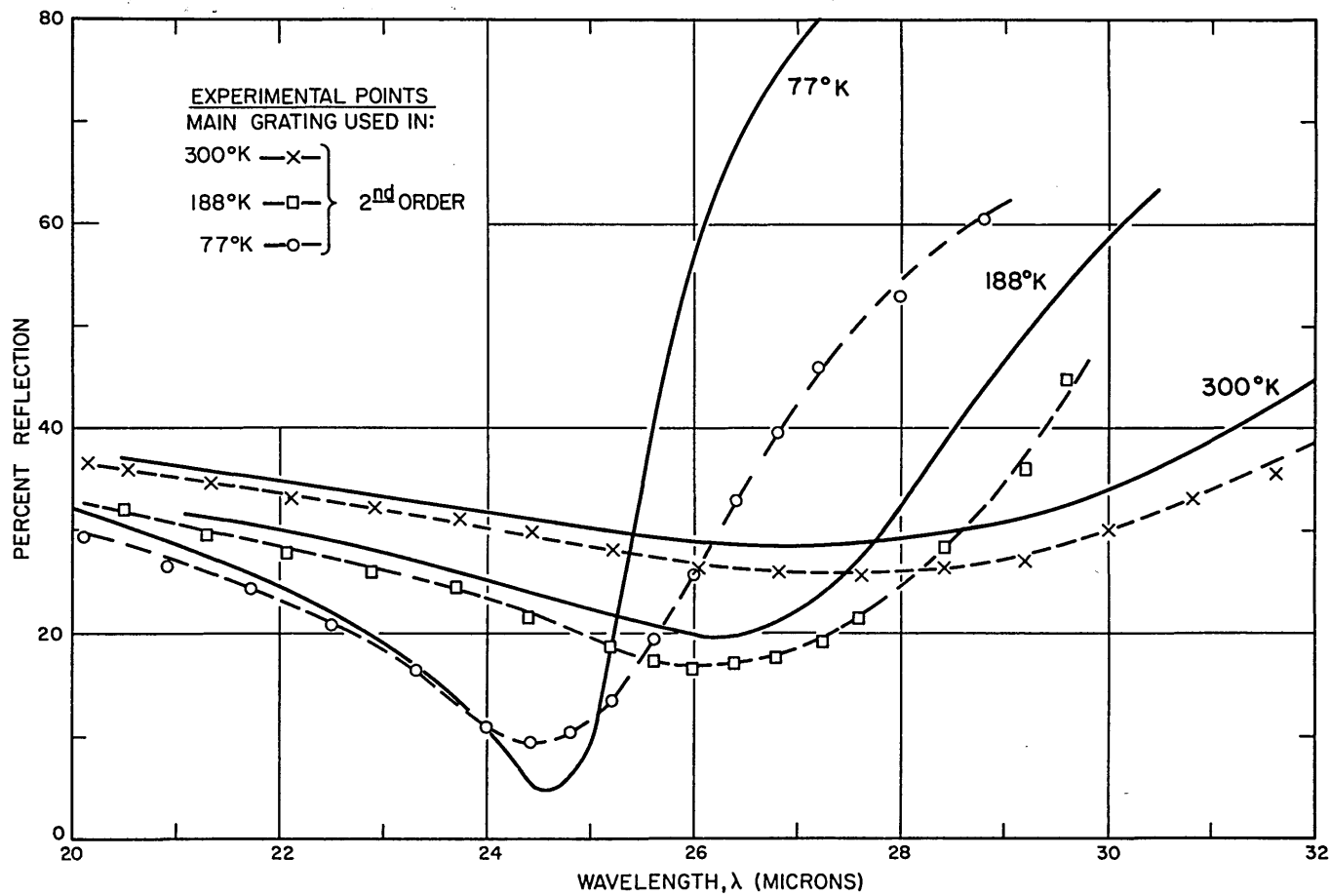


Fig. 5-8 The zero-field infra-red reflectivity of sample 3 as a function of wavelength at 77°, 188°, and 300°K along with theoretical curves at these same temperatures shown as solid curves.

Eq. 5-11 are tabulated below:

T(°K)	$\epsilon_{\infty} = n_0^2$
4	38.2
77	35.6
190	32.2
300	30.0

Table 5-3. Values determined for the relative dielectric constant of the lattice as a function of temperature from Eq. 5-11.

Using these values of  $\epsilon_{\infty}$ , the free carrier concentrations obtained from Hall measurements (Table 5-2), the mobility values shown in Fig. 5-5, and the wavelengths of minimum reflectivity, the conductivity effective masses have been calculated from Eq. 2-10. This information is tabulated below and the resulting conductivity effective masses for samples 1, 2 and 3 are shown plotted as a function of temperature in Fig. 5-3.

Sample #	T (°K)	$\mu$ (m <sup>2</sup> /volt-sec.)	$\lambda_0$ (microns)	$m_c^*$
1	4	undetermined	26.4	0.051
	77	1.15	28.2	0.061
	194	.26	31.2	0.087
	300	.12	32.5	0.108
2	4	undetermined	31.4	0.055
	77	1.4	32.5	0.060
	185	.43	35.9	0.085
	300	.14	37.8	0.110
3	77	0.97	24.5	0.061
	188	0.23	26.2	0.080
	300	0.095	27.3	0.102

Table 5-4. Data pertinent to the calculation of the conductivity effective masses of samples 1, 2, and 3.

It should be noted in conjunction with the above table that the value of the mobility is not required to calculate  $m_c^*$  at 4°K, since at this temperature, and also at 77°K, the approximation  $(\omega\tau)^2 \gg 1$  is valid. Consequently, the

parameter  $\rho$  cancels out of Eq. 2-10.

It is apparent from Fig. 5-3 that the conductivity effective masses calculated in this way exhibit a temperature dependence, increasing with increasing temperature. The actual rate of increase is very similar to that which is observed in the density-of-states effective mass. This result is consistent with the fact that the anisotropy ratio  $K$  does not change significantly with temperature, say from 5.5 at 77°K to 4.0 at 300°K.<sup>15</sup> The consistency of these results follows from the definitions of these quantities, namely

$$m_d^* = N_v^{2/3} m_t K^{1/3} \quad (5-12)$$

where  $N_v$  is the number of equivalent ellipsoids of constant energy in the conduction band, and

$$m_c^* = m_t \frac{3K}{2K + 1} \quad (5-13)$$

For the range of  $K$  values noted above the factors of  $K$  in Eqs. 5-12 and 5-13 are limited to the range of values:

$$1.59 < K^{1/3} < 1.76$$

and

$$1.33 < \frac{3K}{2K + 1} < 1.37$$

From which it follows that the factor contributing most significantly to the temperature dependence of both  $m_d^*$  and  $m_c^*$  is  $m_t$ , thereby producing a similar temperature variation in each case. The fact that a similar temperature dependence was observed in both  $m_d^*$  and  $m_c^*$  increases one's confidence in the validity of the results, since these two were determined by very different methods.

Moreover, from Eqs. 5-12 and 5-13 and from the data for the effective masses, it is possible to determine the number of equivalent ellipsoids in the

conduction band.

$$N_v^{2/3} = \frac{m_d^*}{m_c^*} \frac{3K^{2/3}}{2K + 1} \quad (5-14)$$

The results of these calculations are listed below:

T(°K)	(m <sub>d</sub> <sup>*</sup> ) avg.	m <sub>c</sub> <sup>*</sup>	K (ref.15)	(N <sub>v</sub> ) <sup>2/3</sup>	N <sub>v</sub>
77	0.20	0.060	5.5	2.60	4.2
190	0.25	0.082	4.5	2.50	4.0
300	0.30	0.105	4.0	2.39	3.7

Table 5-5. Data used in Eq. 5-14 for the determination of the number of equivalent ellipsoids in the conduction band.

The results indicate that a four-valley model is to be preferred over an eight-valley model. This result coincides with that obtained by Kuglin, et al., at 4°K. Moreover, the fact that these effective masses result in values of N<sub>v</sub> so close to a theoretical value of 4, a value which has already been deduced at 4°K, further increases our confidence in the temperature dependences and in the absolute values of these masses.

Another comparison between the results of this investigation and of others is afforded at 4°K where a value for m<sub>t</sub> has been determined from the ratio of the oscillatory magnetoresistance obtained at 1.7° and at 4°K for a given magnetic field.<sup>15</sup> The value reported is m<sub>t</sub> = 0.030 ± 0.005. Using the value of K given in the same report, K = 5.5<sup>+2.5</sup><sub>-1.5</sub>, a conductivity effective mass can be calculated. This calculation yields m<sub>c</sub><sup>\*</sup> = 0.041 ± .008 as compared with m<sub>c</sub><sup>\*</sup> 0.052 ± .005 which has been obtained in this investigation. The agreement is reasonably good, especially in view of the fact that the samples investigated here have a carrier concentration which is an order-of-magnitude greater than for the samples utilized in the determination of m<sub>t</sub>, and any non-parabolicity in the conduction band would tend to produce higher effective masses in the material of higher degeneracy.

It has been noted that the data are compatible with a four-valley model for the conduction band. However, a more complicated model, such as a

minimum at the center of the zone in addition to the four minima at the boundary as has been recently proposed,<sup>15</sup> cannot definitely be ruled out. Moreover, in the above analysis it was necessary to utilize  $K$  values reported in the literature. If we now invert the procedure used above, by assuming that the number of ellipsoids is four, it is possible to obtain values of  $K$  and then to compare these values with those reported in the literature. The results of this computation are listed in Table 5-6.

$T(^{\circ}K)$	$(m_d^*)$ avg.	$m_c^*$	$K_{calc.}$	$m_t$	$m_l$
77	0.20	0.060	5.8	0.043	0.25
190	0.25	0.082	4.0	0.062	0.25
300	0.30	0.105	3.0	0.082	0.25

Table 5-6. Data pertinent to the computation of  $K$  values from Eqs. 5-12 and 5-13 on the basis of a four valley energy band model.

The values of  $K$  that are obtained using this inverted procedure are slightly different from those used in the initial computation of  $N_v$ , but they are nevertheless comparable to those reported in the literature. For example, in a recent article the values proposed for  $K$  are  $K = 5.5^{+2.5}_{-1.5}$  at  $4^{\circ}K$  and  $4.0 \pm 0.5$  at  $300^{\circ}K$ .<sup>15</sup> The close comparison between these latter values and those calculated ( $K_{calc.}$ ) implies that a four-valley model for the conduction band is very definitely indicated by the effective mass values determined in this investigation.

It should be noted that  $K$  is actually more than a ratio of  $m_l/m_t$ . The complete expression is  $K = m_l \tau_t / m_t \tau_l$  where  $\tau_l$  and  $\tau_t$  are the longitudinal and transverse relaxation times. A change in  $K$  with temperature can be indicative of a change in the anisotropy of the  $\tau$ 's, which in turn can be indicative of a changing scattering mechanism.<sup>16</sup> On the other hand, if  $\tau$  is assumed to be isotropic, then  $K$  can be considered as simply the ratio  $m_l/m_t$ . The values for  $m_l$  and  $m_t$  listed in Table 5-6 have been calculated on this basis, i.e. an isotropic relaxation time. It is interesting to note that  $m_t$  changes by almost 100% with respect to its value at  $77^{\circ}K$  while  $m_l$  remains constant at 0.25 throughout the temperature range. Thus, if the assumption of an isotropic relaxation time is valid, then this result implies that the ellipsoids of constant

energy, as temperature increases, change in such a way that their longitudinal dimension remains constant while their transverse dimension increases. Thus, they would be assuming a more spherical shape. However, this result depends on the two very important assumptions that the number of valleys is four and that the relaxation time is isotropic. This latter assumption may not be at all justified.

As an additional check between theory and experiment, the conductivity effective mass values obtained from the minima have been inserted into the general dispersion relations for free carriers, Eqs. 2-4 and 2-5, and the theoretical reflectivity curves have been calculated. In making these calculations, the temperature dependence of the dielectric constant of the lattice,  $\epsilon_{\infty}$ , has been taken into account by using the values listed in Table 5-3. The results of these calculations are shown as solid lines in Figs. 5-6, 5-7 and 5-8. The agreement between theory and experiment is quite good for samples 1 and 3 over wide ranges of wavelength. (Sample 2 has many peculiarities and will be discussed at length toward the end of this discussion on n-type reflectivity.) However, there are significant differences and these require additional comment. One notes that in Figs. 5-6 and 5-8 that the theory and experiment match quite well for wavelengths shorter than the reflectivity minimum but that they begin to diverge near the minimum and thereafter. Furthermore, this divergence increases as the temperature is lowered. A similar divergence has been noted in the reflectivity of SnS, and the hypothesis advanced to account for this discrepancy was that the relaxation time  $\tau$  is a strong function of frequency.<sup>17</sup> That is, a shorter time  $\tau$  is said to exist at the longer wavelengths and that this mean free time between collisions increases as the frequency increases. The qualitative explanation for such a phenomenon is based on the idea that impurity scattering is less effective for fast electrons. That such an effect should occur precisely in the vicinity of the reflectivity minimum seems almost too coincidental. Moreover, such an explanation for the present analysis seems very unlikely because impurity scattering is not a dominant factor in the free carrier mobility of the PbS group until very low temperatures ( $\sim 10^{\circ}\text{K}$ ). Instead, as the analysis of the Nernst-Ettingshausen effect has indicated, the predominant scattering mechanism appears to be lattice scattering in this group over a wide temperature range.



The most likely explanation for the observed divergence of experiment from theory lies in the surface condition of the sample. It has been noted by Avery that the surface treatment of PbTe has a very significant effect on the absorption coefficient at wavelengths  $< 3-5$  microns,<sup>18</sup> which is in the region of the absorption edge. Now, the absorption coefficient  $\alpha$  equals the reciprocal of the distance within which the incident radiation is attenuated by a factor  $e^{-1}$ . Consequently,  $\alpha$  is a measure of the depth of the material which interacts with the incident radiation. The absorption coefficient may be expressed in terms of the absorption index  $k$  by the equation

$$\alpha = \frac{4 \pi k}{\lambda} \quad (5-15)$$

On the long wavelength side of the free-carrier reflectivity minimum,  $k$  is increasing rapidly. In fact, this portion of the curve is influenced almost exclusively by the behavior of  $k$ . The sharp rise of the theoretical curves past the minimum gives an indication of how rapidly  $k$  is increasing. Thus, one can see that  $k$  increases much more quickly for the higher mobility material at the lower temperatures. For  $\lambda = 30$  microns, the penetration depth ( $1/\alpha$ ) of the radiation is only 1 micron for  $k \approx 2$ . This means that the surface preparation is very important in this region of the reflectivity. Now, one expects that polishing by means of a wheel and abrasive will produce surface damage of the order of a few times the size of the abrasive particles. Furthermore, this damage can in fact extend somewhat deeper depending on the crystalline properties and on the complete polishing routine, i.e. the complete progression from coarse abrasive to the finest. As has already been noted, Avery reports a significant reduction in the reflectivity below  $6 \mu$  resulting from polishing, and he eventually resorted to cleaved surfaces in his analysis of the energy gap.<sup>13</sup>

With regard to the samples used in this investigation, it is felt that the minimum depth of surface damage resulting from abrasive polishing is of the order of 3-5 microns. Subsequent to polishing with an abrasive, the samples were subjected to a very mild polishing etch (see Chapter III) for a period of about ten minutes. After such treatment good spots were obtained on back-reflection x-ray photographs of the surface. However, this fact alone, without some knowledge of the x-ray penetration in PbTe, does not establish the depth of surface

damage. It is felt that an absolute minimum depth of this damage is on the order of  $1\mu$ . As a result, it would be anticipated that scattering of the radiation due to surface damage could become important for  $k$  values of 1 to 2. This is what is observed, particularly for samples 1 and 3.

In addition to the scattering of radiation at the surface due to damage, another possibility which can account for the observed reduction in the long wavelength reflectivity is a decrease in the apparent mobility of the free electrons should the surface mobility differ from that of the bulk. This is to be distinguished from the effect hypothesized for SnS, where it was suggested that the mobility increases above the bulk low frequency mobility as the frequency increases because of a decrease in the scattering effectiveness of impurities. A reduced surface mobility is highly plausible in view of Levinstein's results with thin films, of a few microns thickness and smaller, of PbTe.<sup>19</sup> This work suggests that the surface mobility could be lower than the bulk mobility for either of two reasons: surface damage or oxidation of the surface. The latter is not considered to be too significant since the polishing of the surface was usually undertaken within a few hours of the time that the samples were placed under a vacuum of  $\sim 10^{-6}\mu$  of Hg in the infra-red reflectivity apparatus. (This was the case for samples 1, 3, 4, and 5.) Moreover, at no time were the samples heated above  $100^{\circ}\text{C}$ . If they were heated to that temperature, it was for only a matter of minutes, and they were always subjected to the polishing etch referred to above just prior to the infra-red investigation. However, the surface damage could have a significant effect on the surface mobility, and this would be most apparent at the lowest temperatures,  $4^{\circ}$  and  $77^{\circ}\text{K}$ , where the bulk mobilities are extremely high.

This latter mechanism, a surface mobility which decreases with increasing absorption coefficient, is strongly suggested by the curves of Figs. 5-6 and 5-8. A significant feature of these curves is the depth of the minima, which is not as great as that predicted by the theory at  $4^{\circ}$  and  $77^{\circ}\text{K}$  while just the opposite is observed at  $190^{\circ}$  and  $300^{\circ}\text{K}$ . From this one concludes that, because of the extremely high mobilities at the lower temperatures, lattice damage and imperfections have a more pronounced effect on the apparent mobility than is the case for the lower mobility conditions at the higher temperatures.

To demonstrate the effect of a decreasing mobility on the reflectivity, sample 3 at 77°K has been chosen as an example. In Fig. 5-9, the experimental data for this sample are replotted along with theoretical curves having different values of  $\tau = m_0\mu/e$ .

It is evident from the figure that a decreasing mobility could account for a considerable amount of the discrepancy between the theoretical and experimental reflectivities, and the scattering of radiation at the surface could account for the remainder.

Assuming that these two mechanisms are completely responsible for the observed discrepancies in Figs. 5-6 and 5-8, it remains to assess their effects on the experimental data. As was pointed out above, the mechanism of a decreasing mobility seems to have its greatest effect at the lowest temperatures, 4° and 77°K, because the bulk mobilities there are so extremely high. Such a mechanism has the effect of raising the minimum reflectivity, and if the mobility change is sufficiently large, it can shift the minimum to shorter wavelengths. These effects are illustrated in Fig. 5-9. It can be seen from this figure that, for such high mobilities, a reduction in  $\tau$  of a factor of two to three is required before the position of the minimum is shifted noticeably. The criterion for whether or not a shift will occur is whether or not  $(\omega\tau)^2$  remains very much greater than unity. If the decrease in  $\tau$  is such that unity is no longer completely negligible with respect to  $(\omega\tau)^2$  then the position of the minimum is shifted to shorter wavelengths. Considering sample 3 as typical, it can be seen from Fig. 5-9 that the change in  $\tau$  at the minimum could not be large enough to cause an appreciable shift in the minimum. To be sure  $\tau$  may decrease more on the long wavelength side of the minimum as  $k$  continues to increase, but this would not affect the position of the minimum. Thus, a decreasing mobility with increasing  $k$  should not give rise to a significant error in the position of the minimum. The other mechanism of scattering at the surface has the effect of suppressing the rise in reflectivity on the long wavelength side of the minima. The result of this effect is to broaden the minima on the long wavelength side. This has the tendency of shifting the minima to longer wavelengths. At the lowest temperatures, where the minima are quite sharp, this broadening should have very little effect. However, at 190° and

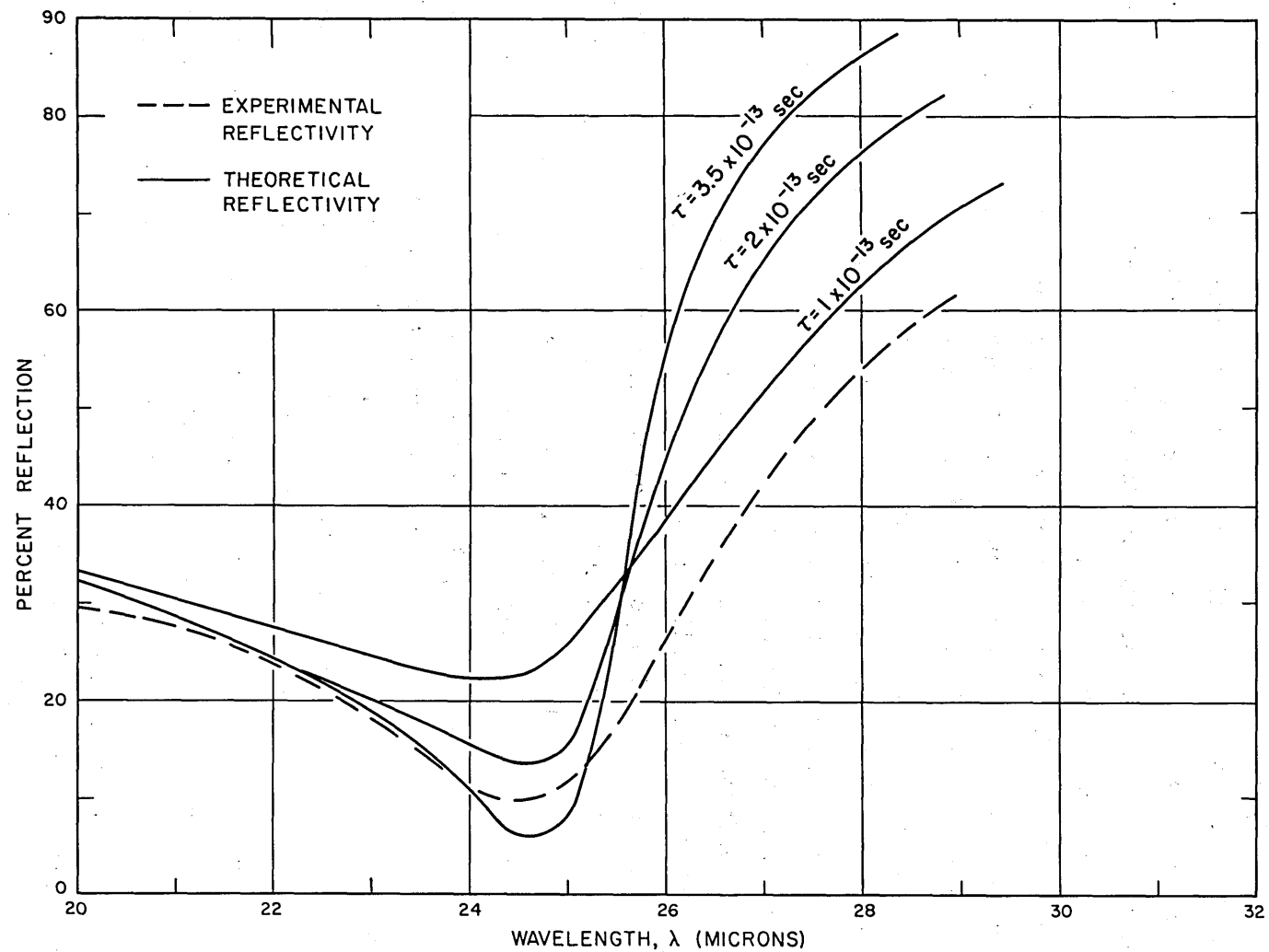


Fig. 5-9 The zero-field reflectivity of sample 3 at 77°K along with theoretical curves for  $N = 3.8 \times 10^{18}$  electrons/cm<sup>3</sup>,  $m_c^* = 0.061$ , and three different values of  $\tau$  ( $3.5$ ,  $2$ , and  $1 \times 10^{-13}$  sec).

300°K, the absorption index at the minima is already of the order of unity, and so this mechanism could have a significant broadening effect at these temperatures. By comparing the shapes of the experimental and theoretical curves at these higher temperatures in Figs. 5-6 and 5-8, we estimate that the broadening due to scattering could give rise to an uncertainty in the wavelength of the minima of approximately  $-0.2\mu$  at 190°K and  $-0.3\mu$  at 300°K. However, over the wavelength range of interest ( $25 - 35\mu$ ), this represents an uncertainty in the position of the minima, arising from the discrepancy in the absorption edge of the reflectivity curve, of about  $-1\%$ . Since  $m_c^*$  is approximately proportional to  $\lambda^2$ , this implies that the uncertainty in  $m_c^*$  from these effects is within  $-2\%$ .

There is still one aspect of the infra-red reflectivity that has not been fully evaluated, i.e. the effect of the lattice polarization on the dispersion has so far been neglected. We will now consider the justification for this omission. Actually, the evaluation of the lattice contribution to the reflectivity is allied with the much broader problem of assessing the true polar character of the compounds in the PbS family. The extent of the uncertainty with regard to this polar character can be appreciated when it is pointed out that static dielectric constants ranging from 17.9 to  $\sim 70$  have been ascribed to PbS. It has been noted that the former value was obtained in 1894 on powdered material<sup>21</sup> while the latter has been deduced from compressibility data.<sup>20</sup> Moreover, the value of  $\epsilon_\infty$  for PbS has been established to be 17.5 by infra-red reflectivity measurements.<sup>13</sup> Thus, it could be that PbS (and also PbSe and PbTe) has almost no polar character at all, i.e. if

$$\epsilon_s - \epsilon_\infty \approx 17.9 - 17.5 = 0.4$$

There is other evidence which causes one to question the degree of the polar character of these compounds. It has already been noted that measurements of the Nernst-Ettingshausen effect have indicated an increasing predominance of acoustical mode scattering, and consequently of homopolar binding, as the temperature increases above 100°K.<sup>2</sup> Moreover, the author of that same report cites, as additional evidence for this conclusion, the experimental result

that the lattice energies of PbS and PbSe, determined by the Born-Haber process, differ significantly from the energies calculated according to the Born theory for ionic crystals. We conclude that the evidence so far seems to favor a predominance of homopolar as opposed to polar binding. However, this is very much unsettled, and we hope to help clarify the situation.

Before proceeding with this analysis, we will outline the steps to be followed so that the reader will understand the relevance of each step. First, we will discuss the infra-red reflectivity and the contribution of the lattice in the wavelength range of interest ( $< 35\mu$ ). This contribution will be evaluated to the extent possible, and the obstacles to a complete evaluation will be determined. Next, we will temporarily leave the reflectivity expression, and turn to the electron mobility. We will consider the mobility of sample 3 and compare the experimental temperature dependence with that synthesized for acoustical mode lattice scattering from the temperature dependences of  $m_c^*$ ,  $m_d^*$  and  $\langle E^{-1/2} \rangle$ . Then, we shall consider the possibility of optical mode lattice scattering for a polar semiconductor. Based on the reasonable assumption that PbTe, being a two atom compound of valence 2, has a mixture of covalent and polar bonding and must therefore have some optical mode scattering, we shall deduce an upper limit on the static dielectric constant. This will be accomplished by requiring that the mobility arising from optical mode scattering must be at least as great as that mobility which is experimentally observed. Finally, we shall return to the infra-red reflectivity and place an upper limit on the effect that the lattice polarization can have on these measurements.

To begin with, the contribution of the ions of a polar crystal AB (with only one absorption band at an angular frequency  $\omega_t$ ) to the dispersion relations is expressed in a form very similar to that of the free electrons. The complete dispersion relations, which include the effects of the lattice, may be expressed as follows:<sup>22,23</sup>

$$n^2 - k^2 = \epsilon_\infty - \frac{Ne^2}{m_c \epsilon_0 \omega^2} \frac{\omega_t^2 \tau^2}{(1 + \omega_t^2 \tau^2)} + \left( \frac{\epsilon_\infty + 2}{3} \right)^2 \frac{N_1 Q^2}{M c \epsilon_0} \left[ \frac{(\omega_t^2 - \omega^2) \tau_1^2}{\omega^2 + (\omega_t^2 - \omega^2) \tau_1^2} \right] \quad (5-16)$$

and

$$2nk = \frac{Ne^2}{m_c \epsilon_0 \omega^2} \frac{\omega \tau}{1 + \omega^2 \tau^2} + \left( \frac{\epsilon_\infty + 2}{3} \right)^2 \frac{N_1 Q^2}{M \epsilon_0} \left[ \frac{\omega \tau_1}{\omega^2 + (\omega_t^2 - \omega^2) \tau_1^2} \right] \quad (5-17)$$

In both equations the last term is the contribution made by the ions. The parameters in the other terms have been defined following Eqs. 2-4 and 2-5.

The new parameters are as follows:

$N_1$  is the concentration of atom pairs AB ( $1.5 \times 10^{22}$  pairs/cm<sup>3</sup> for PbTe).

$Q$  is an effective charge defined by  $Q = SZe$  where  $e$  is the electronic charge,  $Z$  is the valence of the compound ( $Z = 2$  for PbTe), and  $S$  is a measure of the extent to which the ions of charge ( $Ze$ ) are capable of being polarized.

$M$  is the reduced mass,  $1/M = 1/M_A + 1/M_B$  ( $M = 1.45 \times 10^5 m_0$  for PbTe).

$\omega_t$  is the angular frequency of the transverse lattice vibrations (Reststrahlen), and

$\tau_1$  is a relaxation time related to the damping of the lattice vibrations.

To evaluate the contribution of the lattice in these dispersion relations, we consider the specific conditions of this investigation in which  $\omega^2 \gg \omega_t^2$ . (This inequality is based on Eq. 5-21 and the analysis which follows that equation from which it can be inferred that  $\lambda_t > 110\mu$ .) Moreover, to simplify matters we consider the contribution of the lattice at frequencies such that  $\omega > \omega_0$ , where  $\omega_0$  is the angular frequency of the free-carrier reflectivity minimum. In this frequency range, we can assume that  $k = 0$ . In addition, we make the assumption that  $(\omega \tau_1)^2 \gg 1$ . This assumption is not necessary to show that the lattice contribution is small since this contribution decreases with decreasing  $\omega \tau_1$ . However, since  $\tau_1$

is not known, we wish to neglect it in this analysis. There is experimental evidence which indicates that lattice damping is small. (Specifically, for ZnS it has been found that  $\omega_t \tau_1 = 20$  where the  $\omega_t$  involved is less than  $\omega$  in this investigation.<sup>24</sup>) Finally, we assume that  $(\omega\tau)^2 \gg 1$ , a condition which is generally fulfilled except perhaps at 300°K. Equation 5-16 reduces to the expression

$$n^2 = \epsilon_\infty - \frac{Ne^2}{m_c \epsilon_0 \omega^2} - \left( \frac{\epsilon_\infty + 2}{3} \right)^2 \frac{N_1 Q^2}{M \epsilon_0 \omega^2} \quad (5-18)$$

A comparison of the lattice and free electron terms for PbTe yields the ratio:

$$\frac{n^2_{\text{lattice}}}{n^2_{\text{free elec.}}} = \left( \frac{\epsilon_\infty + 2}{3} \right)^2 \frac{N_1 (SZ)^2 / M}{N / m_c} = 1 \times 10^{-2} S^2 \left( \frac{\epsilon_\infty + 2}{3} \right)^2 \quad (5-19)$$

where the values used are  $N_1 = 1.5 \times 10^{22}$  pairs/cm<sup>3</sup>,  $N = 4 \times 10^{18}$  electrons/cm<sup>3</sup>,  $M = 1.45 \times 10^5 m_0$ ,  $m_c = 0.1 m_0$ , and  $Z = 2$ .

The term  $\left( \frac{\epsilon_\infty + 2}{3} \right)^2 \approx 100$  for PbTe so that the relative contribution is approximately represented by the quantity  $S^2$  (for the free carrier concentrations considered here). That is, if the compound PbTe is rather ionic in character, so that  $S$  is nearly unity, these two mechanisms contribute about equally to the dispersion. However, if the bonding is primarily covalent and  $S \approx 0.1$ , the lattice contribution can clearly be neglected with respect to that of the free electrons.

It is also instructive to look at the absolute contributions of the lattice to the relative static dielectric constant  $\epsilon_s$ .

$$n^2 = \epsilon_s = \epsilon_\infty + \left( \frac{\epsilon_\infty + 2}{3} \right)^2 \frac{N_1 Q^2}{M \epsilon_0 \omega_t^2} \quad (5-20)$$

For this calculation, the transverse angular frequency  $\omega_t$  can be estimated since  $\omega_t$  is related to  $\omega_1$  through the Lyddane - Sachs - Teller equation:<sup>25</sup>

$$\omega_t = \omega_1 \left( \frac{\epsilon_\infty}{\epsilon_s} \right)^{1/2} \quad (5-21)$$



Moreover,  $\omega_1 = k \theta / \hbar$  where  $\theta$  has been determined as a function of temperature by Parkinson and Quarrington.<sup>26</sup> To a good approximation, we can assign the value  $\theta = 130^\circ\text{K}$  which yields  $\omega_1 = 1.70 \times 10^{13}$  rad/sec. This corresponds to a wavelength of  $\lambda_1 = 110\mu$ . Thus, from Eq. 5-20 we obtain the result:

$$\epsilon_s - \epsilon_\infty = \left( \frac{\epsilon_\infty + 2}{3} \right)^2 \left( \frac{\epsilon_s}{\epsilon_\infty} \right) 4.56 S^2 \quad (5-22)$$

Again we see that the final result depends upon the degree of ionicity - with very great extremes possible.

We shall now turn our attention to the electron mobility with the ultimate goal of utilizing this property to tell us something about the quantities  $(\epsilon_s - \epsilon_\infty)$  and  $S$ . In the process of comparing the mobility which has been measured experimentally with a theoretical mobility, we wish also to show that the data obtained for the effective masses offer a means of explaining the observed mobility temperature dependence. Consequently, this analysis will serve as a further basis for establishing the validity of the foregoing effective mass determinations.

We have based our early analysis of the data on the belief that acoustical mode lattice scattering predominates at room temperature. To be consistent we should therefore attempt to fit the observed mobility temperature dependence with the temperature dependence theoretically predicted for this scattering mechanism. The theoretical expression for the acoustical mode mobility can be written as follows:<sup>27</sup>

$$\mu_a = \frac{\pi e \hbar^4 C_{11} \langle E^{-1/2} \rangle}{\sqrt{2} E_1^2 k T m_d^{3/2} m_c} \quad (5-23)$$

where  $C_{11}$  is the elastic constant for  $[110]$  longitudinal acoustical waves,  $\hbar = h/2\pi$  and,

$E_1$  is the derivative of the energy of the conduction band edge with respect to the logarithm of the volume of the unit cell.

The two parameters  $C_{11}$  and  $E_1$  have not been measured here (indeed  $E_1$  cannot be measured directly because measurement only yields relative changes between the conduction and valence bands), and so we cannot calculate absolute values for  $\mu_a$ .

However, we have determined  $m_d$ ,  $m_c$  and  $\langle E^{-1/2} \rangle$  as functions of temperature. Thus, if we assume that  $C_{11}$  and  $E_1$  are independent of the temperature (this assumption stems from our lack of knowledge with regard to their temperature dependence), it is possible to plot a mobility which is correct to an arbitrary scale factor. Following this procedure, we show the data obtained for sample 3 in Fig. 5-10 along with a curve which represents the expression:

$$\mu_a = U m_d^{*-3/2} m_c^{*-1} T^{-1} \langle E^{-1/2} \rangle \quad (5-24)$$

where  $U$  is an arbitrary scale factor which has been chosen so as to make the two curves of Fig. 5-10 coincide at room temperature. A better fit between the data and the curve representing Eq. 5-24 could obviously be made by having the point of coincidence at a lower temperature. However, it is felt that the selection of room temperature affords the most meaningful comparison since the proportion of acoustical mode lattice scattering ought to increase with temperature. Also, the experimental data ought to approach, but never cross, the theoretical curve for  $\mu_a$ . (The data utilized in the computation of Eq. 5-24 are listed in Table 5-7.)

T(°K)	$m_c^*$	$m_d^*$	$\langle E^{-1/2} \rangle$
80	0.062	0.205	6.6
100	.066	.208	6.55
150	.075	.225	6.2
200	.087	.250	5.8
250	.097	.275	5.5
300	.105	.305	5.2

Table 5-7. Data taken from Figs. 5-2 and 5-3 for the computation of  $\mu_a$  as given by Eq. 5-24.

Several conclusions can be drawn as a result of the comparison of a theoretical  $\mu_a$  with the actual experimental mobility. In the first place, it is noted that the temperature dependence of a mobility arising from acoustical

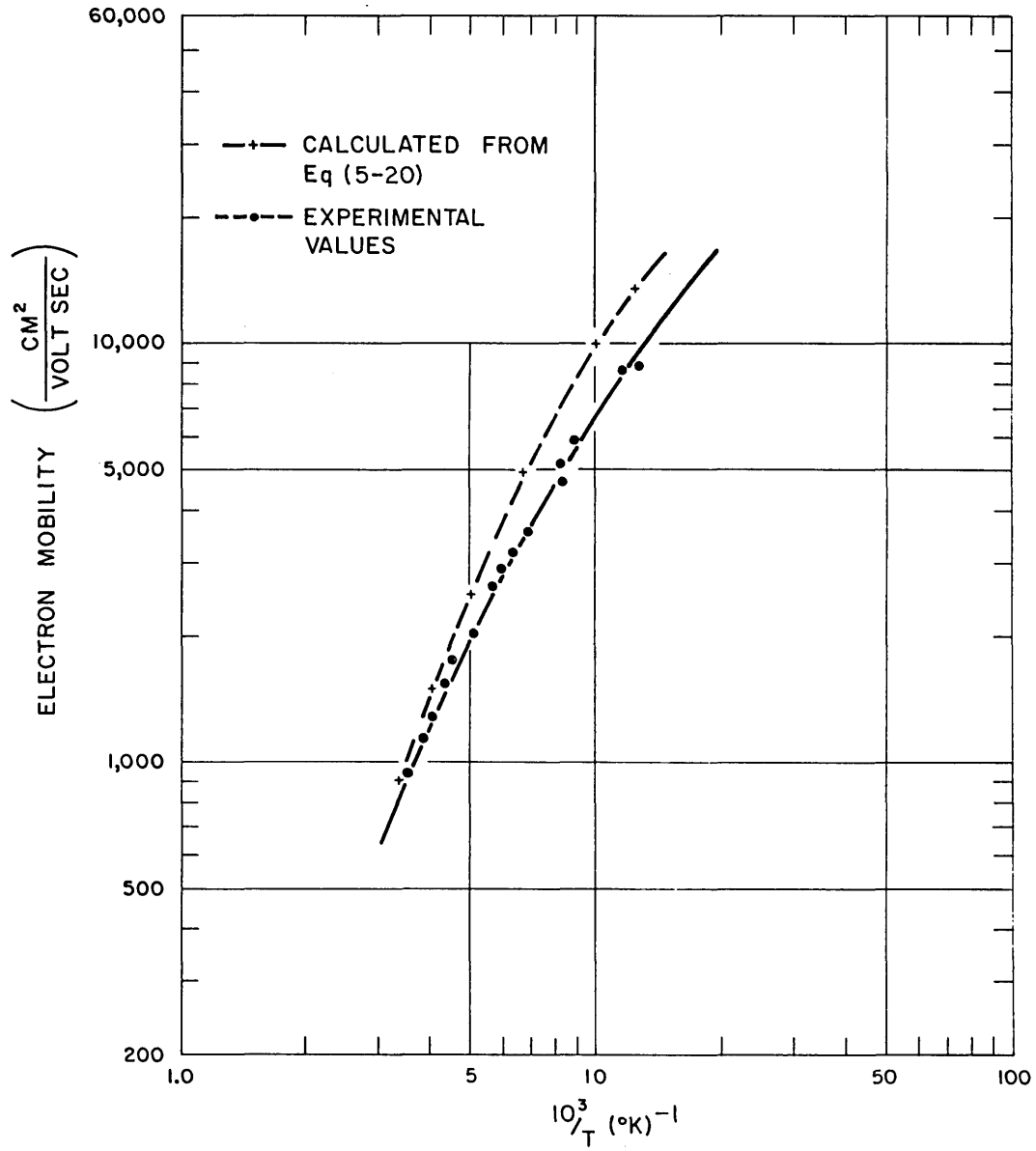


Fig. 5-10 The mobility of sample 3 as determined by experiment along with the temperature dependence predicted by acoustical mode scattering based on data for  $m_c$ ,  $m_d$ , and  $\langle E^{-1/2} \rangle$ .

mode lattice scattering can be considerably greater than the explicit temperature dependence of  $T^{-1}$  to  $T^{-3/2}$  (depending on the degree of degeneracy of the material). This additional temperature dependence results from the variation of the effective masses with temperature. However, we also see that the temperature dependence of the acoustical mode scattering mobility as computed from our data has a slightly greater temperature dependence at room temperature than that of the experimental mobility. Moreover, by matching the two mobilities at room temperature, they fail to match very well around  $100^{\circ}\text{K}$ . The discrepancy is of the order of  $40\%$  at  $80^{\circ}\text{K}$ .

On the basis of this comparison it seems reasonable to postulate that perhaps there is an admixture of two scattering mechanisms instead of just pure acoustical mode scattering. To be specific, we propose that at low temperatures there exists a combination of optical and acoustical mode scattering. Such a combination of scattering mechanisms has been considered for PbS by Petritz and Scanlon.<sup>10</sup> They succeeded in fitting the mobility at low temperatures ( $\sim 100^{\circ}\text{K}$ ), but they were unable to achieve a fit at higher temperatures. In general, the analysis to follow parallels the one made for PbS except in this case it is necessary to consider the optical mode scattering equation for various degrees of degeneracy.

With regard to optical mode scattering, there have been two approaches to the derivation of a theoretical mobility. On the one hand, there is the perturbation-theory approach due to Frohlich and Mott<sup>28</sup> and to Howarth and Sondheimer,<sup>29</sup> and the alternate approach is due to Lee, Low, and Pines.<sup>30</sup> The latter theory is restricted to temperatures such that  $T \ll \theta$  while the former is valid for all temperatures. However, the perturbation-theory approach is based on a power series expansion of a parameter  $\gamma$  which is defined below in Eq. 5-25. (This parameter is denoted by  $\alpha$  in the literature, but we have chosen  $\gamma$  so as not to confuse it with the absorption coefficient appearing in the text.) Thus, it is valid only for  $\gamma < 1$ , and rapid convergence of the theory requires  $\gamma \ll 1$ . The second approach is valid for values of  $\gamma$  as large as 6.

The parameter  $\gamma$  is defined by the equation:

$$\gamma = \frac{e^2}{4\pi\epsilon_0} \left( \frac{m_d}{2\omega_1\hbar^3} \right)^{1/2} \left( \frac{\epsilon_s - \epsilon_\infty}{\epsilon_s \epsilon_\infty} \right) \quad (5-25)$$

where  $\omega_1$  is the angular frequency of the longitudinal polar modes. The remaining parameters are the same as defined earlier in the text. We can establish a maximum limit for  $\gamma$  even without knowing  $\epsilon_s$ . This can be accomplished by taking our highest value for  $m_d$  which occurs at room temperature (i.e.  $m_d = 0.3m_0$ ). Equation 5-25 thus becomes:

$$\gamma = 19.1 \left( \frac{\epsilon_s - \epsilon_\infty}{\epsilon_s \epsilon_\infty} \right) \quad (5-26)$$

It can be seen that  $\gamma$  is zero when  $\epsilon_s$  has its smallest possible value, i.e.  $\epsilon_s = \epsilon_\infty$ , and that  $\gamma$  is a monotonically increasing function of  $\epsilon_s$  having a maximum value for PbTe of  $\gamma = 0.64$ . Moreover, if we should permit  $\epsilon_s$  to have the very high value of 100,  $\gamma$  has decreased to the value of 0.45. Because we find  $\gamma < 1$  under the most extreme circumstances possible, it is reasonable to conclude that the perturbation-theory approach is applicable in the case of PbTe. Moreover, by applying this theory it is possible to calculate an upper limit for  $(\epsilon_s - \epsilon_\infty)$  and thus for  $\gamma$ , by requiring that the resulting optical mode scattering mobility be no smaller than the observed mobility. The value of  $\gamma$  calculated in this way will give an indication of the speed of convergence to be expected for the perturbation theory. Finally, before proceeding with the perturbation-theory approach, it is recalled that this approach is valid for all temperatures.

The perturbation-theory expression for the electrical conductivity in the presence of optical mode lattice scattering is<sup>29</sup>

$$\sigma_0 = \frac{32 \epsilon_0^2 \Delta^3 M \omega_1 k^2 T^2 (e^z - 1) G(z, \eta)}{3 \pi Q_0^2 \hbar^2} \quad (5-27)$$

where  $z = \theta/T$ ,  $\theta = \hbar \omega_1/k$ ,  $G(z, \eta)$  is a very complicated function of  $z$  and  $\eta$  (reduced Fermi potential) but has certain approximate representations,  $\Delta$  is the lattice spacing between ions,  $Q_0$  is the net ionic charge which is effective in producing optical mode scattering and is to be distinguished from the effective ionic charge in Eqs. 5-16, 5-17 and 5-20, and  $M$  is the reduced mass of the ions, as before. [Eq. 5-27 includes a factor  $(4\pi\epsilon_0)^2$  to put it

in MKS units.] The quantity  $Q_0$  requires some additional consideration. It has been shown by Callen<sup>31</sup> that the optical mode which is most effective in scattering electrons is the longitudinal mode of vibration, just as is the case for acoustical mode scattering.<sup>32</sup> Because of this fact the effective charge can be expressed in terms of a modified Born relation as shown by Callen.<sup>31</sup>

$$Q_0^2 = \frac{\epsilon_s - \epsilon_\infty}{\epsilon_\infty} 2\epsilon_0 M \Delta^3 \omega_t^2 \quad (5-28)$$

By combining Eqs. 5-27 and 5-28 we obtain the expression:

$$\sigma_0 = \frac{64\pi\epsilon_0}{3} \left( \frac{kT}{h\omega_t} \right)^2 \omega_1 \frac{\epsilon_\infty^2}{\epsilon_s - \epsilon_\infty} (e^z - 1) G(z, \eta) \quad (5-29)$$

This equation can be further simplified by means of the Lyddane-Sachs-Teller relation<sup>25</sup> and the relation  $\omega_1 = k\theta/\hbar$ . Finally, the optical mode scattering mobility can be obtained from the single-carrier conductivity expression

$$\sigma_0 = Ne \mu_0$$

$$\mu_0 = \frac{32 \epsilon_0 kT}{3hNe} \frac{\epsilon_s \epsilon_\infty}{\epsilon_s - \epsilon_\infty} \frac{(e^z - 1)G(z, \eta)}{z} \quad (5-30)$$

As has already been mentioned, the function  $G(z, \eta)$  is a very complicated function, containing ratios of infinite determinants. The function can be approximated simply by terminating the determinants after a certain number of rows and columns. Fortunately, reasonable accuracy can be achieved with the first order approximation.

In the limit of non-degeneracy, the first order approximation takes the form:

$$G_1(z, \eta) = \chi(z) e^\eta \quad (5-31)$$

where  $\chi(z)$  is approximately unity for  $z \ll 1$ . The exact form of  $\chi(z)$ , as presented in reference 29, is shown in Fig. 5-11. Furthermore,  $G_1(z, \eta)$  is essentially an exact solution in the range of  $z < 1$ .

For an arbitrary degree of degeneracy, the first approximation has been calculated as a function of  $\eta$  and also for the values  $z = 1, 3, 5, 10$ . The results of this calculation are shown in reference 29 and here in Fig. 5-12.

With regard to the optical mode mobility of Eq. 5-30, the free carrier concentration  $N$  is constant,  $\theta$  is known in the range  $20^\circ < T < 200^\circ\text{K}$  from reference 26,  $\epsilon_\infty$  has been calculated as a function of  $T$  on the basis of the value  $\epsilon_\infty = 30$  at  $300^\circ\text{K}$  and  $\epsilon_\infty^2 E_g = \text{constant}$ , and  $\eta$  has been determined on the basis that the dominant scattering mechanism is acoustical mode lattice scattering. The one parameter which has not been established is  $\epsilon_s$ . We shall establish a value, or at least an upper limit, for this quantity. This is possible because the mobility is a monotonically decreasing function for increasing values of  $\epsilon_s$  as can be seen by differentiating the term  $\epsilon_s \epsilon_\infty / (\epsilon_s - \epsilon_\infty)$ . Thus, since the mobility calculated by means of Eq. 5-30 must be at least as great as that measured experimentally, an upper limit on  $\epsilon_s$  can be established.

However, in carrying out this analysis we will be making certain implicit assumptions. The nature of these assumptions can be seen by rewriting Eq. 5-28, making the changes  $2N_1 = 1/\Delta^3$ ,  $\omega_t^2 = (\epsilon_\infty / \epsilon_s) \omega_1^2$ , and  $\omega_1 = k\theta/\hbar$ . This procedure yields the equation:

$$\frac{\epsilon_s \epsilon_\infty}{\epsilon_s - \epsilon_\infty} = \frac{\epsilon_0 M k^2}{N_1 \hbar^2 Q_0^2} \theta^2 \quad (5-32)$$

In the present analysis, we shall allow  $\epsilon_\infty$  and  $\epsilon_s$  to be temperature dependent. However, we assume that their temperature dependences are correlated in such a way that the factor  $\epsilon_s \epsilon_\infty / (\epsilon_s - \epsilon_\infty)$  is constant. We base this assumption on the observation that the right hand side of Eq. 5-32 should not be more than a slowly varying function of temperature.

In the low temperature range,  $40^\circ < T < 140^\circ\text{K}$ , we calculate an optical mode mobility from Eq. 5-30 utilizing values of  $\eta$  from Table 5-1, values of  $G(z, \eta)$  from Fig. 5-12,  $N = 3.8 \times 10^{24}$  electrons/ $\text{m}^3$  (Sample 3), and  $\theta = 130^\circ\text{K}$ . The mobility which is obtained is assumed to be correct within an arbitrary scale factor, namely  $\epsilon_s \epsilon_\infty / (\epsilon_s - \epsilon_\infty)$ . The data utilized in this calculation are listed in Table 5-8 and the results are shown in Fig. 5-13.

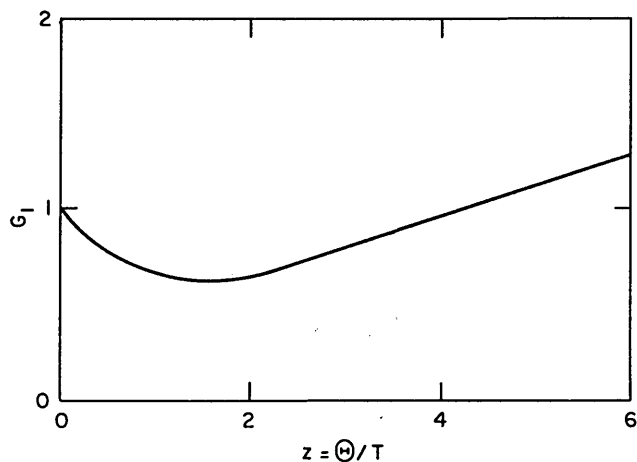


Fig. 5-11 The exact form of the factor  $\chi(z) = G_1(z, \eta) e^{-\eta}$  which is shown as curve 2 in Fig. 1 of reference 28.

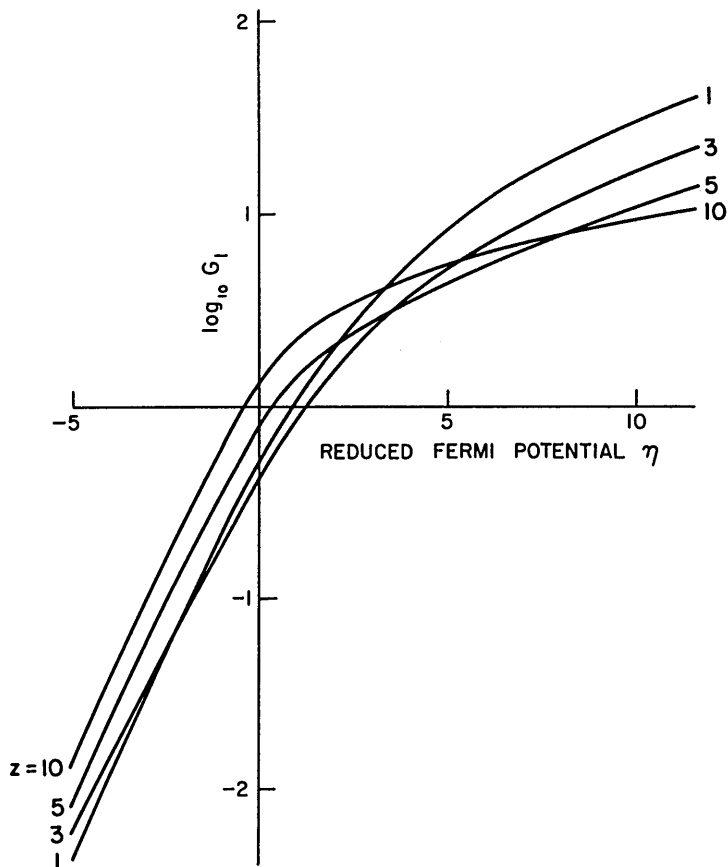


Fig. 5-12 The logarithm of the first approximation  $G_1(z, \eta)$ , which is valid for an arbitrary degree of degeneracy and is shown for values of  $z = 1, 3, 5,$  and 10. This is Fig. 2 of reference 28.



In addition, we have utilized Eqs. 5-30 and 5-31 to calculate the optical mode mobility of a non-degenerate semiconductor at 400° and 500°K. To be sure, Sample 3 would still not be strongly non-degenerate at these temperatures. For example, the equation which relates  $N$  and  $\eta$  in the limit of non-degeneracy, namely  $N = 2(2\pi m_d kT/h^2)^{3/2} e^\eta$ , indicates that  $\eta = -0.94$  and  $-1.3$  for an  $m_d = 0.4m_0$  at 400° and 500°K. However, the approximation is not expected to be too bad. Moreover, the values serve only to give some indication of the optical mode mobility behavior at higher temperatures and as a means of extrapolating the temperature dependence from 140°K. For making these higher temperature calculations we have determined  $\eta$  as indicated above from the relation between  $N$  and  $\eta$  using  $m_d = 0.4m_0$ .  $G_1(z, \eta)$  has been obtained from Eq. 5-31 and Fig. 5-11. The data used are listed in the bottom two rows of Table 5-8 and the results are shown in Fig. 5-13 with those obtained at lower temperatures.

T(°K)	z	$\eta$	$\log_{10} G_1$	$G_1$	$e^z - 1$	$\mu_0 \frac{\epsilon_s \epsilon_\infty}{\epsilon_s - \epsilon_\infty}$
40	3.25	7.5	0.98	9.55	24.8	$9.45 \times 10^{-3}$
60	2.17	6.2	.95	8.9	7.77	6.2
80	1.62	4.9	.85	7.1	4.05	4.6
100	1.30	3.9	.72	5.25	2.67	3.5
120	1.08	3.1	.56	3.63	1.94	2.55
140	.93	2.45	.40	2.51	1.54	1.9
400	.325	-0.94		.33	.384	.505
500	.26	-1.3		.25	.30	.47

Table 5-8. Data pertinent to the calculation of the optical mode scattering mobility of Eq. 5-30. The results are shown in Fig. 5-13.

As we have pointed out in the text, the optical mode mobility which is calculated here has an adjustable scaling factor  $\epsilon_s \epsilon_\infty / (\epsilon_s - \epsilon_\infty)$ . Moreover, we recognize the fact that the mobility, arising from optical mode scattering, must be at least as large as that observed experimentally. With this in mind,

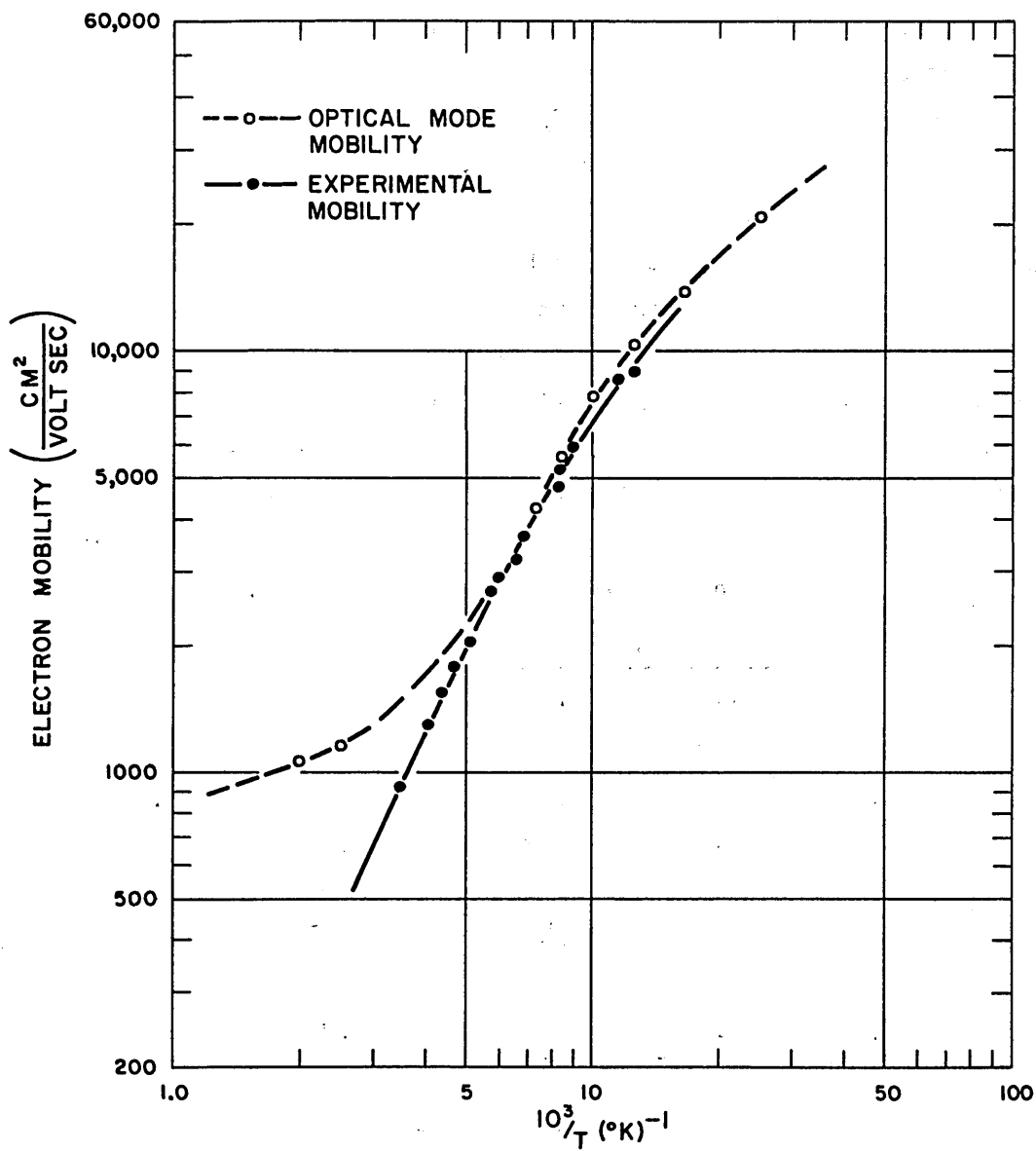


Fig. 5-13 The mobility of sample 3 as determined by experiment along with the temperature dependence predicted by optical mode scattering based on data for  $\eta$  and N.

the results calculated above and recorded in the last column of Table 5-8 are shown in Fig. 5-13 after having been multiplied by a factor equal to (220). This is sufficient to place the values of  $\mu_0$  just above the experimental data. We conclude from this that

$$\frac{\epsilon_s \epsilon_\infty}{\epsilon_s - \epsilon_\infty} > 220 \quad (5-33)$$

Since  $\epsilon_\infty$  is known as a function of temperature, an upper limit for  $\epsilon_s$  can be calculated from this inequality. We calculate that  $\epsilon_s \leq 35$  for  $\epsilon_\infty = 30$  (at 300°K) and  $\epsilon_s \leq 42.5$  for  $\epsilon_\infty = 35.6$  (at 77°K). Furthermore, by inserting this limiting value given by Eq. 5-33 into Eq. 5-26 for  $\gamma$ , the expansion parameter of the perturbation theory, we obtain the result

$$\gamma \leq 0.09 \ll 1,$$

and we conclude that the perturbation theory not only applies for this analysis but that rather rapid convergence should be expected as well.

Before returning to the infra-red reflectivity and the effect of the lattice on the dispersion relations we have gone one step further and combined the acoustical mode mobility shown in Fig. 5-10 with the optical mode mobility of Fig. 5-13. In doing this we recognize that a strictly rigorous approach requires that we add the reciprocals of the relaxation times ( $\tau$ ) characteristic of each of these scattering mechanisms before averaging over the free-carrier kinetic energy. However, since a mean free time can be uniquely defined for optical mode scattering only at temperatures such that  $T > \theta$ , at which temperatures it has been shown that  $\tau_0 \propto E^{1/2}$ , the less rigorous approach of combining mobilities is considerably simpler. Each of these theoretical mobilities contains an arbitrary scale factor which has been adjusted so as to achieve a best fit to the experimental data. The results of this combination procedure are shown in Fig. 5-14.

It can be seen from this figure that a very close fit can be achieved over the entire temperature range of interest. Of course, if one has enough adjustable parameters at his disposal, it is possible to approximate any curve. However, this is not the case here. The only parameters that have been left for

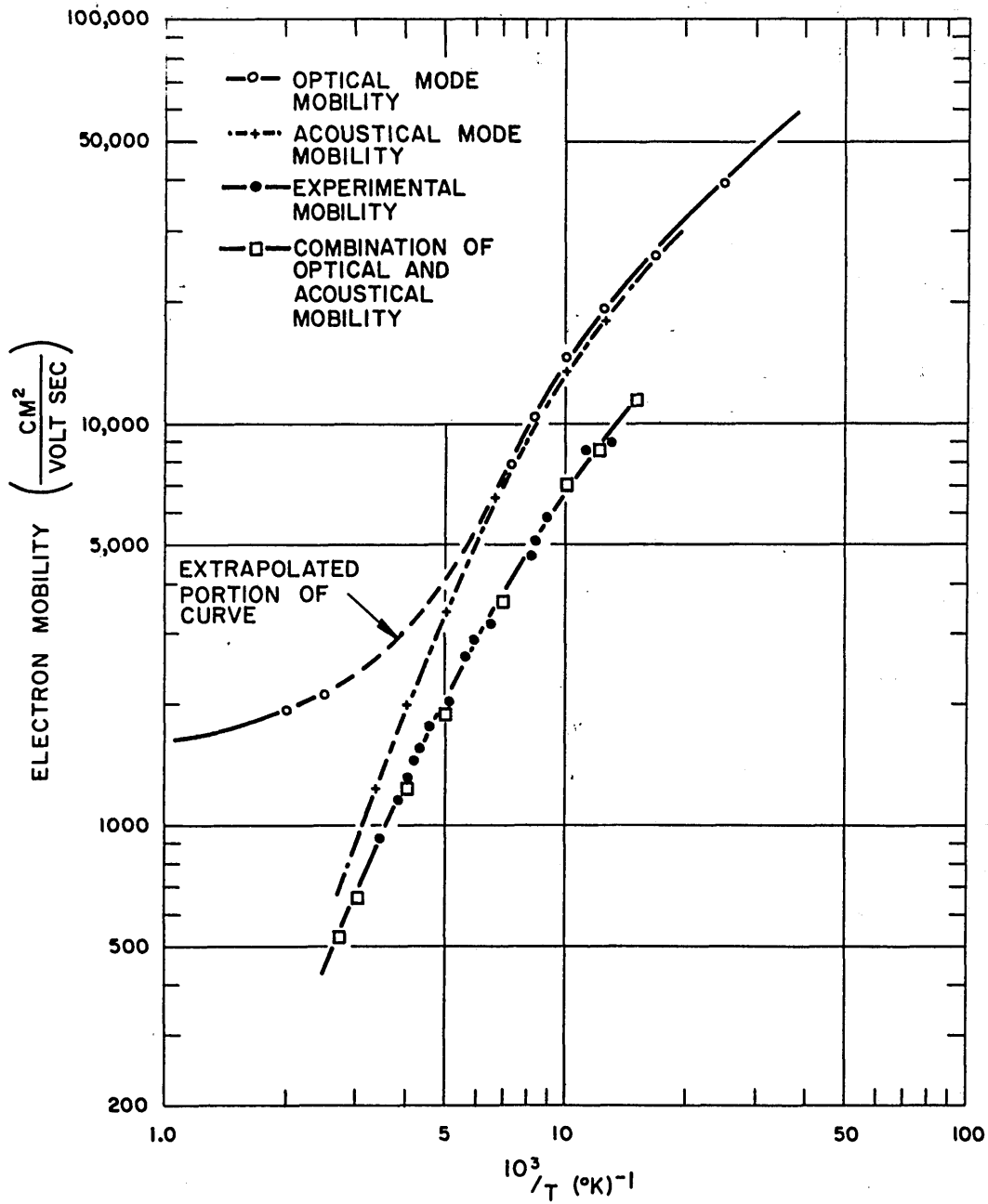


Fig. 5-14 The experimental mobility of sample 3 and the predicted temperature dependences for optical and acoustical mode mobilities which have been scaled so as to "best fit" the experimental data.

final adjustments have been scaling factors for shifting two rather dissimilar curves. Because of this fact, we take heart from the close fit that has been achieved and suggest that the combination of mobilities shown in Fig. 5-14 possibly represents a close approximation to the actual situation. Of course, the primary reason for being able to achieve this fit can be ascribed to the temperature dependences of the effective masses, because this has given us one component mobility,  $\mu_a$ , with a sufficiently high temperature dependence to achieve a fit at the higher temperatures.

The characteristics of the mobilities of Fig. 5-14 will be discussed at greater length as soon as we discuss the uncertainty regarding the contribution of the lattice to the infra-red dispersion. We have established an upper limit for  $\epsilon_s$  from Fig. 5-13, and we can obtain a "most probable" value from Fig. 5-14, specifically the value

$$\frac{\epsilon_s \epsilon_\infty}{\epsilon_s - \epsilon_\infty} = 420 \quad (5-34)$$

Utilizing the results of Eqs. 5-32 and 5-34, we can arrive at the following conclusions.

i. For  $\gamma$ , from Eq. 5-26, we find

$$.09 > \gamma \approx .05$$

a result which completely justifies the applicability of the perturbation-theory approach.

ii. From Eq. 5-22, which was obtained from the expression for the static dielectric constant, we calculate for the ionicity parameter,  $S$ , (assuming an average value for  $\epsilon_\infty = 35$ ):

$$0.09 > S \approx .065$$

This value indicates a rather small degree of ionicity and supports the experimental evidence cited in the Russian literature that homopolar binding predominates in PbTe (and presumably this is also the case for PbS and PbSe).

In passing it is also interesting to note the value that one calculates for the relative static dielectric constant of PbS assuming the same degree of ionicity. For  $N_1 = 1.5 \times 10^{28}$  atom pairs/m<sup>3</sup>,  $Z = 2$ ,  $m = 5.1 \times 10^4 m_0$ ,

$\lambda_t = 80\mu$ , and  $\epsilon_\infty = 17.5$ , one calculates from Eq. 5-20

$$2.3 > \epsilon_s - 17.5 \approx 1.2$$

This leads to a result which is slightly greater than the  $\epsilon_s = 17.9$  value obtained in 1894,<sup>21</sup> but it is considerably less than the value of 70 which has also been put forth.<sup>20</sup> Similarly, for PbTe we conclude that

$$4.8 > \epsilon_s - 30 \approx 2.4$$

iii. Equation 5-19, which compares the contribution of the lattice and of the free electrons to the infra-red dispersion, yields (again assuming an average value for  $\epsilon_\infty = 35$ ):

$$1.2 \times 10^{-2} > \frac{n_{\text{lattice}}^2}{n_{\text{free elec.}}^2} \approx 0.64 \times 10^{-2}$$

From which we conclude that by neglecting the effect of the lattice on the infra-red dispersion, we are neglecting something that amounts to only about 1% of the over-all effect produced by the free electrons. It is to be noted that this is the case for this experiment where the free carrier concentrations are of the order  $3-4 \times 10^{18}$  carriers/cm<sup>3</sup>.

We have now made a complete analytical circle. We started out with an analysis which neglected the effect of the lattice on the infra-red reflectivity, but which enabled us to calculate the free carrier effective masses and their temperature dependences. These effective mass values were checked with existing data and with the energy band structure (i.e. number of valleys). Then, we took these effective mass values and synthesized an electron mobility and compared this mobility with the experimental data. We found that a combination of acoustical and optical mode mobilities could produce a very close fit. From the requirements imposed upon the optical mode component, we have deduced that the material is only very slightly ionic and that the omission of the lattice contribution to the reflectivity is justified.

We wish now to return to Fig. 5-14 and to the composite of acoustical and optical mode mobilities. It can be seen that the acoustical and optical modes are roughly comparable in their scattering effectiveness at the lowest temperatures. At about 150°K the resultant mobilities begin to diverge, with the acoustical modes emerging as the dominant scattering mechanism. Near room temperature and above, the mobility is apparently almost completely determined by the acoustical mode scattering.

This finding is at least qualitatively compatible with the findings reported for the Nernst-Ettingshausen effect.<sup>2</sup> As we recounted earlier, this report recorded a ratio of non-dimensional Nernst-Ettingshausen fields which yielded a function of  $s$ , where  $\tau = \tau_0 E^s$  [see Eq. 5-4]. This function turned out to be zero for  $s = 0$  and positive for negative  $s$ , having a value 0.323 for  $s = -1/2$  as in acoustical mode scattering. Their data are presented below:

Material	Type	$N \times 10^{-18}/\text{cm}^3$	low values		high values	
			$F_y^2/F_x$	T(°K)	$F_y^2/F_x$	T(°K)
PbS	n	6.5	0.1	130	0.25	330
PbSe	p	1.95	.15	130	.3	300
PbSe	p	1.95	.32	300	.34	350
PtSe	n	8.0	.1	135	.22	330
PbTe	n	3.7	.2	200	.31	320
PbTe	n	5.1	.15	200	.25	300
PbTe	n	0.42	.01	125	.03	220

Table 5-9. Data taken from reference 2 pertaining to their measurements of the Nernst-Ettingshausen effect in which the theoretical values for  $F_y^2/F_x$  are 0.323 and zero for  $s = -1/2$  and zero, respectively.

The result that these two scattering mechanisms are comparable over a certain temperature range does force one to recognize that the calculation of the reduced Fermi potential, and subsequently the density-of-states effective mass,

from the thermoelectric power based on the assumption  $s = -1/2$  may be a source of error in the over-all analysis. However, the actual effect of this equivalence of scattering mechanisms could be expected not to be too serious. The basis for this statement is that the equivalence occurs in that temperature range in which the material is strongly degenerate, and the free-carrier kinetic energy is essentially a constant. Moreover, this equivalence of scattering mechanisms should not affect the calculation of the conductivity effective mass. We presume, therefore, that the general picture will not be changed significantly.

In the interest of completeness, there is another bit of information which we have not utilized, namely the scaling factor used to adjust the magnitude of  $\mu_a$  in Fig. 5-14. The significance of this scaling factor can be seen from the equation for acoustical mode mobility.

$$\mu_a = \frac{\pi e \hbar^4 \langle E^{-1/2} \rangle}{\sqrt{2} kT m_d^{3/2} m_c} \frac{C_{11}}{E_1^2} \quad (5-23)$$

Thus, we see that everything except the ratio  $C_{11}/E_1^2$  is calculable from the data obtained in this investigation. Furthermore, the elastic constants for PbTe are reported in a recent abstract.<sup>33</sup> They report the values  $c_{11} = 10.69$ ,  $c_{12} = 0.89$ , and  $c_{44} = 1.31 \times 10^{11}$  dyne/cm<sup>2</sup>. Since  $C_{11}$  is defined by the relation<sup>34</sup>

$$C_{11} = \frac{1}{2} (c_{11} + c_{12} + c_{44})$$

we find that  $C_{11} = 7.10 \times 10^{11}$  dynes/cm<sup>2</sup>. This is to be compared with values of 15.45 and  $19.7 \times 10^{11}$  dynes/cm<sup>2</sup> reported for germanium and silicon, respectively.<sup>35</sup> Moreover, the value of  $E_1$  that is established by means of the scaling factor used for plotting  $\mu_a$  in Fig. 5-14 and this value of  $C_{11}$  is  $E_1 = 14.8$  ev. This value can be compared with values of 13.62 and 12.80 ev which are reported for germanium and silicon.<sup>35</sup> We see that this latter value for  $E_1$  is certainly quite reasonable. This assures us further that we have not imposed any extreme conditions on the properties of PbTe by scaling the acoustical mode component of the mobility as we did in order to fit the experimental data.



Finally, before leaving this discussion of n-type PbTe and passing on to the zero-field reflectivity data for p-type material, we wish to note the unusual behavior which was observed in sample 2 (Fig. 5-7). On the short wavelength side of the free carrier reflectivity minimum at  $4^{\circ}$  and also at  $77^{\circ}\text{K}$ , a very noticeable peak appeared just prior to the reflectivity descent to its minimum. Unfortunately, we have no definite explanation for this behavior. It appears as though something present in the material has a characteristic absorption which is strongly correlated with the free carriers.

In lieu of an explanation we can only recount some of the peculiarities of this particular sample. In the first place, in the order of sample preparation, this sample pre-dates all of the others by several months. (The numbering system 1-5 is indicative of the order in which the samples were placed in the infra-red apparatus.) Moreover, and most probably a contributing factor to this unusual response, this sample was initially rather heavily doped with bismuth. It is the only sample that had any foreign dopant added to it. Since the observed effect appears to be correlated with the free carrier reflectivity, this would seem to indicate the source of this behavior was in some way connected with the free carrier concentration. For this reason, it is strongly felt that the presence of bismuth ions in the lattice is somehow responsible for the observed behavior.

However, this sample has a couple of other very distinguishable variations in its preparation. For instance, its surface was polished as long as two months before it was finally used. Moreover, it was annealed after its surface was polished. This annealing process was otherwise typical -- a temperature of  $750^{\circ}\text{K}$  for 50 hours in an atmosphere produced by a lead-rich mixture of PbTe. Not only did the annealing process pre-date by several weeks its infra-red reflectivity experiment, but it was the only sample which was not subjected to the polishing etch just prior to this phase of the investigation. Finally, the sample contained one very serious crack which fractured completely upon being positioned in the infra-red sample holder.

Considering all of these peculiarities, it is remarkable indeed to see how invariant the principal reflectivity minima are to them. This conclusion is

based on the effective mass behavior which was deduced from the reflectivity minima. It can be seen from Fig. 5-3 that the results obtained for this sample are completely compatible with what was determined for samples 1 and 3.

We turn our attention now to the zero-field reflectivity data of two p-type samples of PbTe. We have already presented the data for the thermoelectric power, Hall coefficient, and free-carrier mobility for these p-type samples in the first pages of this chapter. From these data we determined the contribution by the acoustical mode relaxation time to the mobility temperature dependence and we also obtained the density-of-states effective mass. The temperature dependence of the latter is presented in Fig. 5-4.

The zero-field reflectivity for the two p-type samples is presented in Figs. 5-15 and 5-16. The contrasting shallowness of these reflectivity minima with those of the n-type samples is immediately apparent. For example, no minimum is even distinguishable at 300°K as shown by Fig. 5-15. Part of this shallowness is the result of the inherently lower free-carrier mobility in p-type material. In addition, it can be seen that the correlation between theoretical and experimental curves is much worse for p-type than for n-type material. Certainly the same considerations with respect to the long wavelength absorption edge apply to the p- as well as to the n-type samples. That is, discrepancies arise between the theoretical and experimental curves in the region of high absorption because the depth of penetration becomes very much less, resulting in greater scattering at the surface and in a lower free-carrier mobility. However, the discrepancies between experimental and theoretical curves are not limited to this high absorption region. It can be seen that some of the experimental reflectivities are significantly lower than theory predicts. It is felt that the primary cause of this discrepancy is the fact that p-type material is considerably more difficult to cut and polish without causing extensive damage to the crystal. The p-type samples that were prepared for the infra-red reflectivity measurements has several large cracks in the polished surface. Moreover, the samples were shorter in length than the 2 cm length for which the sample holder was designed. In actual fact, the p-type samples were closer to 1.0 - 1.2 cm in length. These physical defects of cracks and shortness of length make it difficult to obtain absolute values

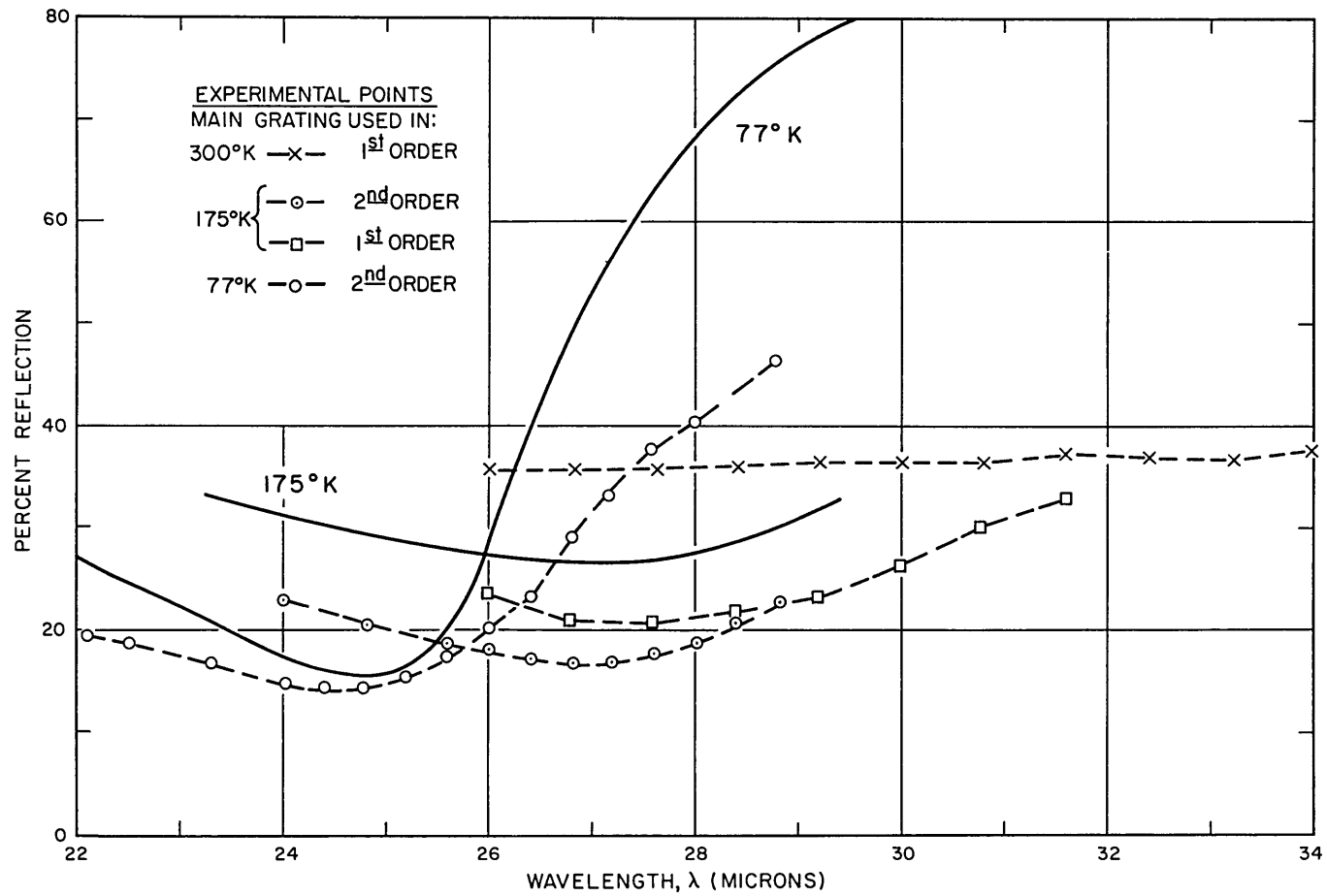


Fig. 5-15 The zero-field infra-red reflectivity of sample 4 as a function of wavelength at 77°, 175°, and 300°K along with theoretical curves at 77° and 175°K are shown as solid curves.

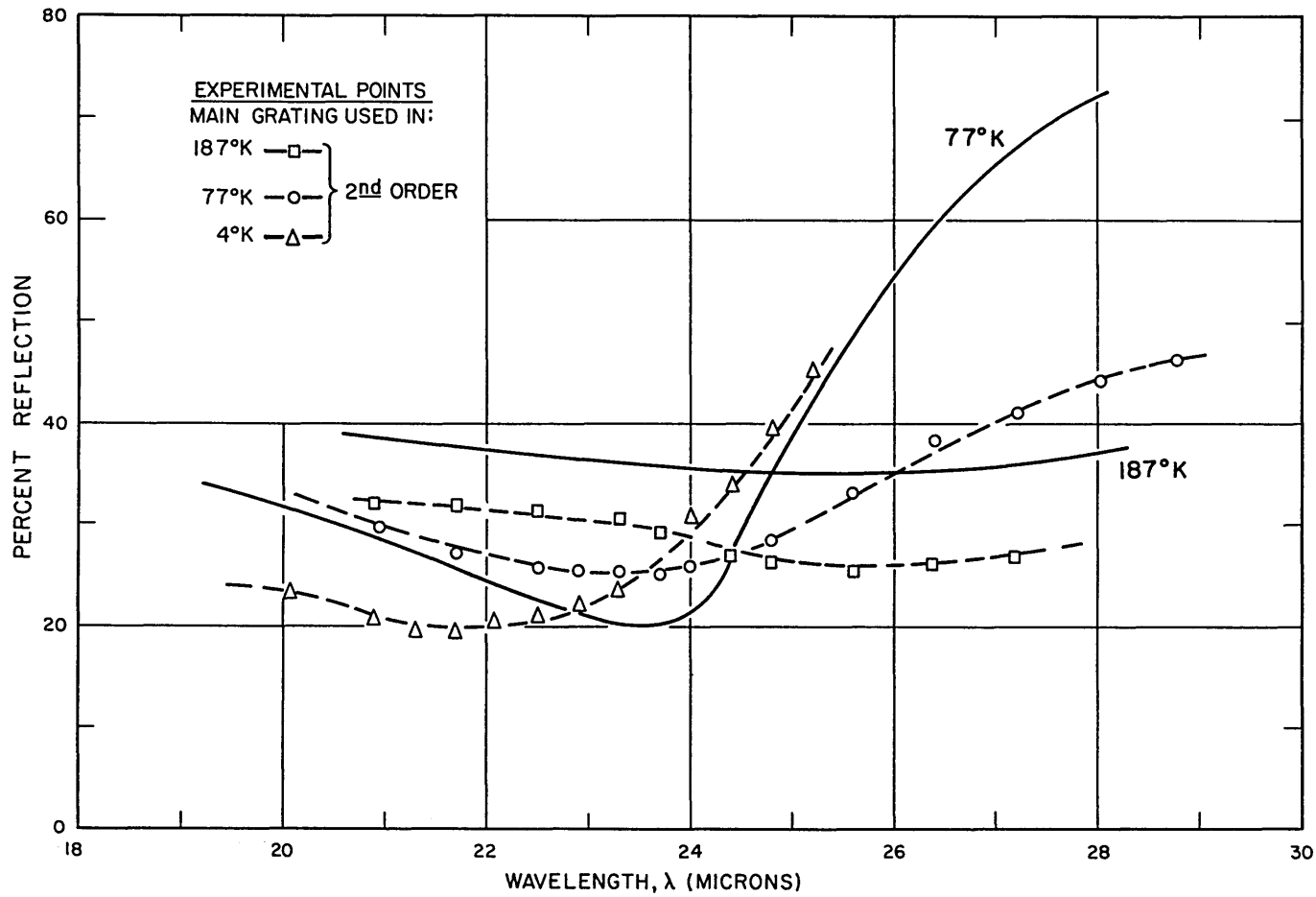


Fig. 5-16 The zero-field infra-red reflectivity of sample 5 as a function of wavelength at 4°, 77°, and 187°K along with theoretical curves at 77° and 187°K shown as solid curves.

of the reflectivity, because some of the incident light gets scattered or else misses the sample altogether. The amount of this loss of signal varies with the position of the sample in the beam. Since the vertical position of the sample was adjustable, it was possible to observe this point. That is, the percent reflection of these two p-type samples could be changed by raising and lowering the sample holder by means of a hand-hydraulic pump. Generally, the vertical position of the sample was adjusted to maximize the reflection, but this was a rather coarse adjustment. It is estimated that such effects could diminish the absolute percent reflection by as much as 15 % . Because of these difficulties with the sample preparation, we estimate that the error in the absolute values of the effective masses obtained for the p-type samples may be as high as  $\pm 15\%$  compared with an estimated error of  $\pm 10\%$  for the n-type samples. However, in both cases we feel that the relative values of  $m_c^*$  determined at different temperatures have a higher degree of accuracy.

In spite of these experimental difficulties encountered with p-type material, the gross features of the infra-red reflectivity are quite similar to those obtained with n-type material. That is, a minimum does appear, for the lower temperatures at least, in this range of wavelengths, and this minimum shifts to longer wavelengths as the temperature is increased.

In analyzing the experimental reflectivities, the procedure that has been followed is exactly parallel to that presented for the n-type material. We take account of the temperature dependence of the high-frequency dielectric constant by using the values listed in Table 5-3. The free-carrier concentrations are those listed in Table 5-2; the free-carrier mobilities are shown in Fig. 5-5, and the wavelengths of the reflectivity minima have been obtained from Figs. 5-15 and 5-16. With these data we have calculated values for the conductivity effective mass as a function of temperature using Eq. 2-10. The data utilized in these calculations and the results are presented in Table 5-10 and the latter are also shown in Fig. 5-4.

Sample	T (°K)	$\mu$ $m^2/\text{volt sec.}$	$\lambda_0$ microns	$m_c^*$
4	77	.48	24.6	0.055
	170	.15	27.1	.079
5	4	undetermined	21.7	.044
	77	.32	23.3	.055
	187	.072	25.6	.086

Table 5-10. Data pertinent to the calculation of the conductivity effective mass of samples 4 and 5. Again, it has been assumed that  $\rho = \omega_0 \tau \gg 1$  at 4°K where the mobility was not determined.

In addition to the results obtained from our infra-red reflectivity data, we show a conductivity effective mass value at room temperature which was deduced from the high absorption region of the infra-red reflectivity of a p-type sample having a hole concentration of  $3 \times 10^{18}$  holes/cm<sup>3</sup>.<sup>36</sup> It can be seen that this value is very compatible with the magnitude and temperature dependence of the conductivity effective mass determined in this study.

It is noted that the temperature dependence of the conductivity effective mass is slightly, greater in p-type material than it is in n-type. A similar increased dependence has been observed with regard to the density-of-states mass.

Having thus calculated values for  $m_{cp}^*$  and  $m_{dp}^*$ , in order to proceed with the analysis in the manner employed for n-type material, it is necessary to establish the value of the anisotropy ratio K. However, at the present time there is some question concerning the true value of K. We have noted that one study has proposed the values of 4.7 at 300°K and 4.2 at 77°K.<sup>37</sup> However, another report suggests that the value to be assigned to K is 6.4 at 4°K.<sup>38</sup> The former values were deduced from magnetoresistance data while the latter was obtained from a study of the de Haas-van Alphen effect in which it was also concluded that there is a valence band maximum at the center of the zone in addition to the ones already confirmed along the  $\langle 111 \rangle$  axes. The discrepancy between the two values may be reconcilable, because in the latter report the 6.4 value is ascribed solely to the  $\langle 111 \rangle$  ellipsoids of revolu-

tion. That is, they distinguish between these maxima and the one at the zone center. Magnetoresistance measurements cannot be so discriminating and so the values resulting from that study would necessarily be averages over the entire valence band energy surface.

The presence of a valence band maximum at the zone center greatly complicates the analysis of the effective masses. The conductivity and density-of-states masses that are obtained from the analysis of the infra-red data and of the reduced Fermi potential are average values associated with the entire valence band. That is, they represent an average of the effective masses of all five valence band maxima. Consequently, the simple relations used in the analysis of n-type material to obtain the number of equivalent ellipsoids,  $m_l$ , and  $m_t$  are not expected to be applicable in the analysis of the valence band. However, it is instructive to apply these simple relations to the effective masses of the valence band just to see what the results of such an analysis might be. To this end we have calculated an  $N_v$  from Eq. 5-14 using the values for K determined from the magnetoresistance data.

$$N_v^{2/3} = \frac{m_d^*}{m_c^*} \frac{3 K^{2/3}}{2 K + 1} \quad (5-14)$$

The results of this calculation are as follows:

T (°K)	$(m_d^*)_{avg.}$	$m_c^*$	K	$(N_v)^{2/3}$	$N_v$
77	0.14	0.055	4.2	2.1	3.1
190	.19	.086	4.5	1.8	2.4
300	.25	.11	4.7	1.8	2.4

Table 5-11. Data used in Eq. 5-14 for the calculation of an "effective" number of equivalent ellipsoids in the valence band.

The number of equivalent ellipsoids of constant energy in the valence band which is deduced from these values for the effective masses is seen to be

something less than four. Although it is difficult to infer very much from this calculation, it does seem reasonable to conclude that the (111) maxima are probably at the zone edge since the "effective" number deduced from Eq. 5-14 is even less than four. Such a conclusion is in line with the results of the investigation of the de Haas-van Alphen effect referred to above.<sup>38</sup> Moreover, these results may also be interpreted to mean that a zone-centered valence band maximum is rather significant in the energy band structure of the valence band. This conjecture is based on the idea that the number of ellipsoids would be four if the (111) maxima dominated, could be as high as five if the (000) and (111) maxima had very similar characteristics, and would be less than four and approach unity as the (000) maximum became the most prominent. In this regard, it should be pointed out that Allgaier has concluded from a careful analysis of the Hall effect that the zone-centered maximum does have an increasing importance as temperature increases.<sup>39</sup>

Even though we cannot be more quantitative with regard to the composition of the effective masses and to the number of equivalent ellipsoids, we can still synthesize an acoustical mode mobility from the data for  $m_d^*$ ,  $m_c^*$  and  $\langle E^{-1/2} \rangle$ . However, we recognize that such a synthesis assumes implicitly that the scattering mechanism is isotropic, or at least has the same energy dependence, in both the (000) and (111) minima. Realizing that this assumption is contained in this analysis, we proceed to calculate an acoustical mode mobility using Eq. 5-20.

$$\mu_a = U m_d^{*-3/2} m_c^{*-1} T^{-1} \langle E^{-1/2} \rangle \quad (5-20)$$

where it is recalled that  $U$  is an arbitrary scaling factor. The data utilized for this calculation are presented below:

$T$ ( $^{\circ}K$ )	$m_c^*$	$m_d^*$	$E^{-1/2}$
80	0.056	0.14	5.5
100	.061	.15	5.5
150	.075	.17	5.45
200	.088	.19	5.3



T (°K)	$m_c^*$	$m_d^*$	$E^{-1/2}$
250	.100	.215	5.15
300	.110	.245	5.00

Table 5-11. Data obtained from Figs. 5-2 and 5-4 and which have been utilized to calculate  $\mu_\alpha$  from Eq. 5-20.

The results of this calculation are shown in Fig. 5-17 along with the data for sample 4. The scaling factor  $U$  has again been chosen so that the two curves give approximately the same mobility at 300°K. It is apparent from the figure that the temperature dependence of the experimental mobility near 300°K is quite well represented by  $\mu_\alpha$ , which has been synthesized from the data. The fit is even better at these temperatures than it was for the n-type material. This result indicates that there is probably an even smaller contribution near 300°K by another scattering mechanism than was deduced for n-type material. However, there is a significant discrepancy between the two curves near 100°K, similar to that which we have observed for n-type material.

By comparing the results for n- and p-type material, it seems reasonable to conclude that a similar combination of scattering mechanisms, i.e. acoustical and optical mode scattering, can be utilized to fit the actual temperature dependence of the mobility. To show that this is, at least, approximately the case, we show also in Fig. 5-17 the mobility values which are obtained by combining the values of  $\mu_\alpha$  (shown in Fig. 5-17) with the optical mobility values (of Fig. 5-14) which were used to obtain a "best fit" to the experimental values for n-type material. To be sure, the optical mode mobility values shown in Fig. 5-14 were calculated on the basis of the data for sample 3. However, since the carrier concentrations of samples 3 and 4 are not very different,  $3.3$  vs.  $3.8 \times 10^{18}$  carriers/cm<sup>3</sup>, and since  $G(z, \eta)$  is not a strong function of  $\eta$  for  $\eta > 5$  (see Fig. 5-12), it does not represent a bad approximation to utilize the optical mode mobility values of Fig. 5-14. The results of this combination of mobilities, the acoustical and optical mode mobility, are in reasonably good agreement with the experimental data. The fact that at the lowest

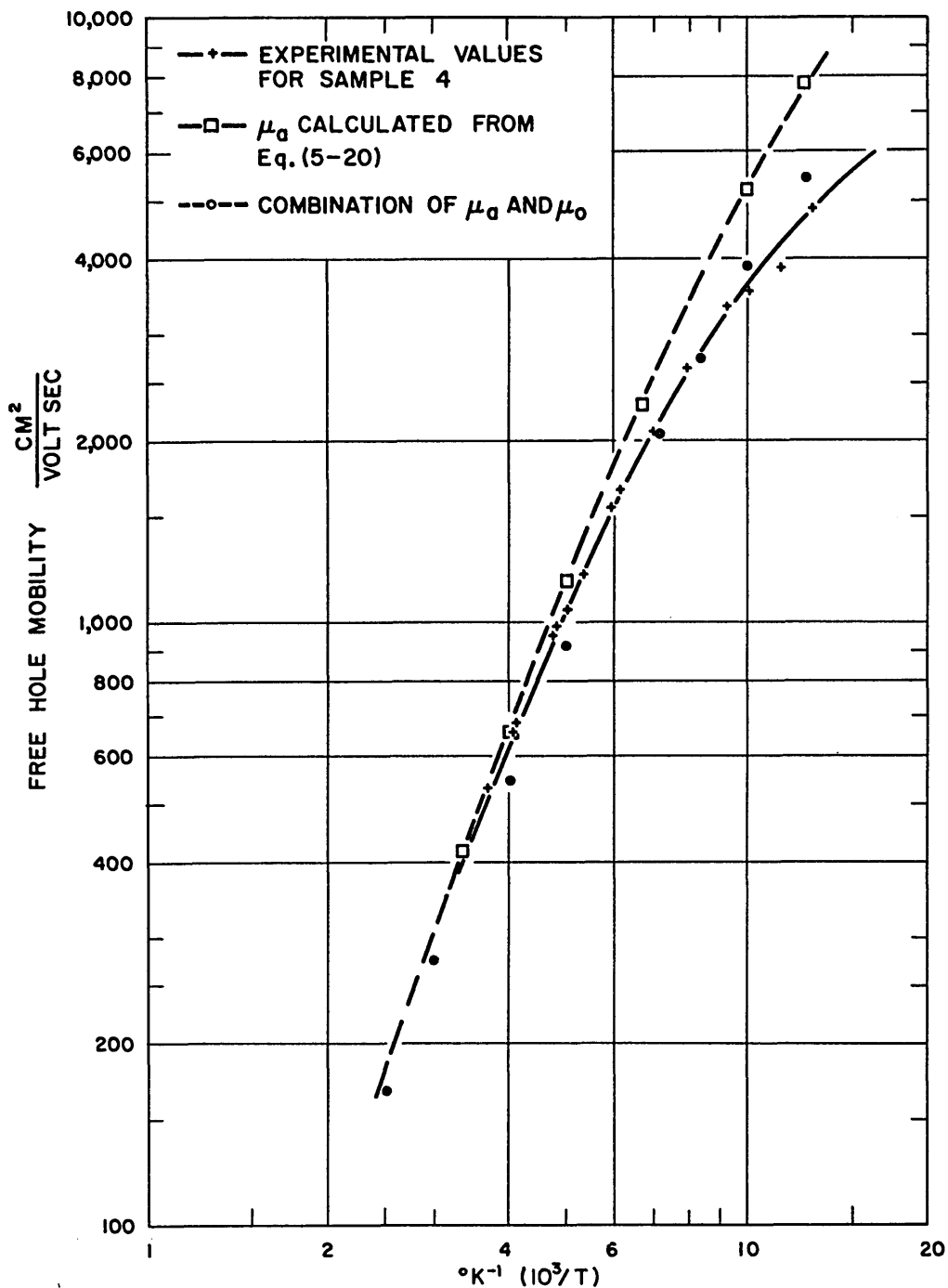


Fig. 5-17 A comparison of the temperature dependence of the free-hole mobility of sample 4 as determined experimentally with that which our data would indicate for acoustical mode scattering. Also included are points calculated from a combination of mobilities  $\mu_a$  (from this figure) and  $\mu_0$  (from Fig. 5-14).

temperatures ( $\sim 100^{\circ}\text{K}$ ) the combined mobility appears to be rising more rapidly than the experimental mobility can possibly be explained by the fact that these p-type samples were not annealed. Thus, the mobility at these lower temperatures could be decreased by scattering at dislocations in the lattice. This idea seems all the more reasonable in view of the fact that after the single-crystalline ingots were grown in the Bridgman furnace, they were quenched from about  $750^{\circ}\text{C}$ . Thus, the dislocations which exist at that relatively high temperature (melting temperature =  $924^{\circ}\text{C}$  for PbTe) were effectively frozen in since these p-type samples were not annealed afterward. However, to examine this point in any detail would require experimental data below  $80^{\circ}\text{K}$ . Nevertheless, above  $100^{\circ}\text{K}$ , we see that a combination of optical and acoustical mode mobility is sufficient to explain the principal characteristics of the observed experimental data for p-type material.

Consequently, we see that even though the condition of the sample surface has been inferior for p-type material, compared with that of the n-type samples, the reflectivity minimum is still observable. The position of the minimum has shifted to longer wavelengths with increasing temperature. It should be noted that this is the exact opposite of the shift that would result if it were assumed that  $m_c$  were constant while  $\epsilon_{\infty}$  decreases and/or  $\mu$  decreases with increasing temperature.

Moreover, the position of the minimum is sufficiently well-defined to calculate the conductivity effective mass for holes in the valence band. It has been noted that the effective mass that is obtained increases with temperature at a rate almost the same but slightly greater than that observed for n-type material. This temperature dependence when combined with that of  $m_d$  and of  $\langle E^{-1/2} \rangle$  in the manner prescribed by acoustical mode lattice scattering, yields a mobility which can account for the observed temperature dependence near room temperature and presumably, therefore, at higher temperatures also. Furthermore, with a small admixture of optical mode scattering, it is possible to fit the observed temperature dependence down to  $100^{\circ}\text{K}$ , which is the desired result.

The third and final area of consideration under the general heading of infra-red reflectivity is that of the magnetoplasma effect. It has already

been pointed out this effect is the splitting and shifting of the infra-red reflectivity minimum in the presence of a magnetic field. In addition to the magnetic field this procedure requires a polarizer in the infra-red beam. The theoretical expressions describing this splitting effect have been presented for the cases:<sup>40</sup>  $\vec{B} \parallel \vec{\phi}$  ( $\vec{\phi}$  is the propagation vector) in the presence of circularly polarized light, and  $\vec{B} \perp \vec{\phi}$  for linearly polarized light such that  $\vec{B} \perp \vec{E}$  (where  $\vec{E}$  is the electric field vector of the incident light). In the case that  $\vec{B} \perp \vec{\phi}$  and the light is polarized such that  $\vec{B} \parallel \vec{E}$ , no shifting of the minimum occurs.

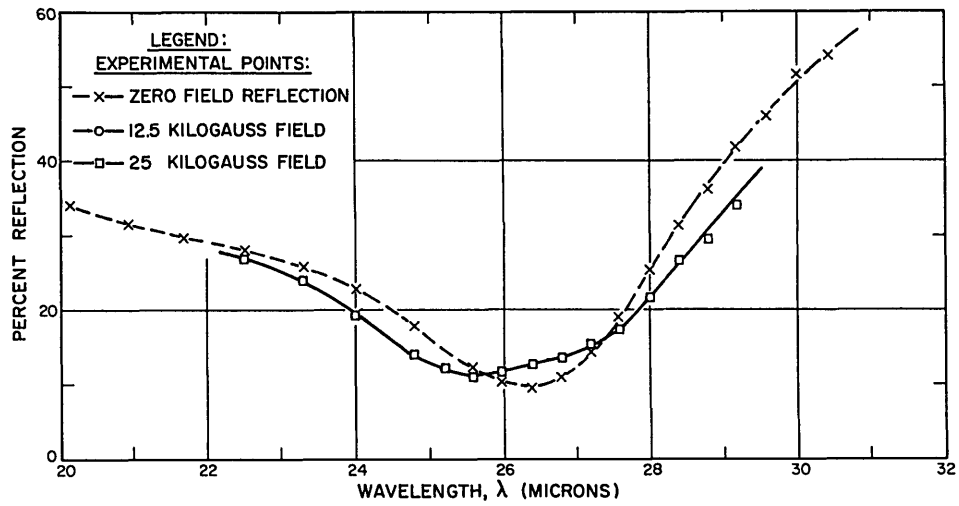
It has also been pointed out that, when a shifting of the minimum does occur which is linear with the magnetic field, the displacement to either side of the zero-field minimum is given by Eq. 2-9.

$$\Delta\omega = \frac{eB}{2 m_t} \frac{K + 2}{2K + 1} \quad (2-9)$$

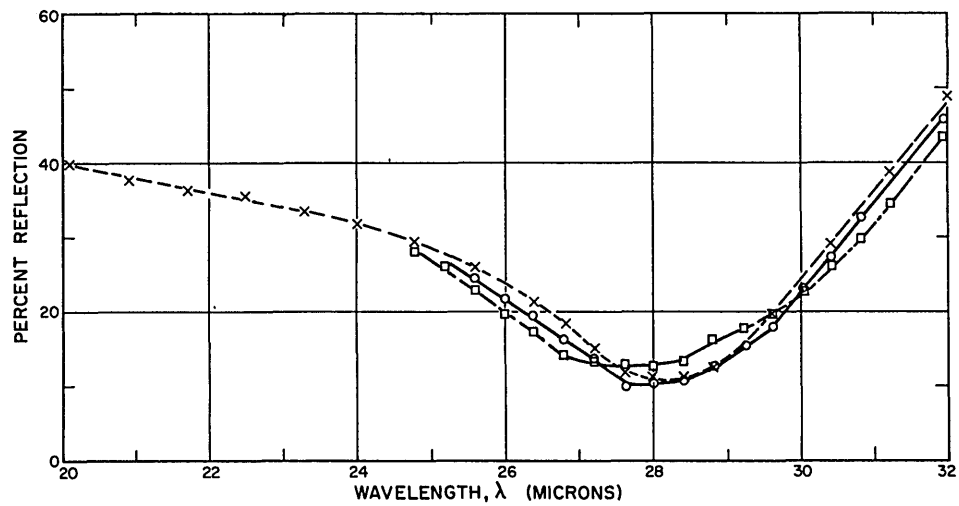
We calculate on the basis of  $m_t = 0.08 m_0$ ,  $K = 4.0$ ,  $B_1 = 25$  kilogauss (maximum available) and a zero-field reflectivity minimum at  $27\mu$  that the expected shift is of the order of one micron.

The actual magnetoplasma shifts which were observed are shown in Fig. 5-18 through 5-21. Perhaps the most striking feature of the magnetoplasma shifts which were observed is their lack of definition. It is almost impossible to determine the amount that the minimum has been shifted because of the broadness of the minima. This is not to imply that the magnetoplasma shift cannot be used to determine the effective mass. However, using our experimental set-up, it is impossible to obtain better than an order-of-magnitude determination of the effective mass from the observed splitting of the zero-field reflectivity minimum.

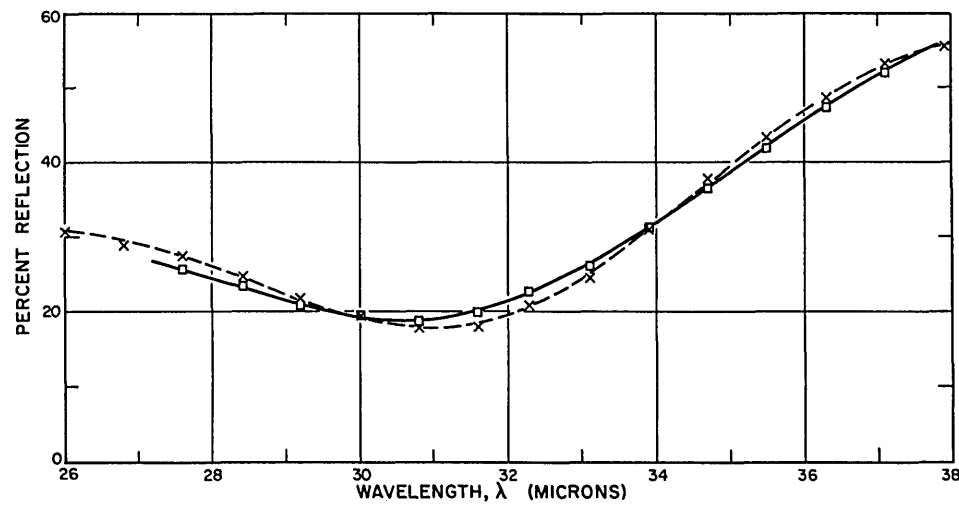
One reason for this has to do with the experimental apparatus used. In this apparatus the magnetic field is perpendicular to the propagation vector, and therefore the infra-red radiation must be linearly polarized such that  $\vec{B} \perp \vec{E}$  for shifting to be observed. Unfortunately, the light in this apparatus is only partially polarized in this manner. That is, there is a significant component of light whose polarization is such that  $\vec{B} \parallel \vec{E}$ .



(a) TEMPERATURE 4°K



(b) TEMPERATURE 77°K



(c) TEMPERATURE 194°K

Fig. 5-18 Magnetoplasma effect in n-type PbTe sample 1.

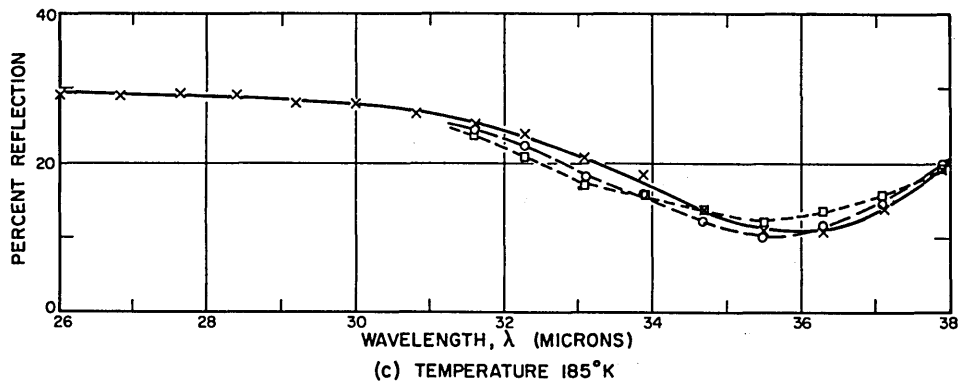
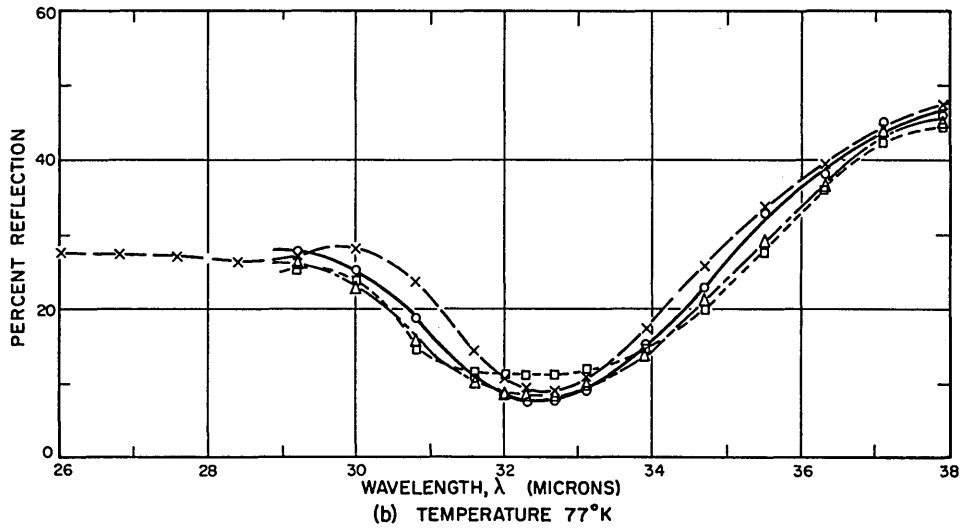
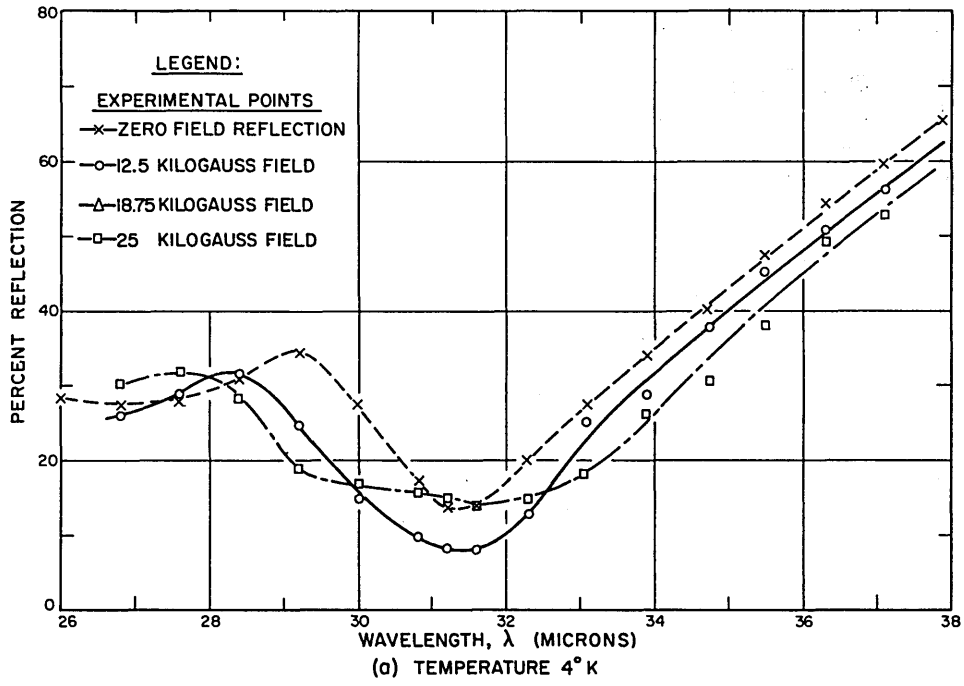


Fig. 5-19 Magnetoplasma effect in n-type PbTe sample 2.

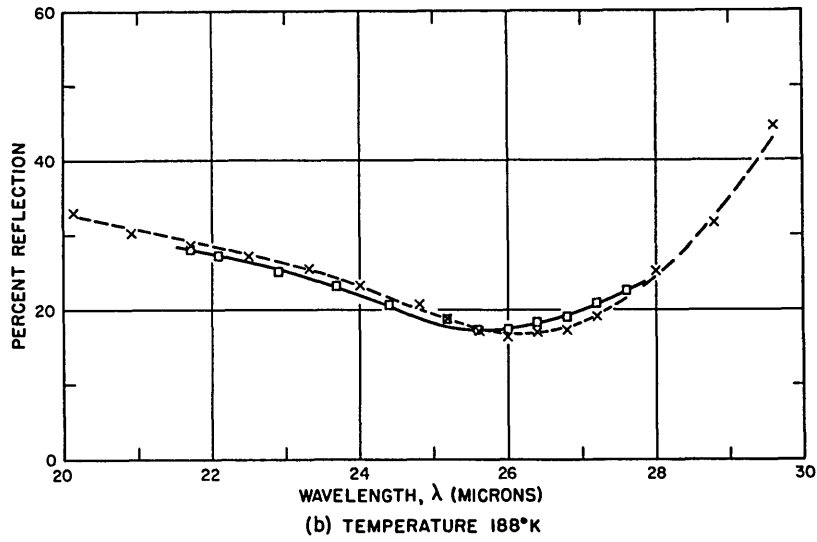
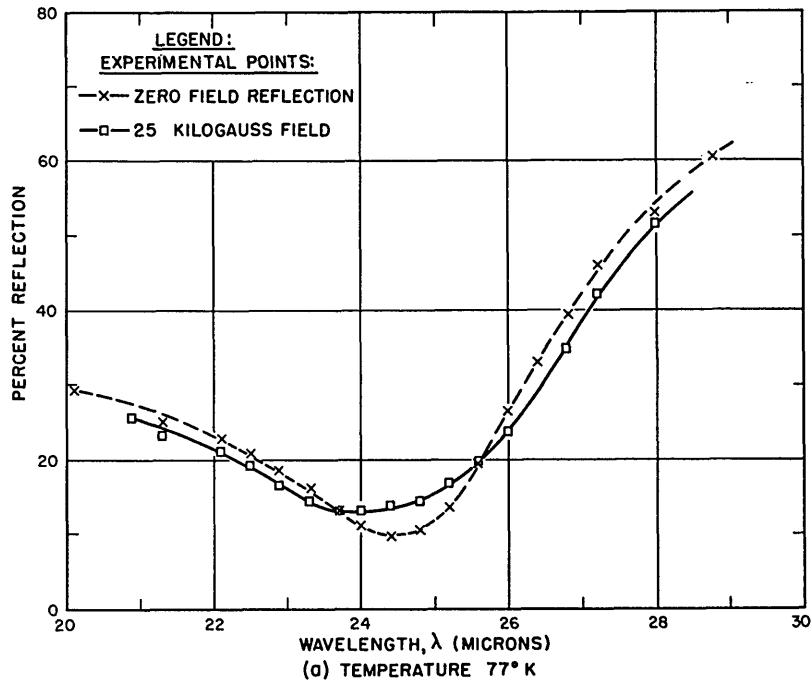


Fig. 5-20 Magnetoplasma effect in n-type PbTe sample 3.

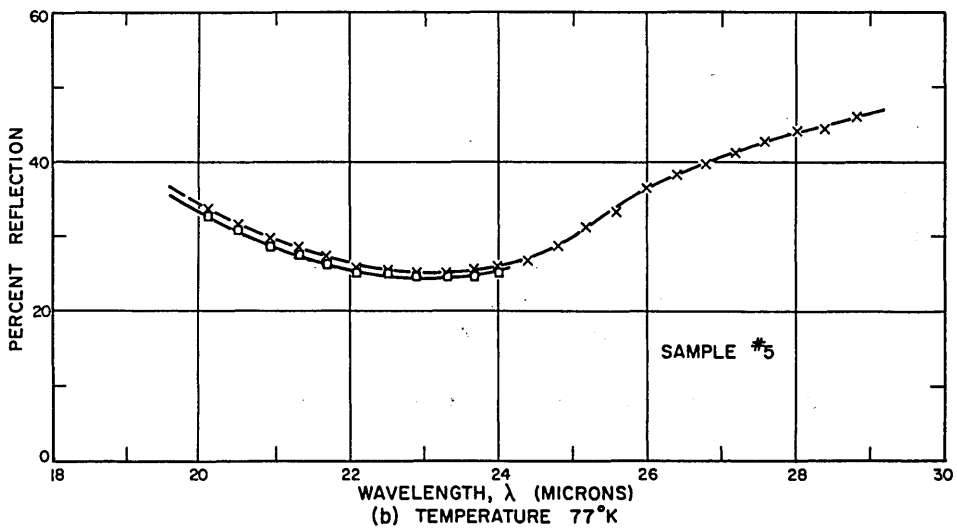
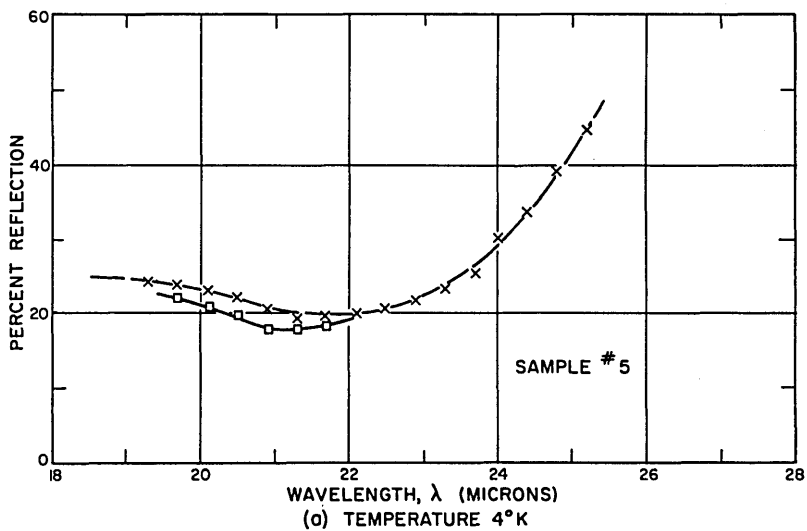
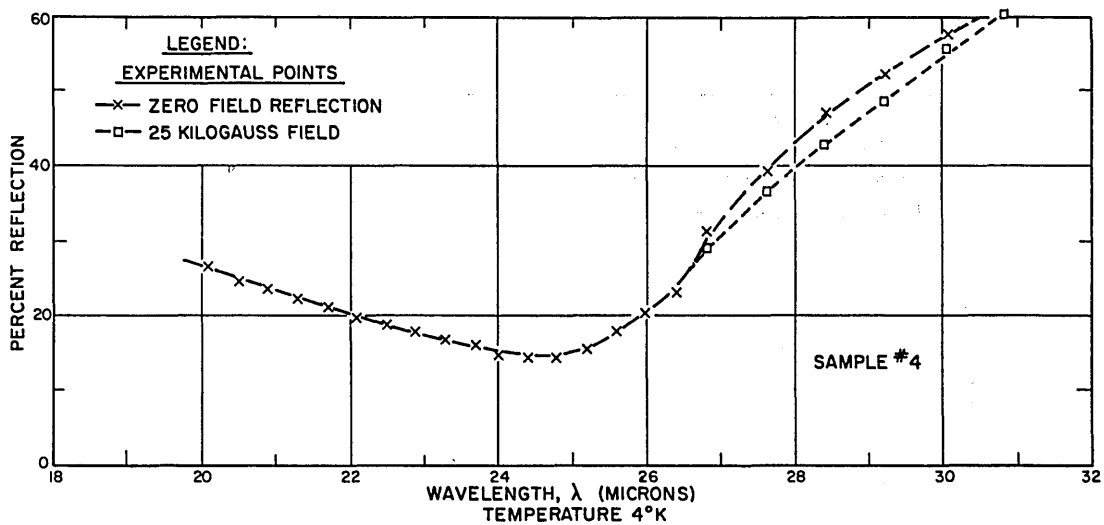


Fig. 5-21 Magnetoplasma effect in p-type PbTe samples 4 and 5.



The reflectivity of this latter polarization is not shifted by the magnetic field so that what we have recorded is a superposition of the shifting which results for  $\vec{B} \perp \vec{E}$  and the zero-field reflectivity. It is no wonder, therefore, that the shifting which we have recorded is less than is expected from Eq. 2-9. The effects on the magnetoplasma shift of incompletely polarized light are so serious that it does not seem worthwhile to speculate concerning the effects of the sample surface on the magnetoplasma shift.

In addition to these difficulties with regard to the determination of the magnetoplasma shift, and therefore of the conductivity effective mass, there are certain limitations which are inherent in this method. In the first place, the size of the magnetic fields that are required to obtain even a nominal amount of shifting represents a serious consideration. Secondly, in this region of the infra-red spectrum, at least, the shifting is quite small and large inaccuracies arise in the process of taking differences of two nearly equal quantities.

Because of these considerations, it is felt that not much significance should be attributed to the results obtained from these magnetoplasma results. However, since a shift has been observed in PbTe, it would be worthwhile for someone to perform the experiment with carefully polished samples and highly polarized infra-red light.

As a matter of interest, the results obtained from the magnetoplasma shift recorded in Figs. 5-18 through 5-21 are tabulated below:

T(°K)	Wavelength shift of minimum for samples 1-5 for B = 25 kilogauss (in microns)					Effective masses from Eq. 2-9					from Eq. 2-10 * m <sub>c</sub>	
	$\Delta\lambda_1$	$\Delta\lambda_2$	$\Delta\lambda_3$	$\Delta\lambda_4$	$\Delta\lambda_5$	* m <sub>c1</sub>	* m <sub>c2</sub>	* m <sub>c3</sub>	* m <sub>c4</sub>	* m <sub>c5</sub>	1-3	4,5
4	0.8	1.0	--	--	0.7	0.091	0.10	--	--	0.071	0.054	0.044
77	0.9	0.8	0.8	--	0.4	0.094	0.137	0.078	--	0.14	0.061	0.055
190	0.7	0.45	0.7	--	--	0.14	0.317	0.10	--	--	0.085	0.085

Table 5-13. Data obtained from Eqs. 5-18 through 5-21 for the magnetoplasma shift and the resultant effective masses calculated from Eq. 2-9.

About the only consistent comparison which exists between the magnetoplasma effective masses and those calculated from the position of the reflectivity minima is that they invariably increase with temperature. However, the absolute magnitudes differ by a minimum of a factor of two, and the rate of change with temperature is generally quite different. It is to be noted also that the effective masses calculated from the magnetoplasma shift are invariably larger than those obtained from the position of the reflectivity minima. This is consistent with the idea that the lack of completely polarized light results in a smaller shift of the minima than that predicted by Eq. 2-9.

Finally, there is one last aspect to this investigation of PbTe. It has been noted in Chapter I that an uncertainty exists with regard to the actual temperature dependence of the thermal conductivity of PbTe. It has been suggested that an extra conduction mechanism of very significant proportions exists in this material. We have made measurements of the thermal conductivity from 100° to 300°K to see if any apparent anomalies of the sort reported could be observed. Since the temperature at which these effects reportedly begin is in the neighborhood of 250° K, and, moreover, since it has been reported that these effects are so significant that the thermal conductivity passes through a minimum very near 300°K, it is reasonable to assume that some indication of this anomalous behavior would be observed within the temperature range of this investigation.

We took extreme care to see that the variables in the system were very closely controlled: the contacts to the sample were made with solder; all leads coming out of the system were thermally grounded to the heat sink; the pressure inside the system was maintained at 1-5 $\mu$  of Hg, and the system was allowed to come to equilibrium for several hours between measurements. Even with this extreme caution it is felt that the results are limited to an accuracy of  $\pm 5\%$ .

The data which have been obtained are shown in Fig. 5-22. For comparison the temperature dependence reported by Deviatkova is reproduced.<sup>41</sup> It is his data which has served as a basis for the existence of an extra thermal conduction mechanism. Also, for comparison we show the results which have been reported by Kanai and Nii.<sup>42</sup> Our data do not agree completely with either of

these other reports in that the thermal resistivity of our samples is somewhat higher than that of Kanaii and Nii at the lower temperatures and does not show any indication of the tendency to reach a maximum and then to decrease as does that of Deviatkova. Moreover, if any change from a linear dependence of the thermal resistivity on temperature is observed, it is such as to cause  $1/\kappa$  to increase and not to decrease. Such a result is not wholly unreasonable if one considers the equation for the thermal conductivity.

$$\kappa = \kappa_e + \kappa_1 \quad (5-35)$$

where  $\kappa_1$  is the contribution made by the lattice and  $\kappa_e$  is the contribution due to free carriers. For an extrinsic conductor of arbitrary degeneracy, the latter is defined by the equation:<sup>6</sup>

$$\kappa_e = L \sigma T \quad (5-36)$$

where

$$L = \frac{(\frac{3}{2} + s)(7/2 + s) F_{1/2 + s} F_{5/2 + s} - (\frac{5}{2} + s)^2 F_{3/2 + s}}{(\frac{3}{2} + s)^2 F_{1/2 + s}^2} \left(\frac{k}{e}\right)^2$$

in which  $s$  and  $F_r$  are again the scattering mechanism parameter and the Fermi-Dirac integral, respectively. If we assume temporarily that  $L$  is a constant and that for lead telluride  $\sigma \propto T^{-5/2}$  and furthermore that  $\kappa_1 \propto T^{-1}$  (as is usually observed in semiconductors at these temperatures), then Eq. 5-35 can be written in the form

$$\kappa = MT^{-3/2} + NT^{-1} \quad (5-37)$$

where  $M$  and  $N$  are constants, independent of temperature.

From these we obtain the result

$$\frac{1}{\kappa} = \frac{T^{3/2} \bar{M}}{1 + \frac{NT}{M}} \quad (5-38)$$

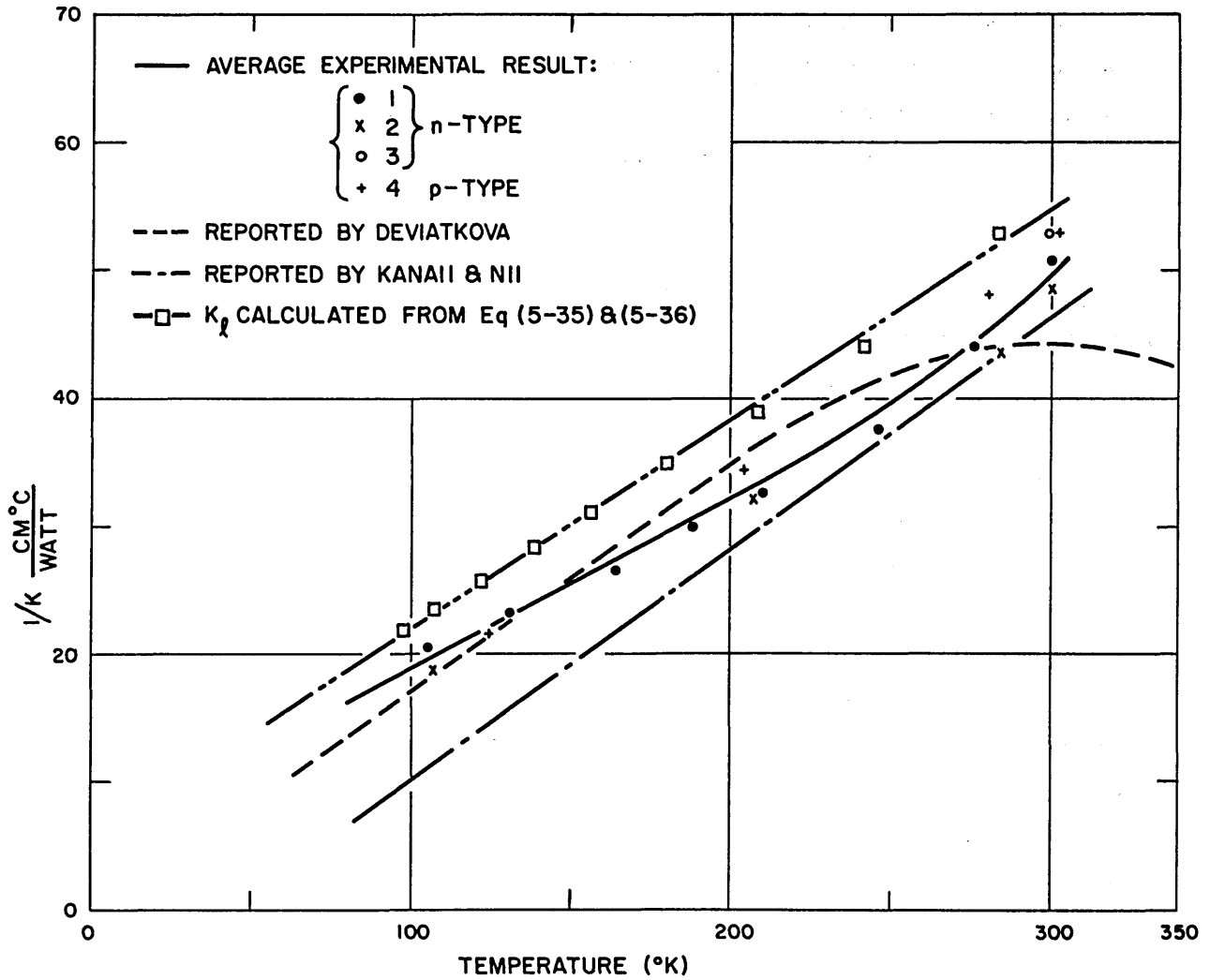


Fig. 5-22 The total thermal resistivity measured for PbTe between 100° and 300°K in this investigation and as reported by Deviatkova and by Kanai and Nii. Also shown is the lattice component of K as deduced from theoretical calculations of  $K_l$ .

We note from Eq. 5-38 that the thermal resistivity can have a temperature dependence which is greater than  $T^{-1}$ . Moreover, as was pointed out in Chapter IV, the neglect of radiative heat losses from the sample surface has the effect of decreasing the thermal resistivity. So the observed increase cannot be attributed to that mechanism. Consequently, we conclude that the slight increase above a  $T^{-1}$  dependence which was observed near room temperature may be really present. However, to be completely sure, it would be necessary to extend these measurements to higher temperatures.

Theoretically, it is possible to utilize thermal conductivity data to deduce the free-carrier scattering mechanism. This can be seen from Eq. 5-36 which in the limit of non-degeneracy reduces to

$$\kappa_e = \left(\frac{5}{2} + s\right) \left(\frac{k}{e}\right)^2 \sigma T \quad (5-39)$$

Consequently, a plot of  $\kappa$  as a function of the electrical conductivity at a fixed temperature and for non-degenerate statistics should yield a straight line of slope  $\left(\frac{5}{2} + s\right) \left(\frac{k}{e}\right)^2 T$ . However, in actual practice this is not a very reliable procedure because of two inherent limitations. First of all, the difficulties encountered in controlling the path of the heat flow and of making good thermal contacts to the sample limit the accuracy of the measurement. Secondly, in order to use Eq. 5-39, which involves  $s$  in a very simplified way compared with the general relation, one is restricted to regions of complete non-degeneracy. This restriction limits one to samples in which the electronic contribution to the total thermal conductivity is 10% or less. This estimate is based on the fact that  $\kappa_e$  of sample 1 has been calculated and at room temperature it amounts to slightly less than 14% of the total thermal conductivity. Moreover, the region of complete non-degeneracy is not reached until 400° to 500°K for these samples. It is also to be noted that the general equation for  $L$ , for an arbitrary degree of degeneracy, involves a difference of two nearly equal quantities, a fact which tends to reduce the reliability of calculations based on this expression. Moreover the value of  $L$  does not change very much between the ranges of total degeneracy and complete non-degeneracy. The change is from  $\frac{\pi^2}{3}$  to  $(5/2 + s)$ .

For these reasons an analysis of the thermal conductivity to yield information about the scattering mechanism has not been attempted. However, the electronic contribution to the total thermal conductivity of sample 1 has been calculated using Eq. 5-36 which is valid for an arbitrary degree of degeneracy. This calculation has been based on an acoustical mode scattering mechanism ( $s = -1/2$ ), the values of  $\eta (T_1)$  listed in Table 5-1, and a short table of Fermi-Dirac integrals.<sup>5</sup> The data pertinent to this calculation are shown in the table below:

$\eta$	$T(^{\circ}K)$	$\sigma \times 10^{-3} \text{ (ohm-cm)}^{-1}$	$\kappa_e \times 10^3 \text{ (watts/cm}^{\circ}C)$
4.0	98	4.3	8.2
3.5	107	3.75	8.8
3.0	122	3.0	7.3
2.5	138	2.45	6.55
2.0	156	2.0	5.8
1.5	180	1.55	5.05
1.0	208	1.2	4.3
0.5	241	0.90	3.65
0.0	283	0.66	3.02

Table 5-14. Data used to obtain the electronic contribution to the total thermal conductivity.

The lattice component,  $\kappa_l$  in Eq. 5-35, has been determined using these calculated values of  $\kappa_e$  and the average values of  $1/\kappa$  represented by the solid curve in Fig. 5-22. The results of this calculation are shown in the same figure. It can be seen that the actual lattice conductivity is quite well approximated by a  $1/T$  dependence. The deviations about the line drawn are less than  $\pm 3\%$ . Moreover, it can be seen that the lattice component determined here parallels very closely the total thermal conductivity reported by Kanai and Nii.<sup>42</sup> The lattice component calculated by them has not been added to the figure because they report a curve which is approximately parallel

to their experimental  $\kappa$  , only shifted upward by about 3-4  $\text{cm}^{\circ}\text{C}/\text{watt}$ . Because of this comparison of the data of Kanaii and Nii with our data and because absolutely no tendency whatsoever for the thermal resistivity to peak or decrease was observed, we conclude that there is no anomalous component present in the thermal conductivity of PbTe of the nature reported, at least, not below  $300^{\circ}\text{K}$ .

## CHAPTER V

### BIBLIOGRAPHY

1. Goldsmid, H. J., Applications of Thermoelectricity, p. 33 (Methuen's Monographs on Physical Subjects, 1960).
2. Tsidil'kovskii, I. M., The Dispersion of Current Carriers in Compounds of the PbS Group, Phys. Metals and Metallography 8, 4, 16-23 (1959).
3. Devyatkova, E. and Smirnov, I., The Thermal Conductivity and the Dependence of the Lorentz Number in PbSe on Temperature and on the Degree of the Electron-Gas Degeneracy, Sov. Phys. Tech. Phys. 2, 1786-92 (Feb. 1961).
4. Gershtein, E., Stavitskaia, T., and Stilbans, L., A Study of the Thermoelectric Properties of PbTe, Sov. Phys. Tech. Phys. 2, 2302-13 (1957).
5. Reference # 1, p. 116.
6. Ibid. p. 35.
7. Smirnov, I., Moizhes, B., and Nensberg, E., The Effective Carrier Mass in Lead Selenide, Sov. Phys. Tech. Phys. 2, 1793-1804 (Feb. 1961).
8. Kuglin, C., Ellett, M., and Cuff, K., Oscillatory Magnetoresistance in n-type PbTe, Phys. Rev. Letters 6, 4, 177-9 (1961).
9. Miller, E., Komarek, K. and Cadoff, I., Interrelation of Electronic Properties and Defect Equilibria in PbTe., J. Appl. Phys. 32, 11, 2457-65 (1961).
10. Petritz, R., and Scanlon, W., Mobility of Electrons and Holes in the Polar Crystal, PbS, Phys. Rev. 97, 6, 1620-6 (1955).
11. Allgaier, R., Weak-Field Magnetoresistance in p-type PbTe at Room Temperature and 77°K, Phys. Rev. 119, 2, 554-61 (1960).
12. Moss, T. S., Optical Properties of Semiconductors, P. 191, Butterworths Semi-Conductor Monograph (London 1959).
13. Avery, D. G., Further Measurements on the Optical Studies of PbS, PbSe, and PbTe, Proc. Phys. Soc. (London) B 67, 2-8 (1954).
14. Gibson, A. F., The Absorption Spectra of Single Crystals of PbS, PbSe, and PbTe, Proc. Phys. Soc. (London) B 65, 378-88 (1952).
15. Cuff, K., Ellett, M., and Kuglin, C., Oscillatory Magnetoresistance in the Conduction Band of PbTe, J. Appl. Phys. (Suppl.) 32, 10, 2179-84 (1961).



16. Goldberg, C., Relaxation Time Anisotropy in n-type Germanium, *Phys. Rev.* 109, 2, 331-5 (Jan. 1958).
17. Haas, C. and Corbey, M., Measurement and Analysis of the Infrared Reflection Spectrum of Semiconducting SnS, *J. Phys. Chem. Solids* 20, 197-203 (Aug. 1961).
18. Avery, D. G., The Optical Constants of PbS, PbSe, and PbTe in the 0.5 - 3 $\mu$  Region of the Spectrum, *Proc. Phys. Soc. (London) B*, 66, 133-40 (1953).
19. Levinstein, H., The Electrical and Optical Properties of PbTe Films, Photoconductivity Conference (1954), pp. 601-18, Wiley (N.Y. 1956).
20. Burstein, E. and Egli, P., The Physics of Semiconductor Materials, *Advances in Electronics and Electron Physics*, vol. 7 p. 23, Academic Press (New York, 1955).
21. Hutson, A. R., Properties of Some Oxides and Sulfides, Semiconductors, A.C.S. Monograph edited by Hannay, N. B., p. 596, Rheinhold Publ. Corp. (New York, 1958).
22. Szigeti, B., Polarizability and Dielectric Constant of Ionic Crystals, *Trans. Faraday Soc.* 45, 155-66 (1949).
23. Ref. 12, chaps. 2 and 16.
24. Haas, C. and Mathieu, J., Infrared Spectra and Longitudinal and Transverse Waves in Cubic Crystals, *J. Phys. Radium* 15, 492 - 4 (1954).
25. Lyddane, R., Sachs, R., and Teller, E., On the Polar Vibrations of Alkali Halides, *Phys. Rev.* 59, 673-6 (1941).
26. Parkinson, D. and Quarrington, J., Molar Heats of Lead Sulfide, Selenide, and Telluride, *Proc. Phys. Soc. (London) A* 67, 569-79 (1954).
27. Shockley, W., *Electrons and Holes in Semiconductors*, Chap. 11, Van Nostrand (Princeton, N.J., 1950).
28. Frohlich, H. and Mott, N., The Mean Free Path of Electrons in Polar Crystals, *Proc. Roy. Soc. (London) A* 171, 496-504 (1939).
29. Howarth, D. and Sondheimer, E., The Theory of Electronic Conduction in Polar Semiconductors, *Proc. Roy. Soc. (London) A* 219, 53-74, (1953).
30. a) Lee, T., Low, F., and Pines, D., The Motion of Slow Electrons in a Polar Crystal, *Phys. Rev.* 90, 297-302 (1953).  
b) Low, F. and Pines, D., The Mobility of Slow Electrons in Polar Crystals, *Phys. Rev.* 91, 193-4 (1953).  
c) *Ibid.*, 98, 414-8 (1955).

31. Callen, H., Electric Breakdown in Ionic Crystals, *Phys. Rev.* 76, 9, 1394-1402 (1949).
32. Ref. 26, Chap. 17.
33. Burke, J., Houston, B., and Allgaier, R., Room-Temperature Piezoresistance and Elastoresistance in p-type PbTe, *Bull. Am. Phys. Soc.*, 6, 136 (March 20, 1961).
34. Ref. 27, p. 527.
35. Brooks, H., Theory of the Electrical Properties of Germanium and Silicon, *Advances in Electronics and Electron Physics* 7, 146, Academic Press (N. Y. 1955).
36. Dixon, J., Reflectivity of p-Type PbTe in the Infra-red Region, *Bull. Am. Phys. Soc.* 6, 312 (Apr. 24, 1961).
37. Allgaier, R., Weak Field Magnetoresistance in p-type PbTe at Room Temperature and 77°K, *Phys. Rev.* 119, 2, 554-61 (1960).
38. Stiles, P., Burstein, E., and Langenberg, D., de Haas-van Alphen Effect in p-Type PbTe and n-Type PbS, *J. Appl. Phys. (Suppl.)* 32, 10, 2174-8 (Oct. 1961).
39. Allgaier, R., Valence Bands in Lead Telluride, *J. Appl. Phys. (Suppl.)* 32, 10, 2185-9 (1961).
40. Iax, B. and Wright, G., Magnetoplasma Reflection in Solids, *Phys. Rev. Letters* 4, 16-18 (Jan. 1, 1960).
41. Deviatkova, E., Investigation of the Thermal Conductivity of PbTe, *Sov. Phys. Tech. Phys.* 2, 414-8 (1957).
42. Kanai, Y. and Nii, R., Experimental Studies on the Thermal Conductivity in Semiconductors, *Phys. Chem. Solids* 8, 338-9 (Jan. 1958).

## CHAPTER VI

### CONCLUDING DISCUSSION

During the course of the present investigation, we have been concerned with a variety of properties of the semiconducting compound PbTe. (Some of these properties are common to other semiconductor materials, especially the very closely related compounds of PbS and PbSe.)

With regard to the growth of single crystals of PbTe, we have found that it is possible to take advantage of the vapor pressure of the molten material. This vapor pressure is sufficient to effect a distillation of the compound. The distillate that is obtained is invariably p-type with a free-carrier concentration of  $3.5 \times 10^{18}$  holes/cm<sup>3</sup> when the starting material is reasonably close to stoichiometric proportions. As it is distilled, many small crystals can be seen to form with cubic and highly reflective surfaces. A typical crystal might be a couple of millimeters on a side. It may very well be possible to grow single crystals either directly from the vapor phase or from a vapor-to-liquid-to-solid progression. In fact, this latter has been carried out with some degree of success during the course of this investigation. An evacuated crucible containing PbTe in one chamber with a connecting tube to allow vapors to pass to another slightly cooler chamber was passed through the Bridgman-Stockbarger furnace described in Chapter III. The rate of progression of the crucible through the furnace was  $\sim 0.4$  cm/hr. The molten material was not sufficiently far removed from the nucleating chamber so that it passed into and through the temperature gradient of the furnace within twenty-four hours after the tip of the nucleating chamber. Nevertheless, a very shiny single-crystalline ingot, one centimeter in diameter and two centimeters long, was grown by this process. However, as pointed out above, the resulting material invariably has a free-carrier concentration of  $3.5 \times 10^{18}$  holes/cm<sup>3</sup>. Moreover, the procedure outlined above simply amounts to combining the distillation and crystal-growth steps. The increased complexity of the crucible container required to effect this combination and the lack of control over the resulting free-carrier concentration weigh heavily against such a combined procedure. This is especially true since it is so simple to

effect the distillation as one step, dope the distillate as required with excess proportions of Pb or Te or with another material as a second step, and then lower that material through the Bridgman furnace. The appearance of the resulting single-crystalline ingots are far superior to others obtained using the alternate methods of Chapter III. This would indicate that the constraining crucible is less likely to introduce strains and defects in the single-crystalline ingot.

The thermal conductivity of 1 p-type and 3 n-type samples of PbTe has been measured. It has been reported that the thermal conductivity of this compound exhibits an extra conduction mechanism which becomes significant at 250°K and which is sufficient to cause the thermal conductivity to increase at temperatures above 300°K. It has been pointed out that this mechanism has not been observed in the related compound of PbSe nor was it observed by Kanai and Nii in PbTe. Our data support this latter finding. We have not observed any indication at all that an additional thermal conduction mechanism exists below 300°K (see Fig. 5-22). We have calculated an electronic contribution to the total thermal conductivity from the general expression for the Wiedemann-Franz coefficient (Eq. 5-35). Upon subtracting this component from our average experimental  $\kappa$ , we obtained values for  $\kappa_1$  which we found obeyed the customary  $T^{-1}$  dependence. As a result we conclude that, below 300°K at least, the thermal conductivity of PbTe exhibits no indication of the anomalous behavior reported by Ioffe and by Deviatkova.

The origin of the observed temperature dependence of the free-carrier mobility in PbTe has been probed. It has often been noted that this temperature dependence obeys a power law ( $T^{-r}$ ), where  $r$  is in the range  $2 < r < 3$  for temperatures above  $\sim 150^\circ\text{K}$ . Such a temperature dependence is not uncommon for semiconductors. Similar behavior has been observed in the related compounds of PbS and PbSe and in p-type Ge and both n- and p-type Si. Nevertheless, such a power law differs from the standard theory for acoustical and optical mode lattice scattering, and one or both of these scattering mechanisms would be expected to dominate over all others at these temperatures.

However, all of the analyses which have attempted to determine the scattering mechanism have indicated that the energy dependence of the relaxation time is the same as that predicted by acoustical mode scattering. This has been deduced

from independent analyses of the Nernst-Ettingshausen effect, of the thermoelectric power, and of the thermal conductivity. This result leads to the apparent contradiction that the kinetic energy dependence of  $\tau$  indicates acoustical mode scattering while the temperature dependence of  $\mu$  is greater than that explicitly predicted by acoustical mode scattering.

The question that arises is whether or not a careful determination of the temperature dependence of the parameters entering the acoustical mode mobility expression can yield a temperature dependence greater than that associated with the factor  $T^{-1} \langle E^{-1/2} \rangle$ . We have undertaken to investigate this very point by determining the temperature dependence of  $m_d$ ,  $m_c$ , and  $E^{-1/2}$ .

The thermoelectric power data has been analyzed on the basis that  $\tau = \tau_0 E^{-1/2}$ . This has yielded the temperature dependence of the reduced Fermi potential. In turn a knowledge of this dependence has been used to establish the temperature dependence of  $\langle E^{-1/2} \rangle$ . It has been observed that, for the carrier concentrations of our samples and for  $T < 300^\circ\text{K}$ , the contribution of this term to the temperature dependence of  $\mu$  is considerably less than the non-degenerate limit of  $T^{-1/2}$ . Thus, the apparent discrepancy between the theoretical and experimental mobilities is even greater than ordinarily considered.

A knowledge of the reduced Fermi potential, along with the free-carrier concentrations deduced from Hall Effect measurements, enables us to calculate the density-of-states effective mass for these five samples of PbTe. The results indicate a very definite temperature dependence for  $m_d$ , increasing with increasing temperature. The absolute values that were obtained were compared with values reported for various temperatures in the literature, and they were shown to be compatible with a majority of these reports.

For obtaining the temperature dependence of the conductivity effective mass, a new method of utilizing the infra-red dispersion due to free-carriers has been developed. Heretofore, for measuring  $m_c$  using infra-red radiation it has been necessary to perform either the magnetoplasma experiment or else to consider the entire infra-red reflectivity curve. The latter method is by far the more straightforward of the two. However, it too has certain disadvantages. The principle disadvantage is that the free carrier absorption on the long wavelength side of the reflectivity minimum must be analyzed to obtain the absorption coefficient  $k$ . This means that the surface of the sample must be very care-

fully polished so that surface damage does not affect the reflectivity in this wavelength range. We have seen that surface damage can have the effect of reducing the steepness of the reflectivity rise in this region. This reduction can come about from scattering at the surface and/or from a decreased surface mobility. Consequently, the results that one obtains from an analysis of this kind are dependent on the condition of the surface. This becomes an even greater problem in PbTe at temperatures of  $4^{\circ}$  and  $77^{\circ}$ K, because the bulk mobility is extremely high. As a result, it does not require much surface damage to seriously affect the mobility. Moreover, the depth of penetration of the infra-red is substantially reduced in the high mobility material.

Because of these difficulties, the alternate procedure developed here for obtaining the effective mass from the free-carrier dispersion simplifies this determination considerably. The procedure that has been developed enables one to calculate  $m_c$  directly from the wavelength of the reflectivity minimum, along with data for  $N$ ,  $\mu$ , and  $\epsilon_{\infty}$ . This has a distinct advantage in that the position of the minimum is relatively insensitive to many sample defects. For example, the two noted above, scattering at the surface and a decreased surface mobility, are not nearly as serious in the proximity of the reflectivity minimum as they are at longer wavelengths. Furthermore, undersized samples have the effect of reducing the resolution of the minimum, but this has no effect on its position.

Thus, we see that this method is quite capable of providing useful data under what are normally considered to be very adverse conditions.

We have calculated values for  $m_c$  using this procedure (Eq. 2-10) and the results are shown together with  $m_d$  in Figs. 5-3 and 5-4. It has been found that  $m_c$  has a temperature dependence which is similar to that observed for  $m_d$ . The values of  $m_c$  and  $m_d$  have then been utilized to deduce the number of equivalent ellipsoids. We have deduced the existence of four ellipsoids in the conduction band and something less than four ( $\sim 2.5$ ) in the valence band. The latter we have interpreted as indicating an important role for the zone-centered maximum which has been postulated in the literature. The former result is taken to mean that the energy minima along the  $\langle 111 \rangle$  axes occur at the zone boundary.

Having obtained values as a function of temperature for  $m_c$ ,  $m_d$  and  $\langle E^{-1/2} \rangle$ , it has been possible to synthesize the temperature dependence predicted by acoustical mode scattering. This synthesis has been based on the assumption that the elastic constant  $C_{11}$  and the deformation potential  $E_1$  are independent of temperature. Upon comparing the resulting temperature dependence for both n- and p-type material with the respective experimental mobilities, we conclude that they agree very well at the higher temperatures ( $> 200^\circ\text{K}$ ). However, this acoustical mode mobility is incapable of matching the observed mobilities at the lowest temperatures ( $\sim 100^\circ\text{K}$ ).

The PbS family of compounds, heretofore, has been considered to have a predominately polar character. Realizing that PbTe is a two atom compound of valence two, it is reasonable to assume that it does have some polar character. Whether this is its dominant character is another question. However, on the basis that it does have some polar character, it follows that there must exist some optical mode scattering.

An optical mode scattering mobility has been calculated for sample 3 using the perturbation theory of Frohlich and Mott and of Howarth and Sondheimer. Before applying this theory, it has been shown that the expansion parameter  $\gamma$  for PbTe always satisfies the criterion of applicability of the theory, namely  $\gamma < 1$ . Consequently, an optical mode mobility has been calculated using Howarth and Sondheimer's expression which is valid for an arbitrary degree of degeneracy at  $T < \theta$  ( $\theta$  is the Debye temperature) and their expression which is valid in the non-degenerate limit at  $T > 400^\circ\text{K}$ . This procedure yields a mobility with an arbitrary scaling factor of the form  $\epsilon_s \epsilon_\infty / (\epsilon_s - \epsilon_\infty)$ . In order that this optical mode mobility be at least as great as the experimental mobility for PbTe, this factor must be such that  $\epsilon_s - \epsilon_\infty < 5$ . This result has placed an upper limit on the polar character of PbTe. Moreover, adjusting the scale factors for  $\mu_a$  and  $\mu_o$  to achieve a "best fit" to the experimental mobility yields "most probable" values of  $\epsilon_s = \epsilon_\infty + 2.5$  and  $S = 0.07$  for the static dielectric constant and the effective ionic charge.

These results have two very important implications. In the first place, we see that these values imply that the contribution of the lattice to the infra-red dispersion is negligible ( $\sim 1\%$ ) with respect to that of the free

carriers. We conclude that it is valid to analyze the infra-red reflectivity of PbTe by considering only the contribution of the free carriers, which is the procedure that has been followed. Moreover, it should be noted that this conclusion regarding the insignificance of the lattice contribution to the dispersion is in no way dependent on the original interpretation of the reflectivity data. That is, an optical mode mobility could have been calculated before the conductivity effective masses were determined from  $\lambda_0$  since  $m_c$  does not enter into the calculation of  $\mu_0$ .

The second major implication of these results for  $\epsilon_s$  and S is that PbTe, and presumably also PbS and PbSe, have been wrongly considered to be polar semiconductors. Instead they should be considered to be very predominately covalent. There have been other indications that this might in fact be the case. For example, the static dielectric constant reported for PbS in the International Critical Tables is very close to the known high-frequency dielectric constant; the apparent predominance of acoustical mode scattering at high temperatures is also indicative of a predominance of covalent bonding.

Moreover, by inserting this "most probable" value of  $\epsilon_s$ , or for that matter the upper limit of  $\epsilon_s$ , into the expansion parameter  $\gamma$  of the optical mode perturbation theory, we conclude that one should expect reasonably fast convergence of the theory.

Finally, and probably most important of all, the "best fit" combination of  $\mu_a$  and  $\mu_0$  can be seen to approximate the experimental mobility over the entire temperature range of this investigation. We conclude from this that the observed temperature dependence of the mobility is well-explained by the temperature dependence of both the conductivity and density-of-states effective masses.

This result, a variation of  $m_c$  and  $m_d$  with temperature, can be due to non-parabolic bands, to a change in the scattering mechanism, or to changes in the energy gap or in the lattice.

We are unable to make any final conclusion regarding which, if any, of these mechanisms is the cause of the temperature dependence observed for  $m_c$  and  $m_d$  in PbTe. However, we can note the following points:

- i. The theory for non-parabolic bands at the zone center indicates that the effective mass increases as the Fermi level moves farther into



the energy band. Assuming that the same result characterizes non-parabolic bands away from the zone center, we deduce that this effect is not the cause of the observed behavior. This follows from the fact that, as the temperature increases, the Fermi level in our samples approaches and even passes out of the energy band while at the same time, the effective masses are increasing. This is just the opposite of what the non-parabolic band theory predicts. However, it cannot be concluded that non-parabolic bands are completely absent. It can only be concluded that some other mechanism must be producing the observed temperature dependence, and that this other mechanism is capable of masking the effect of non-parabolic bands if they should be present.

- ii. We have observed that the scattering mechanism does change somewhat as the temperature increases. It is apparently a combination of acoustical and optical mode scattering up to  $\sim 150^\circ\text{K}$ . Around this temperature acoustical mode scattering begins to emerge as the dominant mechanism. However, since the temperature dependence of the mobility is the same up to very high temperatures where the scattering mechanism is almost exclusively acoustical mode scattering, a changing scattering mechanism would not seem to be the basic cause of the observed behavior.
- iii. This leaves the two remaining mechanisms - an expanding lattice and a changing direct energy gap as the two most likely sources of this temperature dependence of  $m_c$  and  $m_d$ . That this is at least plausible can be seen from the equation<sup>1</sup>

$$\frac{1}{m^*} \approx \frac{1}{m_0} \left( 1 + \frac{2 \hbar^2 G^2}{m_0 (\Delta E)} \right) \quad (6-1)$$

where  $m^*$  is the component of the inverse effective mass along the direction of the vector from the center of the zone to the symmetry point G and  $(\Delta E)$  is the direct energy gap to that energy band which has the highest probability of

interacting with the free carriers (assuming there is only one such band.)

If it is assumed that the energy gap reported by Avery and by Gibson is the direct gap then  $\Delta E = E_g$ , and it increases with temperature. Moreover,  $G \propto \alpha_0^{-1}$  where  $\alpha_0$  is the lattice spacing. Now, the lattice expands with temperature, and therefore  $G$  has a negative temperature dependence. Both of these temperature dependences are such as to cause  $m^*$  to increase with temperature, which is the behavior that has been observed. However, final quantitative conclusions with regard to the cause of the temperature dependence of  $m_c$  and  $m_d$  must await further improvement and clarification of the theory.

## CHAPTER VI

### BIBLIOGRAPHY

1. Ziman, J. M., *Electrons and Phonons*, Chapter II, Clarendon Press (Oxford, 1960).

APPENDIX A DIFFERENTIATION OF THE EQUATION FOR THE REFLECTIVITY OF FREE CARRIERS

$$R = \frac{(n - 1)^2 + k^2}{(n + 1)^2 + k^2} \quad (A-1)$$

and the free carrier dispersion relations

$$n^2 - k^2 = \epsilon \quad (A-2)$$

and

$$nk = \beta \quad (A-3)$$

where

$$\epsilon = \epsilon_{\infty} - \frac{Ne^2}{\epsilon_0 m_c} \frac{\tau^2}{1 + (\omega\tau)^2} = A - \frac{B}{1 + \rho^2}$$

$$\beta = \frac{1}{\omega\tau} \frac{Ne^2}{2m_c \epsilon_0} \frac{\tau^2}{1 + (\omega\tau)^2} = \frac{B}{2\rho(1 + \rho^2)}$$

$$\rho = \omega\tau \quad \text{and} \quad B = \frac{Ne^2 \tau^2}{m_c \epsilon_0}$$

The assumption is made that  $\tau$  is not a function of frequency (or if it is that it varies very slowly in region of the reflectivity minimum so that in that region it is essentially a constant).

The condition  $\frac{\partial R}{\partial \rho} = 0$  yields the equation:

$$\left[ n^2 - 1 - k^2 \right] n' + 2nk k' = 0$$

where the prime signifies  $\partial/\partial \rho$   
 Substituting  $k = \beta/n$ ,  $k' = \beta'/n - \beta n'/n^2$  and

simplifying yields:

$$\left[ n^4 - n^2 - 3\beta^2 \right] n' + 2\beta n\beta' = 0 \quad (\text{A-4})$$

Combining (A-2) and (A-3)

$$n^4 = \epsilon n^2 + \beta^2 \quad (\text{A-5})$$

which when substituted into (A-4) yields the result

$$\left[ (\epsilon - 1)n^2 - 2\beta^2 \right] n' + 2\beta n\beta' = 0 \quad (\text{A-6})$$

Now,  $n' = \frac{(n^2)'}{2n}$ . Therefore, (A-6) is written

$$(\epsilon - 1)n^2 - 2\beta^2 (n^2)' + 4n^2 \beta\beta' = 0 \quad (\text{A-7})$$

Moreover, from (A-5) it follows that:

$$2n^2 = \epsilon + \sqrt{\epsilon^2 + 4\beta^2} = A - \frac{B}{1 + \rho^2} + \sqrt{\left( A - \frac{B}{1 + \rho^2} \right)^2 + \frac{B^2}{\rho^2(1 + \rho^2)^2}}$$

$$2n^2 = A - \frac{B}{1 + \rho^2} + \sqrt{A^2 - \frac{2AB}{1 + \rho^2} + \frac{B^2}{\rho^2(1 + \rho^2)^2}}$$

where the positive root is chosen to keep  $n$  real.

$$2 \frac{\partial n^2}{\partial \rho} = \frac{2B\rho}{(1 + \rho^2)^2} + \frac{\frac{2AB\rho}{(1 + \rho^2)^2} - \frac{B^2(1 + 2\rho^2)}{\rho^3(1 + \rho^2)^2}}{\sqrt{A^2 - \frac{2AB}{1 + \rho^2} + \frac{B^2}{\rho^2(1 + \rho^2)^2}}} \quad (\text{A-8})$$

Now,

$$\beta = \frac{B}{2\rho(1 + \rho^2)} \quad \text{and} \quad \beta' = - \frac{B(1 + 3\rho^2)}{2\rho^2(1 + \rho^2)^2}$$

Therefore, the terms in Eq. (A-8) may be rewritten in terms of  $\beta'$ .

$$\frac{2B\rho}{(1+\rho^2)^2} = - \frac{4\rho^3}{(1+3\rho^2)} \beta'$$

$$\frac{2AB\rho}{(1+\rho^2)^2} = - \frac{4\rho^3 A}{(1+3\rho^2)} \beta'$$

$$- \frac{B^2(1+2\rho^2)}{\rho^3(1+\rho^2)^2} = \frac{2B(1+2\rho^2)}{\rho(1+3\rho^2)} \beta'$$

and

$$\sqrt{A^2 - \frac{2AB}{1+\rho^2} + \frac{B^2}{\rho^2(1+\rho^2)}} = 2n^2 - A + \frac{B}{1+\rho^2}$$

Thus, Eq. (A-8) takes the form:

$$(n^2)' = \left\{ - \frac{2\rho^3}{(1+3\rho^2)} + \frac{\frac{B(1+2\rho^2)}{\rho(1+3\rho^2)} - \frac{2\rho^3 A}{(1+3\rho^2)}}{2n^2 - A + \frac{B}{1+\rho^2}} \right\} \beta' = C(\rho) \beta' \quad (A-9)$$

The factor  $C(\rho)$  can be simplified to the following form:

$$C(\rho) = \frac{1}{\rho(1+3\rho^2)(2n^2 - A + \frac{B}{1+\rho^2})} \left[ - 4n^2 \rho^4 + \frac{B(1+3\rho^2)}{1+\rho^2} \right] \quad (A-10)$$

Combining (A-7), (A-9) and (A-10) yields:

$$\left[ (\epsilon-1)n^2 - 2\beta^2 \right] \left[ - 4n^2 \rho^4 + \frac{B(1+3\rho^2)}{(1+\rho^2)} \right] + 2n^2 \frac{B(1+3\rho^2)}{1+\rho^2} \left[ 2n^2 - A + \frac{B}{1+\rho^2} \right] = 0 \quad (A-11)$$

where, of course, it has been assumed that  $\beta = \frac{B(1+3\rho^2)}{2\rho^2(1+\rho^2)} \neq 0$ .

However, this is obviously not a restrictive condition.

Equation (A-11) can be rewritten in the form

$$n^4 - G(\rho) n^2 - H(\rho) \beta^2 = 0 \quad (\text{A-12})$$

where

$$G(\rho) = \frac{\left[ -\frac{2B^2\rho^2}{(1+\rho^2)^2} - (\epsilon-1) \frac{B(1+3\rho^2)}{1+\rho^2} + \frac{2AB(1+3\rho^2)}{(1+\rho^2)} - \frac{2B^2(1+3\rho^2)}{(1+\rho^2)^2} \right]}{4 \left[ \frac{B(1+3\rho^2)}{1+\rho^2} - (\epsilon-1)\rho^4 \right]}$$

and

$$H(\rho) = \frac{\frac{B(1+3\rho^2)}{1+\rho^2}}{2 \left[ \frac{B(1+3\rho^2)}{1+\rho^2} - (\epsilon-1)\rho^4 \right]}$$

and from (A-5), we have a general relation of the same form which must hold everywhere including at the reflectivity minimum.

$$n^4 - \epsilon n^2 - \beta^2 = 0 \quad (\text{A-5})$$

Equating (A-5) and (A-12), yields

$$n^2 = \beta^2 \frac{(H-1)}{\epsilon - G} \quad (\text{A-13})$$

and by substituting (A-13) into (A-5), a relationship between the coefficients  $\epsilon$ ,  $\beta$ ,  $H$ , and  $G$  is established, namely

$$\beta^2 \frac{(H-1)}{\epsilon - G} - \frac{\epsilon - G}{H - 1} = \epsilon$$

and

$$\beta^2 = \frac{(\epsilon - G)(H\epsilon - G)}{(H-1)^2} \quad (\text{A-14})$$

By redefining the coefficients

$$G = g/f \quad \text{and} \quad H = h/f$$

where  $f = 4 \left[ \frac{B(1+3\rho^2)}{1+\rho^2} - (\epsilon-1)\rho^4 \right]$

Then, Eq. (A-14) takes the form:

$$\beta^2 = \frac{(f\epsilon - g)(h\epsilon - g)}{(h-f)^2} \quad (\text{A-15})$$

Now, these new parameters  $f$ ,  $g$ , and  $h$  can be reduced to the forms:

$$\begin{aligned} f &= 4 \left[ \frac{B(1+3\rho^2 + \rho^4)}{1+\rho^2} - (A-1)\rho^4 \right] \\ g &= (A+1) \frac{B(1+3\rho^2)}{1+\rho^2} - B^2 \frac{(1+5\rho^2)}{(1+\rho^2)^2} \\ h &= \frac{2B(1+3\rho^2)}{1+\rho^2} \end{aligned} \quad (\text{A-16})$$

When these are combined in the manner prescribed by Eq. (A-15) and after much simplification, the following equation is obtained:

$$B^3 + 2\rho^2 (1+2\rho^2)(3A-2) B^2 - \rho^2 (1+5\rho^2+8\rho^4)(3A^2 - 4A+1) B + 4A (A-1)^2 \rho^6 (1+3\rho^2) = 0 \quad (A-17)$$

Defining

$$B = \frac{\rho^2}{m_c^*} \quad Z = \frac{\rho^2}{m_c^*} \quad \frac{Ne^2}{m_o \omega_o^2 \epsilon_o} \quad \text{where } \omega_o = \text{radial frequency of minimum reflectivity}$$

Eq. (A-17) can be rewritten in the form:

$$m_c^{*3} - \frac{(3A-1)}{4A(A-1)} \frac{\frac{1}{Z} + 5 + 8\rho^2}{(1+3\rho^2)} Z m_c^{*2} + \frac{(3A-2)}{2A(A-1)^2} \frac{(1+2\rho^2)}{(1+3\rho^2)} Z^2 m_c^* + \frac{Z^3}{4A(A-1)^2(1+3\rho^2)} = 0 \quad (A-18)$$

which is the form of Eq. (2-10).

Finally, it should be noted that many limiting conditions, for checking the validity of Eqs. (A-17) and (A-18), simply are non-physical. For example,  $A \neq 1$  but must be greater than unity, because the total relative dielectric constant must be greater than that of free space. Also,  $\rho^2 \neq 0$  because the dispersion relation (A-3) has a singularity at  $\rho = 0$ . These two serve as examples; there are several other limiting conditions which are similarly non-allowable.



APPENDIX B. APPLICATION OF EQ. 2-10 TO THE CASE OF N-TYPE GERMANIUM.

From the data of Spitzer of Fan:

$$\begin{aligned}\lambda_0 &= 23 \mu \\ \epsilon_\infty &= 16 \\ \mu_h &= 520 \text{ cm}^2/\text{volt-sec.}\end{aligned}$$

Initial estimate:  $m_c^* = 0.12$  (from cyclotron resonance).

Equation 2-10 becomes:

$$m_c^{*3} - 0.249 m_c^{*2} + 0.0147 m_c^* + 1.65 \times 10^{-5} = 0 \quad (\text{B-1})$$

The last term represents a small correction, on the order of 1 % , so it is neglected. Solving the remaining quadratic yields:

$$m_c^* = 0.152 \quad (\text{B-2})$$

Second estimate:  $m_c^* = 0.15$

Equation 2-10 now becomes:

$$m_c^{*3} - 0.246 m_c^{*2} + 0.0146 m_c^* + 1.07 \times 10^{-5} = 0 \quad (\text{B-3})$$

Again, neglecting the last term, we obtain the result:

$$m_c^* = 0.146 \quad (\text{B-4})$$

It is apparent that (B-2) and (B-4) are not very different so that it can be anticipated that  $m_c^* = 0.146$  represents a solution to the quadratic approximation to Eq. 2-10. Since the last term is only about 1 % as great as the other terms, a reasonable third estimate is:  $m_c^* = 0.145$ . This value does, in fact, satisfy the cubic Eq. 2-10.

## BIOGRAPHICAL NOTE

Henry A. Lyden was born in Youngstown, Ohio on February 11, 1935. For his undergraduate education he participated in a "Combined Program" between Williams College in Williamstown, Massachusetts and the Massachusetts Institute of Technology. This program involved five years of study. The first three years from 1952 to 1955, he attended Williams College as a Physics major, and during the next two years he attended the Massachusetts Institute of Technology in the Electrical Engineering Department. In June, 1957 he received both his A.B. degree from Williams College and his S.B. degree from M.I.T. During the following summer he worked for the Sperry Gyroscope division of Sperry Rand Corporation in the Transport Flight Control Department. After returning to M.I.T. in the fall of 1957 as a research assistant in the Solid-State Energy Conversion Group of the E.E. Dept., he received his S.M. degree in February 1959. Subsequently he has been associated with the same Energy Conversion Group, and he received an appointment as instructor in the Electrical Engineering Department in June 1961.

He is a member of Tau Beta Pi, Eta Kappa Nu and Sigma Xi.